UCSF
UC San Francisco Electronic Theses and Dissertations

**Title**
N-WASP at the Membrane-Actin Interface

**Permalink**
https://escholarship.org/uc/item/8jr992g4

**Author**
Co, Carl

**Publication Date**
2007-04-02

Peer reviewed|Thesis/dissertation

eScholarship.org Powered by the California Digital Library
University of California

# N-WASP at the Membrane-Actin Interface

by

Carl Co

DISSERTATION

Submitted in partial satisfaction of the requirements for the degree of

DOCTOR OF PHILOSOPHY

in

Cell Biology

in the

GRADUATE DIVISION

of the

UNIVERSITY OF CALIFORNIA, SAN FRANCISCO

*To team actin.*

**ACKNOWLEDGMENTS**

Many people shared their minds, hearts and time to help see this project to fruition. This work is the result of the insight, creativity, passion and storytelling of Jack Taunton. His careful analysis of experiments and acute attention to details molded our initial observations into the story we have presented. I owe so much to two extremely talented and tireless scientists, Derek Wong and Sarah Arriola. They helped breathe life into this project with their efforts, enthusiasms and perseverance every day.

I would also like to share my gratitude to the community of scientists I was fortunate to have at UCSF. The Lim lab and the Mullins lab were responsible for my training as an actinologist. I especially would like to thank John Dueber, Ken Prehoda, Roby Bhattacharyya, Orkun Akin and Mark Dayel. In recent times, I have had great discussions with Dan Fletcher, Allen Liu and Sapun Parekh. To my thesis committee members, Ron Vale and Wendell Lim: thank you for your guidance and interest in my future after graduate school.

Life in the lab was a melting pot of personalities that blended so well. These included Mike Cohen, Jennifer Garrison, Vicky Chang, Sarah Maifeld and Julia Kardon, who I would like to acknowledge for her work on N-WASP speckling.

And finally to my family and friends for their support and inspiration; especially to Liz Mack, my editor and partner.

I would like to acknowledge the Herbert Boyer PIBS Tetrad program for their support and Sue Adams, whose door was always open for me.

**ABSTRACT**

Actin polymerization occurs on membrane surfaces in cells. Signal transduction cascades activate nucleation promoting factors (NPFs) that are recruited to and activated at the membrane to produce polarized actin networks. These cytoskeletal structures generate force against membranes such as at the leading edge of chemotaxing cells, at the basal membrane of invasive podosomes in cancerous cells, and at the surface of rocketing intracellular vesicles. The molecular mechanisms that regulate the establishment and maintenance of polarized actin networks on the membrane are not well understood. Specifically, it is unknown how the actin network remains attached to the membrane as it pushes against it.

Formation of polarized actin networks has been reconstituted *in vitro* on the surface of polystyrene beads. Because these systems used NPFs that are fixed to the bead surface, the physiological relevance of the membrane and of signal transduction activation could not be assessed on the formation and/or maintenance of polarized actin networks.

We used the vesicle motility system to study the role of the NPF, N-WASP, at the membrane-actin interface of rocketing vesicles. We found that the actin monomer binding domain, the WH2 domain, was necessary and sufficient to localize to the membrane-actin interface. To dissect the mechanism of this localization, we created a novel biomimetic motility system using pure components. This system included a lipid bilayer substrate and a set of soluble

signaling proteins including autoinhibited N-WASP and inactive Cdc42/RhoGDI complex. Using this system, we made two critical observations: first, we demonstrated that WH2 mutants that were defective in localization to the membrane-actin interface formed comet tails that prematurely detached from the membrane. N-WASP maintained membrane-actin attachment by WH2-mediated capture of actin filament barbed ends. Further, we observed in cells that these mutations resulted in defects in organization of large podosome structures. The second observation has initiated a new study. We demonstrated that the concurrent activation of Cdc42 and N-WASP with actin polymerization yielded a new form of symmetry breaking on membranes. This result, which mimics a more physiological experimental scenario, highlights the necessity to study signal-dependent actin assembly on membranes *in vitro*.

**TABLE OF CONTENTS**


| | | |
|---|---|---|
| Preface | Acknowledgements | iv |
| | Abstract | v |
| | Table of Contents | vii |
| | List of Tables | x |
| | List of Figures | xi |
| Chapter 1: | Introduction | 1 |
| Chapter 2: | N-WASP localization to the membrane-actin interface of rocketing vesicles | 10 |

Abstract

Introduction

Results

- N-WASP localizes to the membrane-actin interface of moving vesicles
- The C-terminal WH2 domain ($WH2_b$) is required for N-WASP localization to the membrane-actin interface
- The polybasic motif and WH2 domains are sufficient to localize to the membrane-actin interface
- The $WH2_a$ motif is not sufficient to localize N-WASP to the membrane-actin interface
- Mutations in the $WH2_b$ motif abrogate membrane-actin localization but not actin polymerization
- Mutations in the $WH2_b$ motif affect the ability of N-WASP to promote robust vesicle motility
- Polarization mutant K444Q N-WASP clustering

on moving vesicles

Mutations in the WH2 motif that abrogate localization of N-WASP to the membrane-actin interface do not abolish N-WASP oligomerization

Discussion

A new polarization motif

Materials and Methods

Chapter 3: Reconstitution of Cdc42/GDI activated actin assembly on synthetic PIP2 lipid bilayers with pure proteins reveals a new mechanism for membrane-actin adhesion and a new mechanism of symmetry breaking 55

Abstract

Introduction

Results

Reconstitution of intersectin-dependent Cdc42/GDI activation at the membrane surface

Reconstitution of Cdc42 activated vesicle motility with pure proteins

Two modes of symmetry breaking on lipid-coated beads

N-WASP mutants defective in asymmetric localization create comet tails but catastrophically detach from the membrane

Membrane-actin detachment is highly dependent on actin monomers and this counteracts the detaching effects caused by capping protein

Inhibition of Arp2/3 activity does not lead to membrane-actin detachment

Actin filament capture of F-actin barbed ends by WH2 domains requires actin monomers

WH2 domains are sufficient to maintain attachment of a dendritic network to the membrane surface

Discussion

Materials and Methods

Chapter 4: N-WASP regulates the formation of large podosome structures in cells 104

Abstract

Introduction

Results

Podosome formation in v-Src transformed cells requires N-WASP

RA/RA N-WASP forms podosomes and nucleates actin polymerization almost equivalently to WT N-WASP

Podosomes require v-Src kinase activity

Live imaging of podosomes

RA/RA N-WASP is defective in the formation of large podosome structures and circular podosomes

Dynamics of WT and RA/RA N-WASP podosome structures

Discussion

Materials and Methods

Chapter 5: Discussion and Future Directions 128

Appendix A: Pathogen motility in WT and RA/RA cells 138

Appendix B: References 144

## LIST OF TABLES

Table 1 22

Table 2 30

## LIST OF FIGURES


| | |
|---|---|
| Figure 1 | 6 |
| Figure 2.1 | 17 |
| Figure 2.2 | 19 |
| Figure 2.3 | 24 |
| Figure 2.4 | 27 |
| Figure 2.5 | 28 |
| Figure 2.6 | 31 |
| Figure 2.7 | 33 |
| Figrue 2.8 | 36 |
| Figure 2.9 | 38 |
| Figure 2.10 | 39 |
| Figure 2.11 | 41 |
| Figure 2.12 | 45 |
| Figure 2.13 | 50 |
| Figure 2.14 | 53 |
| Figure 3.1 | 62 |
| Figure 3.2 | 64 |
| Figure 3.3 | 67 |
| Figure 3.4 | 69 |
| Figure 3.5 | 71 |
| Figure 3.6 | 75 |
| Figure 3.7 | 79 |

Figure 3.8 80

Figure 3.9 85

Figure 3.10 87

Figure 3.11 90

Figure 3.12 92

Figure 3.13 96

Figure 4.1 110

Figure 4.2 111

Figure 4.3 112

Figure 4.4 113

Figure 4.5 115

Figure 4.6 116

Figure 4.7 119

Figure 4.8 120

Figure 4.9 122

Figure A1 141

Figure A2 142

# Chapter 1

# Introduction

## Introduction

Many cellular events utilize localized actin polymerization to create force against membrane structures (Pollard and Borisy, 2003). Actin polymerization extends the plasma membrane for cell movement, deforms membranes to engulf particles for cellular intake and can be hijacked by pathogens for use as a motor to spread from one cell to another (Kaksonen et al., 2003; Welch and Mullins, 2002). In cancerous cells, large actin-rich structures called podosomes are asymmetrically formed at the base of the cell and degrade the surrounding extracellular matrix (ECM) to allow invasion (Mizutani et al., 2002; Yamaguchi et al., 2005). Localized actin assembly creates polarized networks that allow these forms of membrane movement.

Most cells are not inherently polarized. They use complex sets of molecules and intricate schemes to generate global cell polarity or asymmetrical membrane structures. For example, both pathogenic bacteria and intracellular vesicles form polarized actin structures, termed comet tails, that propel them around the cell. The pathogenic bacteria *Shigella flexneri*, produces a surface protein, IcsA which is expressed in a polarized fashion on the bacterial cell surface (Egile et al., 1999; Snapper et al., 2001). The localization of this membrane protein serves as a polarization zone, which targets and spatially restricts actin machinery to one end of the bacteria. On the cellular plasma membrane and on the surface of endosomes and lysosomes, polarization zones do not exist. Nonetheless, asymmetrical structures are created: cell motility is

driven by leading edge actin structures and endosome rocketing is propelled by actin comet tails.

Polarization of membrane structures can be achieved by systems of self-organization that rely on various mechanisms of reinforcement. The budding yeast, *Saccharomyces cerevisiae,* becomes polarized cell mating. Cell polarization is initiated by gradients of extracellular mating pheromones. This forms a polarization zone and initiates cell asymmetry. However, in the absence of external cues, yeast cells will spontaneously generate sites of polarity along the membrane (Kirschner et al., 2000; Wedlich-Soldner et al., 2003). This self-organization is driven by a form of positive reinforcement based on a system of signaling components and the actin cytoskeleton. First, the RhoGTPase, Cdc42, and its interacting proteins are recruited to the membrane. Next, components of this pathway recruit actin filaments to the site of signaling and through an unknown mechanism tether the filaments to the membrane. Finally, more Cdc42 molecules are transported along the newly laid actin filament tracks to the site of signaling, creating a form of feedback, or positive reinforcement (Wedlich-Soldner et al., 2003). This process is an example of cell polarization at the membrane generated initially by a self-organizing system, and then reinforced by signaling molecules and the actin cytoskeleton.

In mammalian cells and intracellular vesicles, there are also no inherent polarization zones. Instead, cellular polarity is achieved by the generation of a

polarized actin network and possibly maintained at the membrane surface in a process similar to yeast. It is interesting to consider the commonalities among these quite different biological processes of yeast polarization, mammalian podosome formation and vesicle motility. First, the molecular players in the signal transduction pathways are similar among all 3 biological systems. Second, the requirement of component localization to the membrane and interaction with cytoskeletal networks is conserved. Thus, the mechanisms of reinforcement discussed here may be generalizable to other biological systems.

Vesicle motility is a model system to study signal transduction-dependent polarized actin assembly at the membrane surface (Papayannopoulos et al., 2005; Rozelle et al., 2000; Taunton et al., 2000; van der Gucht et al., 2005). Like previous biomimetic systems involving bacteria or plastic beads, a polarized actin comet tail generates the force for movement (van der Gucht et al., 2005). However, this system is unique for two important reasons of physiological relevance. First, actin network assembly is activated by signaling cascades that exchange components between the cytosol and the membrane. Second, polarized actin assembly occurs on fluid membranes that allow components and the cytoskeleton to interact and diffuse along the surface.

In one vesicle motility model system involving Xenopus extracts, motility is initiated by the stimulation of Protein Kinase C (PKC) by phorbol ester which mimics diacylglycerol (Taunton et al., 2000). This activates the RhoGTPase

signaling cascade and recruits Cdc42 from the solution to the surface of endosomes and lysosomes. Formation of the actin network on the membrane is initiated by the recruitment of the nucleation promoting factor (NPF), neural Wiskott Aldrich Syndrome protein (N-WASP) by activated Cdc42 and the phosphoinositide $PI(4,5)P_2$ (PIP2) (Papayannopoulos et al., 2005; Taunton et al., 2000). N-WASP recruits components of actin machinery and orchestrates the formation of the actin comet tail at the membrane surface (Fig.1).

A

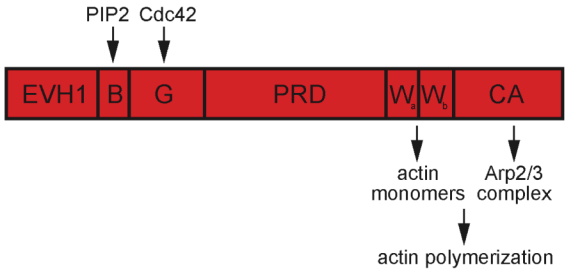
PIP2
Cdc42
EVH1
B
G
PRD
W
W
CA
actin monomers
Arp2/3 complex
actin polymerization

B

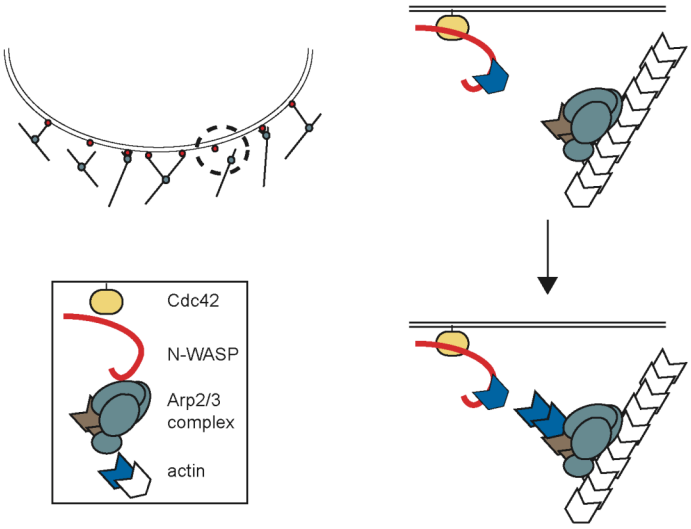
Cdc42
N-WASP
Arp2/3 complex
actin

**Fig.1 Model of N-WASP-dependent actin assembly at the membrane surface.**

(A) The domain structure of N-WASP. Arrows indicate the respective interactions of each domain with PIP2, Cdc42, actin monomers and Arp2/3 complex. The following abbreviations are used: enabled-VASP homology domain 1, EVH1; polybasic motif, B; GTPase binding domain, G; proline-rich domain, PRD; WASP Homology domain 2, $W_a$ and $W_b$; connecting region, C; and acidic region, A. Actin polymerization requires N-WASP, actin monomers and the Arp2/3 complex.

(B) Model of the membrane-actin interface of rocketing vesicles. Sticks represent actin filaments. Red circles represent N-WASP. Grey circles represent the Arp2/3 complex. The actin network interacts with the membrane surface. Magnified inset of actin polymerization at the membrane interface. Membrane-bound N-WASP recruits actin monomers and shuttles them to the filament bound Arp2/3 complex for dendritic nucleation of the actin network.

N-WASP is a multidomain scaffolding protein that nucleates actin network assembly by activating the Arp2/3 complex. Membrane localization is governed by a polybasic motif (B) and GTPase binding domain (G), which interact with PIP2 and Cdc42, respectively. The WASP Homology domain 2 (WH2) binds actin monomers and the Central and Acidic domain (CA) binds to the polymerization motor, known as the Arp2/3 complex (Marchand et al., 2001). N-WASP initiates the formation of actin networks by shuttling actin monomers to the Arp2/3 complex (Fig.1A). This complex, bound to actin filaments, nucleates a daughter filament, which elongates towards the membrane surface (Kelly et al., 2006). This polymerization process produces a dendritic actin network that pushes against the membrane surface (Fig.1B).

In studying this process in the model systems described, several key questions have emerged. As vesicles rocket around the cytoplasm, the comet tail remains bound to the membrane and structurally polarized there. Thus, over time there is only one comet tail. What remains puzzling is: by what mechanism does the polarized actin comet tail remain stably bound to the fluid membrane surface? In a similar observation, cancerous cells maintain large podosome structures over long periods of time which are used to degrade their surroundings (Mizutani et al., 2002; Spinardi et al., 2004; Yamaguchi et al., 2006). If signal transduction cascades occur continuously and signaling and actin machinery components are continually recruited to the membrane surface, the question is:

how are these polarized structures maintained over time? In budding yeast polarization, actin filaments serve as guidance tracks to the membrane. This simple observation leads to the question: how do filaments interact with the membrane surface?

In the following work, we use a combination of 3 systems (the Xenopus extract vesicle motility system, a reconstituted-pure protein signal transduction actin assembly system on fluid membrane surfaces and a podosome model system in mammalian cells) to address these questions. Importantly, we determine that the components of these systems are similar and can be used to further explain how the actin machinery interacts with a membrane surface to establish and maintain polarized actin networks.

# Chapter 2

## N-WASP localization to the membrane-actin interface of rocketing vesicles.

**Abstract**

Nucleation promoting factors localize asymmetrically on the surface of rocketing vesicles, at the interface between the actin network and the membrane. One potential explanation for this polarized localization on a fluid bilayer is that NPFs directly interact with a component of actin comet tails. Identification of a polarization domain within N-WASP would allow us to elucidate the molecular mechanisms that govern the interactions between the membrane and actin network, to test its functional relevance and to potentially provide insight into the mechanism by which a polarized actin structure is established and maintained.

## Introduction

*In vivo*, actin polymerization occurs on fluid membrane surfaces such as the leading edge of lamellipodia and filipodia and on the surface of rocketing endocytic vesicles (Welch and Mullins, 2002). *In vitro*, actin polymerization is studied using an assay that employs purified proteins in bulk solutions in monitoring the polymerization of pyrene-labeled actin (Mullins et al., 1998). While this assay has been useful in deciphering the kinetics and mechanisms of Arp2/3 complex activation, it does not reveal information regarding the organization of the actin network, the ability of this network to generate force, or the localization of NPFs and the Arp2/3 complex.

The creation of actin-based bead motility systems in cell-free extracts was a major advance towards our understanding of actin nucleation in cells (Yarar et al., 1999). These experiments allowed for examination of the actin network structure and the players involved in this process *in vitro*. For example, platinum replica electron microscopy demonstrated that the actin comet tail was organized in a dendritic network reminiscent of the organization of the actin network at the leading of motile cells and further, that the actin network is attached to the bead surface (Cameron et al., 2001). It also allowed for the examination of the relationship between actin network assembly and the resulting force generation (Boukellal et al., 2004; Giardini et al., 2003; Kuo and McGrath, 2000; Marcy et al., 2004).

Characterizing the localization patterns of signaling molecules could provide fundamental insights into the mechanisms by which polarized actin networks form. NPFs are dynamic proteins whose activity must be regulated and who must interact with both membrane proteins and lipids in the plasma membrane. Recently, we developed a cell-free model system that reconstitutes actin nucleation on the surface of intracellular vesicles (Taunton et al., 2000). Upon activation of PKC, prenylated Cdc42 is exchanged from its inhibitory factor GTPase Dissociation Inhibitor (GDI) to the membrane. Upon interaction with PIP2 and membrane-bound Cdc42, N-WASP is released from its autoinhibited state and stimulates Arp2/3 complex-dependent actin polymerization at the membrane surface (Papayannopoulos et al., 2005; Rohatgi et al., 1999).

To dissect the mechanisms by which N-WASP activity is regulated at the membrane surface, we characterized the localization of N-WASP on the surface of motile vesicles in Xenopus extracts. To understand the mechanism of polarized membrane localization, we identify the elements that regulate N-WASP localization to the membrane-actin interface and further examine the functional relevance of this localization in N-WASP-powered vesicle motility. By probing the behavior of N-WASP molecules on the surface of moving vesicles, we provide insight into the general mechanisms by which a polarized actin structure is established and maintained on a fluid membrane bilayer.

## Results

### N-WASP localizes in a polarized manner to the membrane-actin interface.

The molecular mechanisms that regulate interactions between the polarized actin network and the fluid membrane surface are not well understood. It has been proposed that attachment of the actin network to the membrane surface is governed by the Arp2/3 complex, which transiently links the sides of membrane-proximal filaments to the CA domain of N-WASP prior to generating a new barbed end (Mogilner and Oster, 2003). In an alternative proposed mechanism, attachment is mediated by direct interactions between N-WASP and membrane-proximal barbed ends. This mechanism is central to filament end-tracking models of *Listeria monocytogenes* movement (Dickinson and Purich, 2002). As a third possibility, both side-binding and barbed-end binding mechanisms are required for mediating the membrane-actin network adhesion. Finally, clustering of N-WASP molecules may be regulated by N-WASP's ability to oligomerize on the membrane. There is little experimental evidence to support any of these mechanisms. The vesicle motility system is used experimentally to probe the interactions between the membrane, N-WASP and the polarized actin network.

Previous immunoelectron microscopy studies demonstrated that N-WASP molecules were intimately associated with the vesicle membrane and appeared biased to the region of the vesicle contacting the actin comet tail (Taunton et al.,

2000). Here, we use live fluorescence imaging to probe N-WASP dynamics on the surface of rocketing endosomes. We find that N-WASP localization is polarized (Fig. 2.1B, C): N-WASP fluorescence is most intense at the membrane-proximal ends of actin comet tails, where N-WASP appears to connect the membrane surface and the F-actin network (Fig. 2.1 C, Fig. 1 B).

The most likely explanation for N-WASP asymmetry on a fluid membrane bilayer is that N-WASP directly interacts with a component of the actin comet tail (e.g., actin itself, the Arp2/3 complex, or another structural component). In addition, N-WASP asymmetry may be driven by the oligomerization of membrane-bound-N-WASP molecules. These mechanisms may cluster N-WASP and regulate actin assembly and force generation at the membrane surface.

Initially, we searched for a candidate polarization domain, defined as the minimal N-WASP fragment that localizes to the membrane-actin interface of rocketing vesicles. We labeled a panel of bacterially-expressed N-WASP fragments with fluorophores and added them to phorbol ester-stimulated Xenopus egg extracts, a well-established system for studying vesicle motility (Papayannopoulos et al., 2005; Taunton et al., 2000). At low concentrations (50 nM), labeled N-WASP fragments had neither inhibitory nor stimulatory effects on vesicle motility, which is driven in these experiments by unlabeled endogenous N-WASP. We used live imaging to determine whether labeled fragments localized to the membrane-actin interface.

We assessed that deletion of the amino-terminal EVH1 domain which facilitated expression in E. coli had no effect on asymmetric localization, as Alexa488 N-WASP$^{151-501}$ localized to the polarization zone of all moving vesicles. In this experiment we simultaneously imaged a rhodamine-labeled BG fragment (rhod-BG). In contrast to N-WASP$^{151-501}$, the BG fragment was evenly distributed along the entire surface of the vesicle (Fig. 2.1 B, C n=100). In several cases, rhod-BG was even excluded from the membrane-actin interface. Thus, interactions with acidic phospholipids and Cdc42, previously thought to be essential for the recruitment of N-WASP to endosomal vesicles in this system (Papayannopoulos et al., 2005; Prehoda et al., 2000), are not sufficient to mediate colocalization of rhod-BG with Alexa488-N-WASP$^{151-501}$ to the membrane-actin interface, despite robust recruitment of this fragment to the membrane.

When the WH2, central, and acidic domains ($W_aW_bCA$) were fused to BG (Fig. 2.2 A), the resulting BG-$W_aW_bCA$ (BG-WCA) fragment now localized to the membrane-actin interface (Fig. 2.2 B). This result suggested that the polarization activity lies within the carboxy-terminal, Arp2/3-activating portion of N-WASP. Given that the Arp2/3 complex can simultaneously bind to the N-WASP CA domain and the sides of actin filaments (Egile et al., 2005), we hypothesized that this region mediates the interaction with the actin comet tail. We were therefore surprised to find that the BG-$W_aW_b$ fragment, which lacks the Arp2/3-binding

A

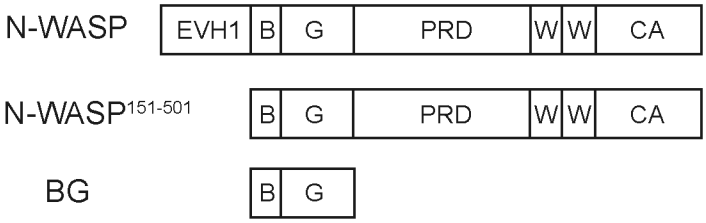
N-WASP
EVH1
B
G
PRD
W
W
CA
N-WASP151-501
B
G
PRD
W
W
CA
BG
B
G

B

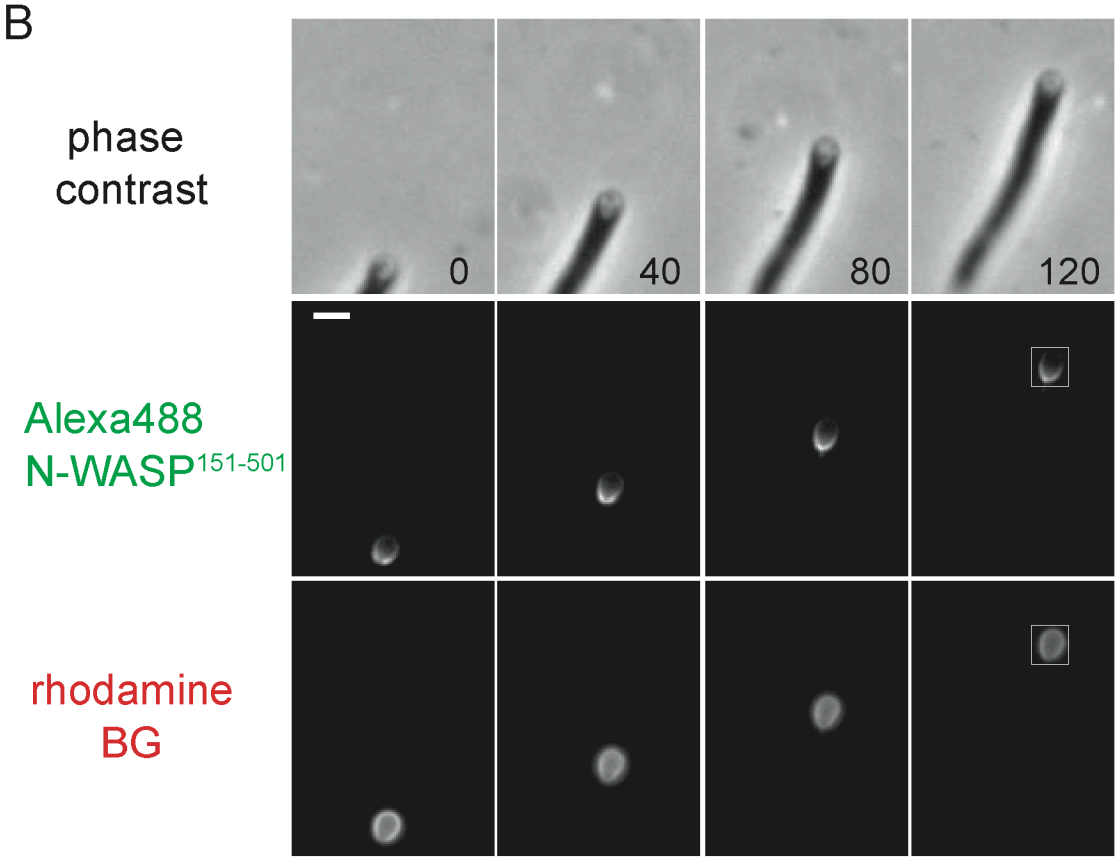
phase contrast
0
40
80
120
Alexa488 N-WASP151-501
rhodamine BG

C

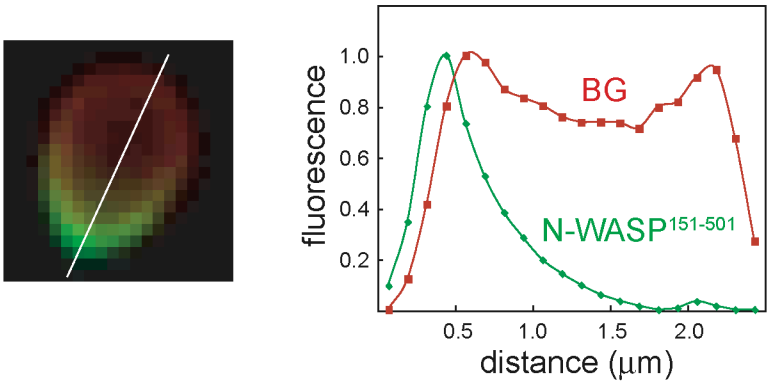
fluorescence
1.0
0.8
0.6
0.4
0.2
BG
N-WASP151-501
0.5
1.0
1.5
2.0
distance (μm)

**Fig. 2.1 N-WASP localizes to the polarization zone of moving vesicles.**
(A) The domain structure of N-WASP and derived fragments. Abbreviations: EVH1, Enabled-VASP homology domain 1; B, polybasic region; G, GTPase-binding domain; PRD, proline-rich domain; W, WASP homology domain 2; CA, central and acidic domain. Internally deleted domains were replaced with a $(Gly\text{-}Ser)_4$ linker.
(B) Alexa488 $N\text{-}WASP^{151\text{-}501}$ and rhodamine-BG (each at 50 nM) were added to phorbol ester-stimulated Xenopus egg extracts, and rocketing vesicles were imaged every 40 s by phase contrast and fluorescence microscopy.
(C) Magnified inset from (B). Linescan analysis was performed to quantify the localization of fluorescent N-WASP constructs along the moving vesicle surface.

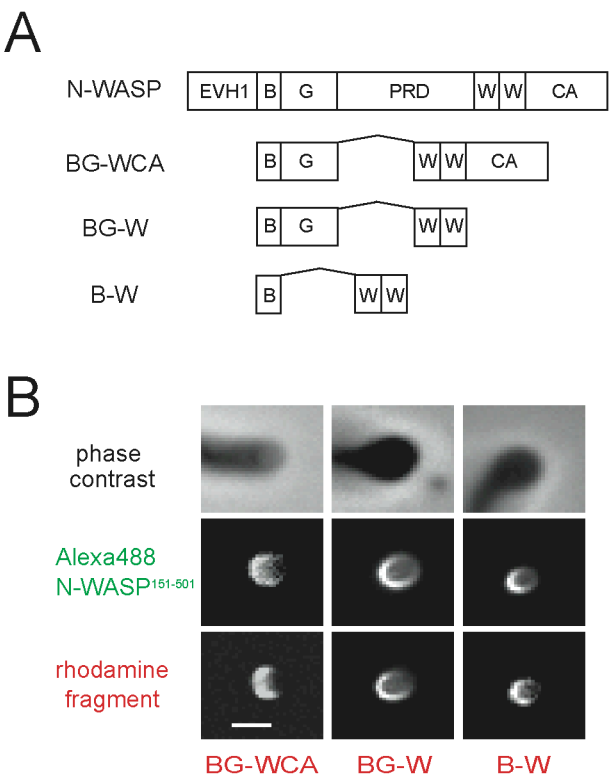


**Fig 2.2 N-WASP WH2 domains are sufficient to localize to the polarization zone of moving vesicles.**

(A) Domain structure of N-WASP fragments used in (B). Abbreviations: EVH1, Enabled-VASP homology domain 1; B, polybasic region; G, GTPase-binding domain; PRD, proline-rich domain; W, WASP homology domain 2; CA, central and acidic domain. Internally deleted domains were replaced with a $(Gly\text{-}Ser)_4$ linker. (B) Alexa488 N-WASP$^{151\text{-}501}$ and the indicated rhodamine-labeled fragments (final concentration, 50 nM) were imaged as in (Fig 2.1). Images are representative of >50 rocketing vesicles for each rhodamine-labeled fragment. Bar = 2 μm.

central and acidic domains, perfectly colocalized with N-WASP$^{151-501}$ to the membrane-actin interface (Fig. 2.2 B). Further deletion of the carboxy-terminal $WH2_b$ domain from this fragment abolished its asymmetric distribution, despite efficient recruitment to the membrane (Fig. 2.4 B, n>100). Thus, one or both WH2 domains are required for localization of N-WASP fragments to the membrane-actin interface. In addition, localization to the membrane-actin interface does not absolutely require an interaction between N-WASP and the Arp2/3 complex.

The presence of WH2 domains is sufficient to localize N-WASP to the membrane-actin interface. A minimal fragment comprising only the polybasic motif and the WH2 domains (B-$W_aW_b$) localized to the polarization zone (Fig. 2.3 A, B). This was visualized using time-lapse video microscopy of extracts containing Alexa488-actin, in which rhodamine-labeled B-$W_aW_b$ fragments precisely colocalized to the point of contact between the actin network and the surface of moving vesicles (Fig.2.3 A, B). In several examples, small actin networks appeared to nucleate peripherally to the main comet tail and were subsequently swept into the main comet tail. In these cases, fluorescent B-W is also swept into the membrane-actin interface (Fig.2.3 B). By contrast, fragments containing only the polybasic motif or the tandem WH2 domains did not localize asymmetrically to either moving or stationary vesicles (data not shown). Thus, our deletion analysis (summarized in Table I) revealed that asymmetric localization of WH2-containing N-WASP fragments cannot be explained by

interactions with the Arp2/3 complex, Cdc42, WASP interacting protein (WIP), or SH3 domains (e.g., the adaptor protein, Nck). Rather, the polarization determinant appears to be within the WH2 domains, suggesting a novel function for these domains, independent of its role in promoting actin nucleation by the Arp2/3 complex.

Localization of N-WASP to the membrane-actin interface was specific to the C-terminal WH2 domain ($W_b$). The $W_a$ domain was not sufficient to cause polarization of the BG domain (Fig. 2.4). Unlike other members of the WASP/Scar family of NPFs, N-WASP is the only member with more than one WH2 domain, the reasons for which is unclear. In another NPF, Spire, recent data suggests that its tandem WH2 domains position actin monomers in a pseudo-filament-like organization for polymerization (Quinlan et al., 2005). While this specific mechanism may not be similar to that used by N-WASP WH2 domains, this result implies that WH2 domains may have additional roles aside from coordinating actin monomers for polymerization by the Arp2/3 complex (Kelly et al., 2006).

| Construct | | | Membrane Recruitment | Polarization |
|---|---|---|---|---|
| N-WASP | | | + | + |
| N-WASP$^{124-501}$ | | | + | + |
| N-WASP$^{136-501}$ | | | + | + |
| N-WASP$^{151-501}$ | | | + | + |
| N-WASP$^{151-501}$ | Δ 403-418 | | + | + |
| N-WASP$^{151-501}$ | Δ 432-446 | | + | - |
| BG | 178-274 | | + | - |
| BG | 178-244 | | + | - |
| G | 196-274 | | - | - |
| G-WCA | 196-274-$(SG)_4$-392-501 | 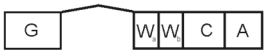 | - | - |
| BG-W*CA | 178-274-$(SG)_4$-392-501 | 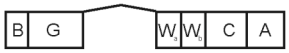 | + | + |
| BG-W*C | 178-274-$(SG)_4$-392-481 | 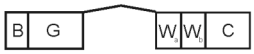 | + | + |
| BG-W* | 178-274-$(SG)_4$-392-446 | 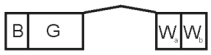 | + | + |
| BG-$W_a$ | 178-274-$(SG)_4$-392-427 | | - | + |
| BG-$W_a$ | 178-274-$(SG)_4$-419-446 | | + | + |
| B-W*CA | 178-204-$(SG)_4$-392-501 | | + | + |
| W*CA | 178-204-$(SG)_4$-392-501 | | - | + |
| B-W* | 178-204-$(SG)_4$-392-446 | | + | + |
| B-$W_a$ | 178-204-$(SG)_4$-392-427 | 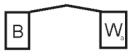 | + | - |
| B-$W_b$ | 178-204-$(SG)_4$-419-446 | | ND* | ND |

**Table 1 Deletion analysis of N-WASP constructs**

N-WASP constructs and their corresponding amino acids are listed. These proteins were expressed in *E. coli*, purified, fluorescently labeled and examined for their abilities to be recruited to (membrane recruitment) and localized to the membrane-actin interface (polarized localization) in PMA-stimulated Xenopus HSS. $(SG)_4$ is a serine-glycine linker. W* represents $W_aW_b$. ND = not done. ND* = B-$W_b$ could not be tested because the protein precipitated upon fluorescent labeling.

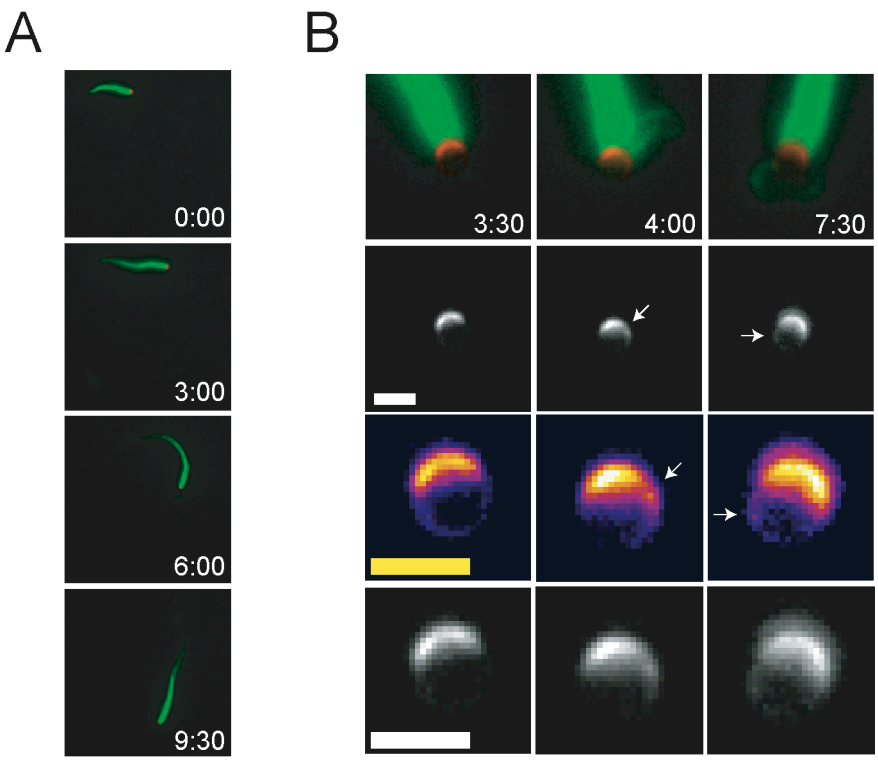


**Fig. 2.3 Localization of B-W on the surface of moving vesicles.**
Rhodamine B-W (50 nM) localizes to the polarization zone of a moving vesicle in phorbol ester-stimulated Xenopus egg cytosol containing Alexa488 actin. Fluorescence images were acquired every 30 s. (A) Time-lapse images of Rhod B-W on a moving vesicle. (B) Magnified insets of a moving vesicle highlighting the localization of rhod B-W to the membrane-actin interface. Scale bar = 2 μm.

**Point mutations in the $WH2_b$ domain uncouple its asymmetric localization and nucleation functions.**

To assess the functional relevance of polarized localization in membrane movement, we searched for WH2 domain point mutations that would selectively abolish the localization function without affecting Arp2/3-promoted actin nucleation. N-WASP has two WH2 domains whose functions are at least partially redundant (Yamaguchi et al., 2000). To address this issue, we deleted the amino-terminal WH2 domain ($W_a$), which was neither necessary nor sufficient for localization to the membrane-actin interface (Fig. 2.5). The resulting construct ($\Delta W_a$ N-WASP$^{151-501}$) had slightly diminished Arp2/3-stimulatory activity in a pyrene actin polymerization assay (Fig. 2.5) but was indistinguishable from N-WASP$^{151-501}$ in its ability to restore vesicle motility to extracts immunodepleted of endogenous N-WASP (data not shown). One difficulty in identifying a mutant with wild type polymerization activity stems from the likelihood that the functions at the membrane, including nucleation and tethering may involve similar interactions with the barbed ends of actin monomers and/or filaments. Mutations that inactivate one function were thus likely to inactivate the other. Indeed, many of the WH2 mutants that we tested were severely defective in pyrene actin nucleation assays, making it impossible to interpret their effects on vesicle motility (Table 2).

We obtained two $WH2_b$ mutants, R438A and K444Q, whose Arp2/3-dependent actin nucleation activities were identical to that of $\Delta W_a$ N-WASP$^{151-501}$ (hereafter referred to as "WT N-WASP") over a range of concentrations. (Fig. 2.7) Interestingly, both mutants displayed lower binding affinities for actin monomers (Fig.; $K_D$ for WT = 0.9 μM; R438A ≥ 30 μM; K444Q = 10 μM). Binding of actin to a $W_bCA$ fragment containing the R438A mutation was barely detectable in a fluorescence anisotropy assay, yet it was at least as effective as WT WCA at stimulating Arp2/3-dependent actin nucleation (data not shown).

A

$W_b$ ALLDQIRQGIQLKSV
$W_a$ ALLDQIREGAQLKKV

B

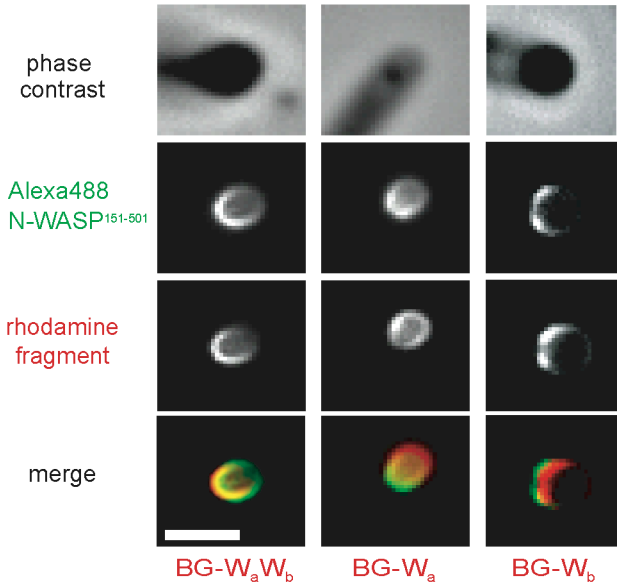


**Fig. 2.4 $W_a$ is not sufficient to localize N-WASP to the membrane-actin interface.**

(A) Amino acid sequence of $W_a$ and $W_b$

(B) $W_b$ is sufficient to localize to the membrane-actin interface, whereas $W_a$ is not. Alexa488 WT N-WASP and either rhodamine BG-$W_aW_b$, BG-$W_a$ or BG-$W_b$ (final concentrations, 50 nM) were added to phorbol ester-stimulated Xenopus egg extracts and rocketing vesicles imaged as in Fig. 2.1. BG-$W_a$ is symmetrically localized and partially excluded from the polarization zone (representative of >50 rocketing vesicles). Bar = 2 μm.

A

N-WASP151-501
B
G
PRD
W
W
CA
N-WASP151-501 ΔWa
B
G
PRD
W
CA

B

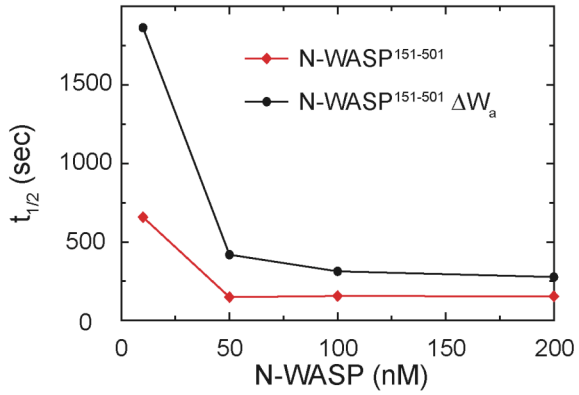
N-WASP151-501
N-WASP151-501 ΔWa
t1/2 (sec)
1500
1000
500
0
0
50
100
150
200
N-WASP (nM)

C

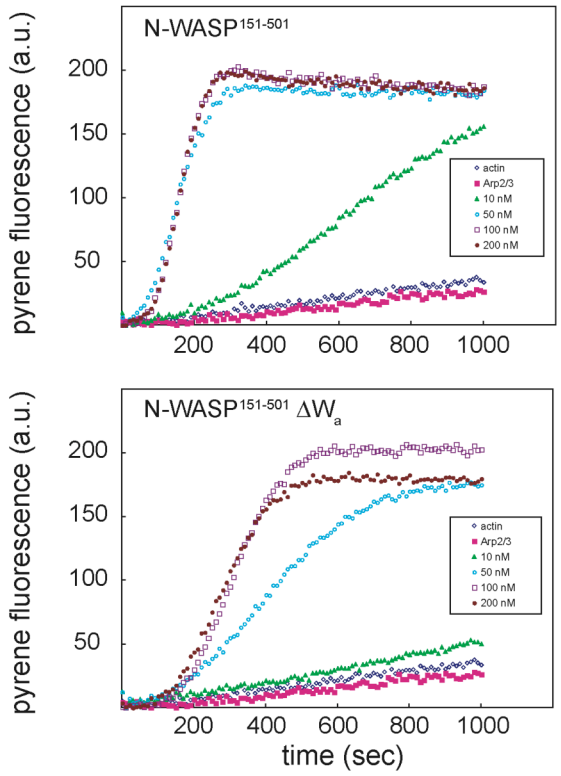
N-WASP151-501
pyrene fluorescence (a.u.)
200
150
100
50
actin
Arp2/3
10 nM
50 nM
100 nM
200 nM
200
400
600
800
1000
N-WASP151-501 ΔWa
pyrene fluorescence (a.u.)
200
150
100
50
actin
Arp2/3
10 nM
50 nM
100 nM
200 nM
200
400
600
800
1000
time (sec)

**Fig. 2.5 Deletion of $W_a$ from N-WASP$^{151-501}$ yields "WT N-WASP".**
(A) The domain structures of N-WASP$^{151-501}$ and ΔWa N-WASP$^{151-501}$. (B) Pyrene actin polymerization kinetics comparing N-WASP$^{151-501}$ and ΔWa N-WASP$^{151-501}$. Graph is the time to half maximal polymerization ($t_{1/2}$) using various N-WASP concentrations. (C) Pyrene actin polymerization curves used to create graph in (B); various concentrations of N-WASP were activated by 6 μM Cdc42/GTPγS (nonprenylated, expressed in *E. coli*), 20 nM Arp2/3 complex and 2.5 μM actin (5 % pyrene-labeled).

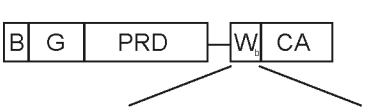


| | | Polarized | Actin Polymerization |
|---|---|---|---|
| WT $W_b$ | ALLDQIRQGIQLKSV | + | ++ |
| WT $W_a$ | ALLDQIREGAQLKKV | - | ++ |
| | AEEDQIRQGIQLKSV | - | - |
| | ALLDAIRAGIALKSV | + | ND |
| | ALLDQERQGIQLKSV | - | - |
| R438A | ALLDQIAQGIQLKSV | - | ++ |
| $W_b \rightarrow W_a$ | ALLDQIREGAQLKKV | - | +/- |
| | ALLDQIRQPIQLKSV | + | ND |
| | ALLDQIRQGEELKSV | - | - |
| | ALLDQIRQGIQAKSA | + | - |
| | ALLDQIAQGIQLQSV | - | - |
| K444Q | ALLDQIRQGIQLQSV | - | ++ |
| | ALLDQIRQGIQLDDV | - | + |

**Table 2 Mutagenesis of WT N-WASP**

Point mutations in WT N-WASP were created by site-directed mutagenesis. Highlighted in red are the amino acids mutated in each construct. Also shown are the results of the characterization of these mutants in the membrane-actin localization assay (polarized or not) and the pyrene actin polymerization assay as performed in Fig. 2.5 C. ND = not done.

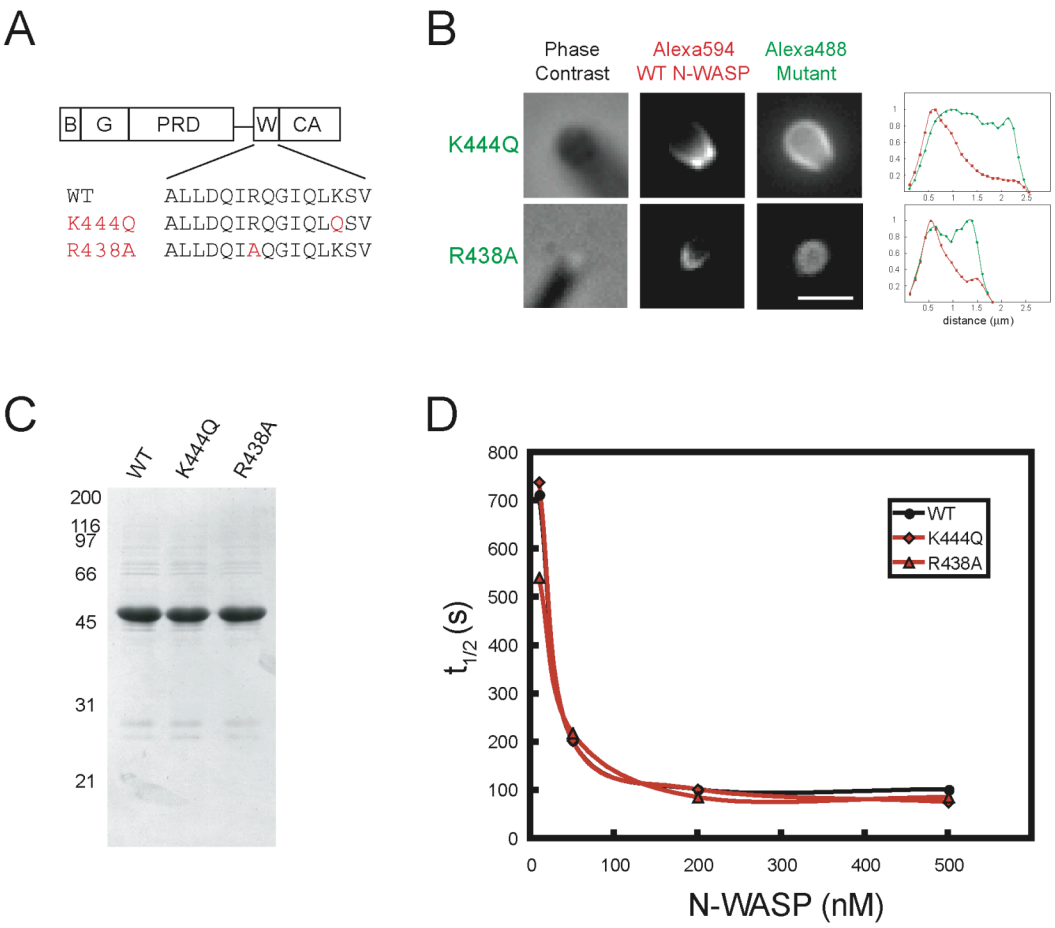


**Fig. 2.6 Polarization defective N-WASP mutants.**

(A) Amino acid sequence of the WH2 domain of N-WASP$^{151-501}$ $\Delta W_a$, WT N-WASP, highlighting the K444Q and R438A mutations.

(B) Alexa594 WT N-WASP and either Alexa488 K444Q or Alexa488 R438A N-WASP (final concentrations, 50 nM) were added to phorbol ester-stimulated Xenopus egg extracts and rocketing vesicles imaged as in Fig. 2.1. Line-scan analysis indicates asymmetric localization of WT N-WASP (red lines), whereas K444Q and R438A N-WASP (green lines) are symmetrically localized or partially excluded from the polarization zone (representative of >50 rocketing vesicles). Bar = 2 μm.

(C) SDS-PAGE of purified N WASP proteins stained with Coomassie blue.

(D) Pyrene actin polymerization kinetics were measured with increasing concentrations of WT, K444Q, and R438A N-WASP in the presence of saturating Cdc42/GTPgS (6 μM), 2.5 μM actin monomers (5% pyrene labeled), and 20 nM Arp2/3 complex. Plots indicate the time to half-maximal polymerization ($t_{1/2}$) as a function of N-WASP concentration.

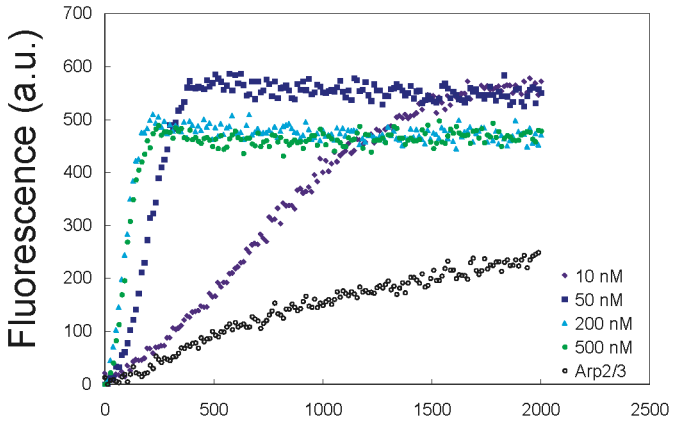


WT

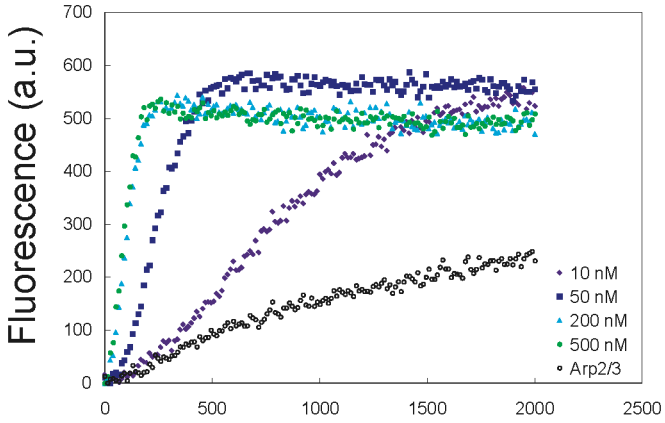


K444Q

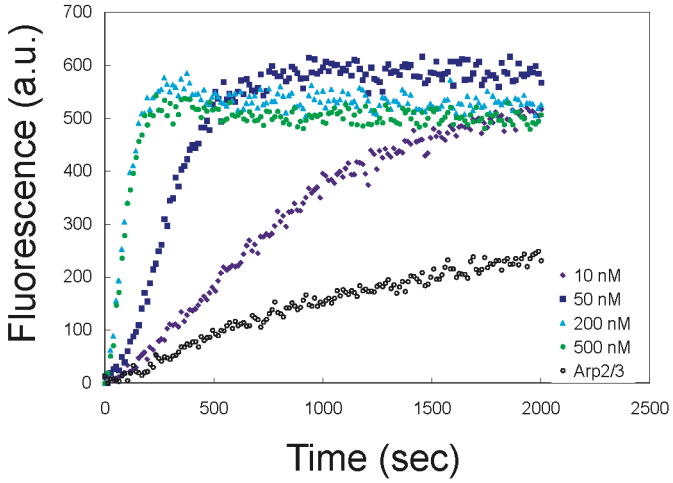


R438A

**Fig. 2.7 Pyrene actin polymerization assays comparing WT, R438A, and K444Q $\Delta W_a$ N-WASP$^{151-501}$ constructs.**

Polymerization kinetics were measured with a SpectraMax Gemini XS fluorescent plate reader (Molecular Devices, excitation: 365 nm, emission: 407 nm) as previously described (Dueber et al., 2003). Polymerization reactions contained 2.5 μM purified rabbit skeletal muscle actin (5% pyrene labeled), 20 nM bovine Arp2/3 complex, and 6 μM GTPγS-bound Cdc42 (nonprenylated, expressed in *E. coli*).

Competition experiments with unlabeled WT and mutant $W_b$CA constructs displayed qualitative similarities for actin monomer binding. Interestingly, the competition curves of both mutants did not plateau to the same anisotropy level as WT $W_b$CA competition (Fig. 2.8 C). One possible explanation for this result is that there are two possible binding surfaces for actin monomers on the $W_b$CA construct and that these mutations disrupt only one binding surface. Despite the significant decrease in actin binding affinity, both WH2 mutants had nucleation activity comparable to WT N-WASP. Thus, high affinity actin binding by the WH2 domain is not required for potent nucleation promoting activity, as noted in previous studies of WASP WH2 mutants (Marchand et al., 2001).

Remarkably, neither R438A nor K444Q N-WASP (labeled with Alexa488) localized to the membrane-actin interface of rocketing endosomes when added to Xenopus egg extracts containing unlabeled endogenous N-WASP (Fig. 2.6). By contrast, rhodamine-labeled WT N-WASP, imaged simultaneously on the same vesicles, localized to the membrane-actin interface in every case (Fig. 2.6, n=100). Thus, mutation of either one of two conserved residues in the $WH2_b$ domain prevents co-localization with WT N-WASP to the point of contact between the actin network and the membrane. These results suggest that mutations in the WH2 domain may cause specific defects in membrane-actin attachment.

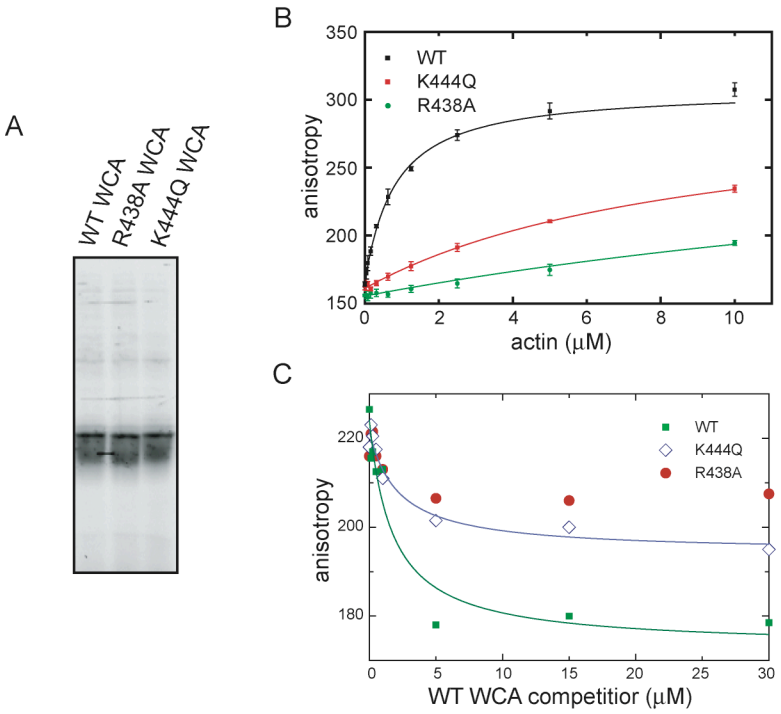


**Fig. 2.8 Actin monomer binding to N-WASP $W_bCA$ constructs.**

(A) Scanned gel of Oregon Green-labeled N-WASP (WT, K444Q, and R438A $W_bCA$ fragments) separated by SDS PAGE and imaged using Typhoon gel imaging station.

(B) Fluorescence anisotropy of Oregon Green-labeled N-WASP (100 nM of WT, K444Q, and R438A $W_bCA$ fragments) was measured in the presence of increasing actin monomer concentrations. Data shown are mean ± S.D., performed in quadruplicate. Curves represent the best fit of data to a quadratic binding equation, providing equilibrium dissociation constants ($K_d$) as follows: WT = 0.9 μM, K444Q = 10 μM, and R438A ≥ 30 μM.

(C) Unlabeled $W_bCA$ peptides were used in the competition experiment. OregonGreen488-WT $W_bCA$ was pre-bound to actin at 0.6 μM and unlabeled $W_bCA$ constructs were added to compete off bound labeled WT $W_bCA$ peptide.

To determine the functional relevance of the WH2 domain mutations, we asked whether R438A or K444Q N-WASP (N-WASP is N-WASP$^{151-501}$) could support motility of Xenopus vesicles or synthetic PIP2 liposomes in N-WASP-immunodepleted extracts (Fig. 2.12). Unlike recombinant WT N-WASP, both point mutants were unable to fully rescue vesicle motility (Fig. 2.9). There were far fewer actin comet tails in extracts containing either the R438A or K444Q mutant as the only source of N-WASP. Most comet tails were small and seemed to be jagged and frayed (Fig. 2.9 A). Time-lapse imaging revealed a significant number of tails that did not grow at either end and apparently were not attached to a vesicle. We note that in rescue experiments using fluorescently labeled R438A or K444Q N-WASP, asymmetric localization to the membrane-actin interface was observed only in rare cases in which the vesicles were actually moving (data not shown). These results suggest that the R438A and K444Q mutations strongly impair, but do not eliminate interactions between the membrane and the actin network.

**N-WASP clustering on the membrane.**

Imaging of N-WASP on moving vesicles demonstrated that N-WASP is tightly associated with a component of the membrane-actin interface (Fig. 2.3). To better assess the dynamics of WT and mutant N-WASP on moving membranes, we needed an imaging method that would allow us to detect slow movements of fluorescent molecules. Fluorescent speckle microsopy images result from stochastic variations in the number of fluorescent molecules within

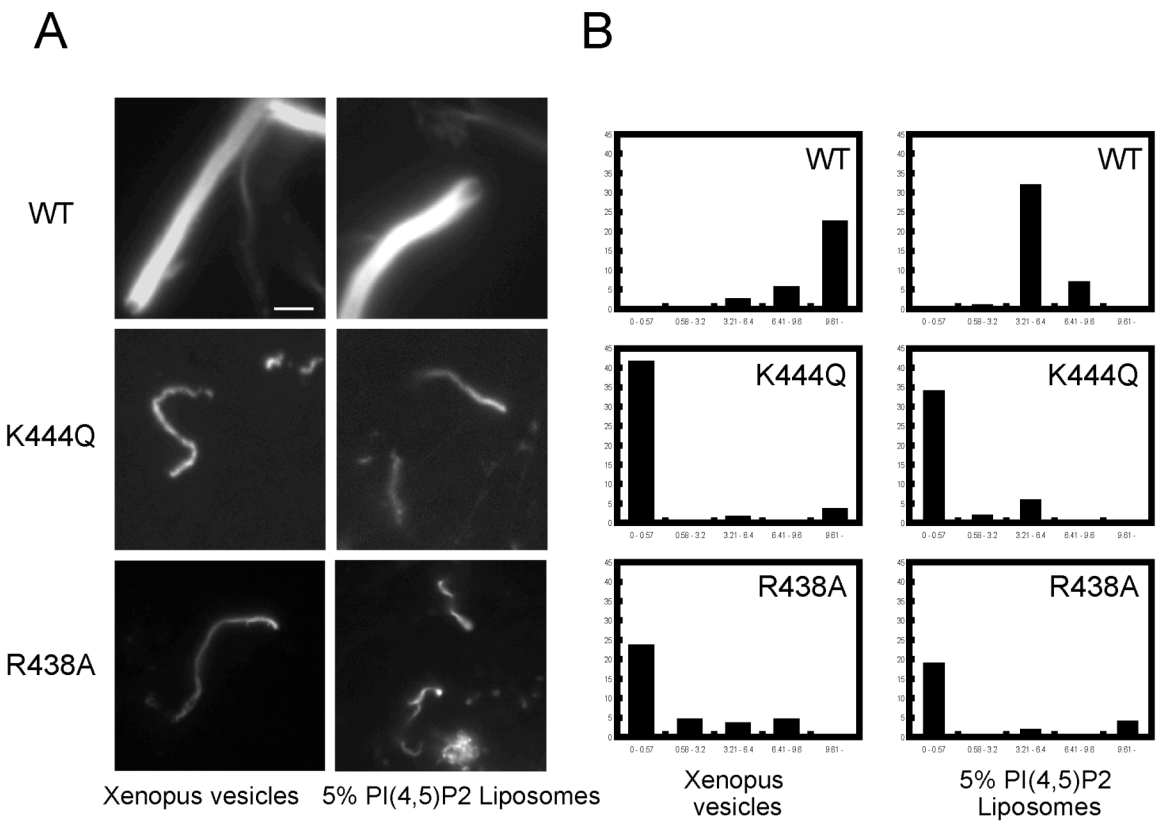


**Fig. 2.9 Polarization mutants are defective in vesicle motility.**

(A) Representative images of rocketing vesicles formed by WT, K444Q and R438A N-WASP (250 nM) in N-WASP-depleted HSS and using either Xenopus vesicles or PIP2 liposomes. Scale bar = 2 μm. (B) The majority of comet tails formed by K444Q and R438A are not motile. Quantitation of speeds of rocketing vesicles in (A). Graphs are the number of rocketing vesicles at a given speed. Speeds (μm/m) are binned accordingly: 0-0.57, 0.58-3.2, 3.21-6.4, 6.41-9.6, 9.61 and greater, in μm/min.

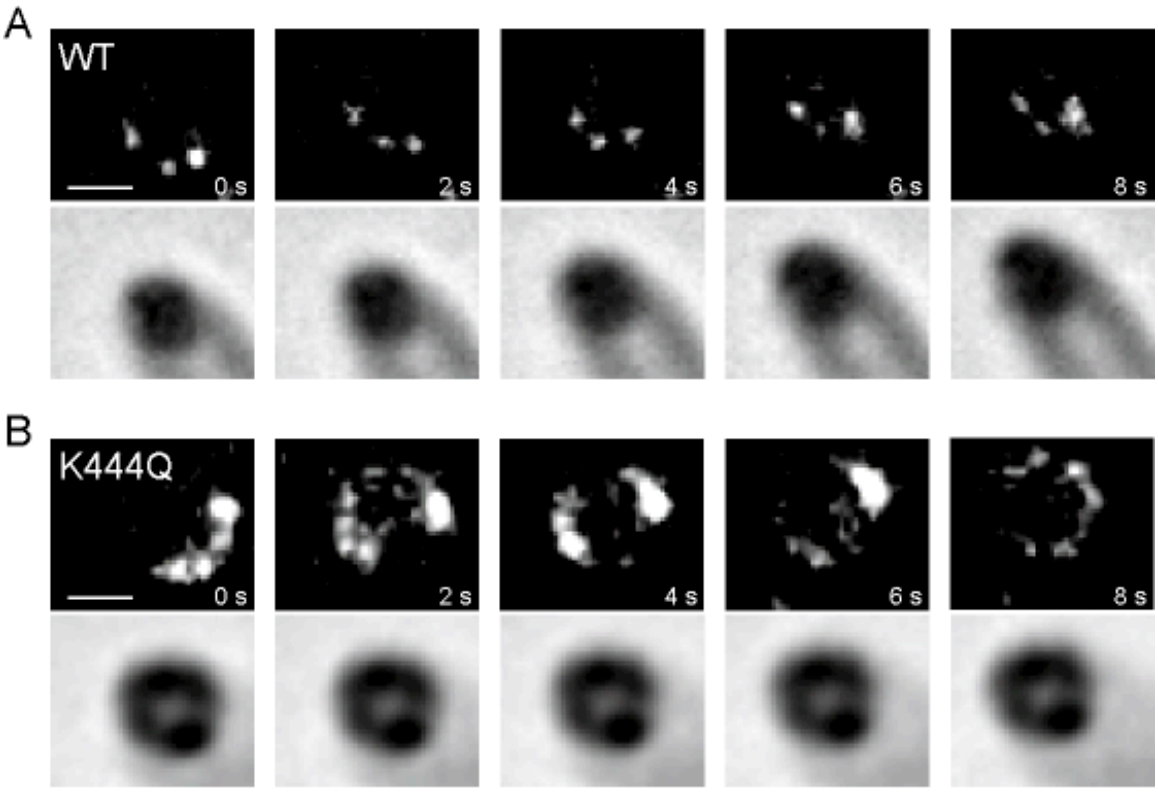


**Fig. 2.10 Speckle microscopy of WT and K444Q N-WASP on moving vesicles.**

Timelapse fluorescence and phase contrast images were acquired at 2 frames/s. (A) Alexa488 WT and (B) Alexa488 K444Q N-WASP (~170 pM WT and ~130 pM K444Q; fluorescence images taken with 750 ms FITC exposure) on moving vesicles in phorbol ester-stimulated extracts. Scale bars = 2 μm.

minimal regions resolvable by light microscopy. Speckles serve as fiduciary marks allowing measurement of movement and turnover of molecules that are anchored to cytoskeletal polymers (Kapoor and Mitchison, 2001; Waterman-Storer et al., 1998). We used time-lapse microscopy at 2 frames/s to visualize motility extracts containing very low concentrations of labeled WT and K444Q N-WASP (~170 and 130 pM final concentration respectively). Qualitatively, WT N-WASP clustered into discrete foci that were relatively static during vesicle movement. Conversely, K444Q N-WASP speckles appeared be more dynamic on the membrane and did not seem to form stable clusters. We cannot distinguish between K444Q N-WASP diffusion on the membrane and exchange of molecules from the cytoplasm. Nevertheless, these results support a WH2 domain-dependent interaction with a component of the membrane-actin interface to promote clustering of N-WASP molecules.

**Mutations in the WH2 domain that abolish localization to the membrane-actin interface do not affect N-WASP oligomerization.**

Initially, we hypothesized that one mechanism that may regulate the polarized localization of N-WASP on the membrane was its ability to self-organize on the membrane surface. We used chemical crosslinking to assess the ability of N-WASP to homo-oligomerize on membranes. First, WT and K444Q N-WASP were incubated with synthetic PIP2 liposomes and activated Cdc42. Next, a cysteine reactive bis-maleimide crosslinker was added to the reaction for 30 min at RT and the reaction was run out on an SDS PAGE

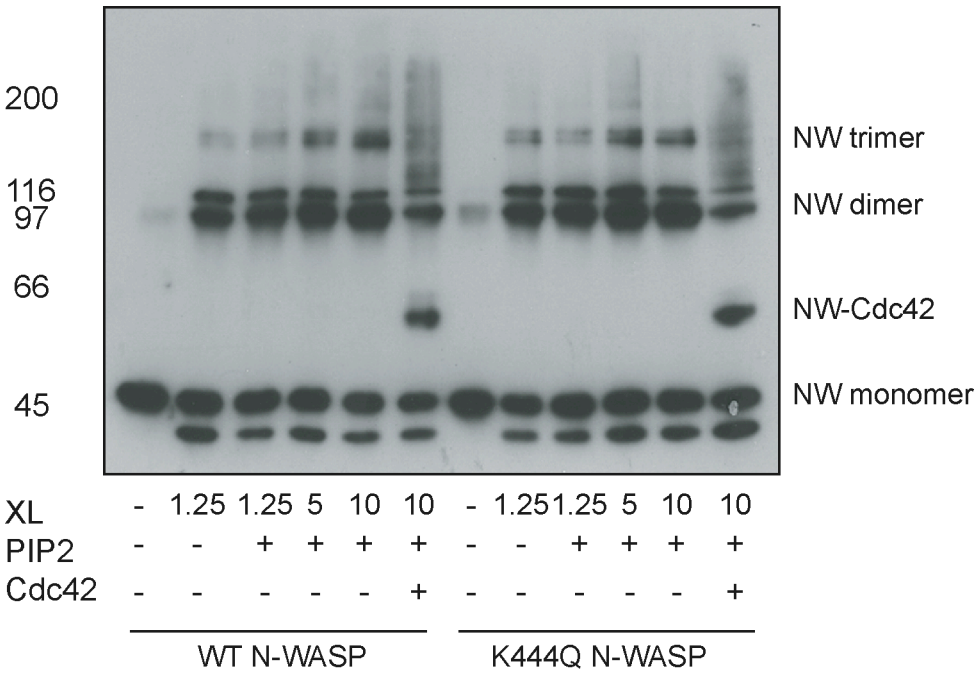


**Fig. 2.11 X-linking to detect N-WASP oligomerization.**

WT or K444Q N-WASP were tested in their ability to oligomerize in the presence of PIP2 liposomes and activated Cdc42. N-WASP (250 nM) was incubated in the presence of PIP2 liposomes (12.5 μM, 5% PIP2) and 2.5 μM activated Cdc42. Bis-maleimide cross-linker (XL) was added at different concentrations (1.25, 5, and 10 μM) in cross-linking buffer (10 mM Hepes pH 7.5, 100 mM NaCl) and incubated at RT for 30 min. The reaction was stopped by adding sample buffer, boiled, separated by SDS PAGE and processed for western analysis. 12CA5 anti-HA was used at 1:1000 to detect HA-tagged N-WASP constructs. Indicated on the right of the gel are bands representing monomeric N-WASP, N-WASP dimers, trimers and N-WASP-Cdc42 cross-linked complexes.

denaturing gel. Oligomerization was assessed by the presence of higher order bands using the 12CA5 antibody against HA tagged N-WASP constructs. There are two cysteines in these constructs: one in the Cdc42-binding region and one between the two WH2 domains. If there is a correlation between asymmetric localization and oligomerization, then WT N-WASP, which polarizes, and K444Q, which does not, should exhibit different abilities to self-associate in the presence of membranes and activated Cdc42. However, the crosslinking patterns between WT and K444Q N-WASP were indistinguishable in the absence or presence of PIP2 liposomes. Crosslinking allowed us to detect the interaction between N-WASP and Cdc42 as a new band at approximately 75 KDa. Thus, we can conclude that the mutations in the WH2 domain that abrogate polarized localization do not eliminate N-WASP oligomerization. Further, we can preliminarily rule out N-WASP self-association as a primary mechanism to explain its polarized localization on moving membranes. Nevertheless, the crosslinking data are consistent with (but don't prove) N-WASP oligomerization on the membrane. Further work is needed to test whether a direct N-WASP/N-WASP contact or whether N-WASP clusters within PIP2 microdomains.

In summary, mutation in either one of two conserved amino acids in the WH2 domain interferes with the ability of N-WASP to localize to the polarization zone (in the presence of WT N-WASP) and severely inhibits vesicle motility in Xenopus egg extracts lacking endogenous N-WASP. R438A and K444Q N-WASP are equivalent to WT N-WASP in Arp2/3-dependent actin nucleation

assays, despite a striking decrease in actin binding affinity. These data provide evidence for a critical new role for the WH2 domain in actin-powered vesicle motility beyond its previously established role in delivering actin monomers to the Arp2/3 complex (Kelly et al., 2006).

## Discussion

In this study, we used live fluorescent imaging to characterize the dynamics of N-WASP on the membrane and to show that the WH2 domain is required. Mutations in the WH2 domain that inactivate this function, but that do not affect actin polymerization, cause defects in N-WASP's ability to propel robust vesicle motility. Collectively, these results point to a new role for the WH2 domain in formation and/or maintenance of polarized actin networks on membrane surfaces. We propose that the molecular interactions responsible for concentrating N-WASP molecules in a WH2-dependent manner at the membrane-actin interface are also responsible for physically attaching comet tails to the membrane. However, the Xenopus extract system did not allow us to test this possibility (see Chapter 3).

### Organization of N-WASP molecules at the membrane-actin interface.

Clustering of N-WASP molecules may serve various roles in membrane motility: (1) increasing the activity of N-WASP as proposed by Papayanopolus and colleagues (2005), (2) restricting new actin assembly to an N-WASP enriched surface, yielding signal amplification, (3) creating a high local

concentration of barbed ends that may be important for increased actin network branching or recruitment of factors that may assist in actin assembly.

Clustering can be a powerful mechanism to restrict the activation of a protein to the membrane surface. Regulation of protein activity at the membrane surface has been relatively unexplored. There are few well-characterized examples of this type of regulation. The kinesin motor Unc104p translocates cargo vesicles along microtubule tracks (Klopfenstein et al., 2002). Unc104p is a monomeric PIP2 binding motor protein in solution. However, experimentally increasing PIP2 density on these cargo vesicles increases Unc104p activity in a cooperative manner suggesting that Unc104p clustering on the membrane surface is required for maximal and efficient motor activity. Likewise, N-WASP is extremely sensitive to PIP2 density (Papayannopoulos et al., 2005). Upon membrane association, N-WASP may organize through PIP2 clustering, weak oligomerization or interactions with actin filaments directly. Our crosslinking results (Fig. 2.11) are consistent with actin-independent, PIP2-dependent clustering.

The interaction between N-WASP and the F-actin network may be another mechanism that explains clustering of N-WASP molecules. Carlier and colleagues (1999) demonstrated that N-WASP may interact with F-actin directly. In their model, a basic region N-terminal to the PIP2 binding region is critical for F-actin interactions (Egile et al., 1999). Interestingly, the addition of these N-

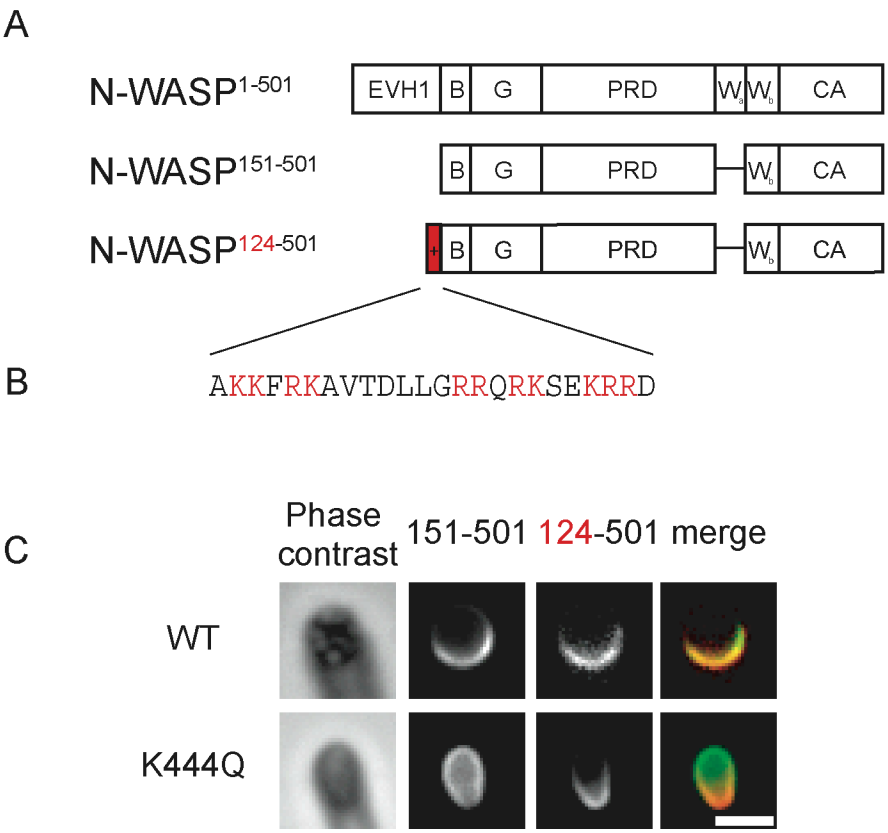


**Fig. 2.12 A basic stretch of amino acids N-terminal of the PIP2 binding region is another polarization domain**

(A) The domain structures of full length N-WASP$^{1-501}$, WT N-WASP$^{151-501}$, and an extended N-WASP$^{124-501}$. Highlighted in red are the extended regions.

(B) Amino acid sequence of the extended basic region (aa124-148). Highlighted in red are the basic amino acids in this region.

(C) Extending K444Q N-WASP$^{124-501}$ to contain this basic region rescues its ability to localize to the membrane-actin interface. Alexa488 WT N-WASP$^{151-501}$ and Alexa594 WT N-WASP$^{124-501}$ were imaged on moving vesicles in phorbol ester stimulated extracts as in Fig. 2.1 B. Likewise, Alexa488 K444Q N-WASP$^{151-501}$ and Alexa594 K444Q N-WASP$^{124-501}$ were imaged on moving vesicles. Scale bar = 2 μm.

terminal basic motifs rescued the ability of K444Q to localize to the membrane-actin interface of moving vesicles (Fig. 2.12). However, in preliminary experiments, this construct was not able to fully rescue the vesicle motility defects in N-WASP-depleted extracts (data not shown). Interestingly, the most N-terminal part of this extended basic region may be part of the EVH1 domain (Volkman et al., 2002). Also, this region may be required by N-WASP to activate the IcsA protein from *Shigella flexneri* in Arp2/3-dependent actin nucleation (unpublished data, John Dueber). The study of this new polarization motif may yield additional insights into the interactions between the N-WASP and the actin network. It seems plausible that this region, rather than interacting directly with F-actin, constitutes a second PIP2 binding motif (albeit one with very low affinity).

**A new function for the WH2 domain.**

Recently, the structure of the WH2 domain bound to an actin monomer was solved (Chereau et al., 2005). The mutations in this domain that specifically abrogate polarized N-WASP localization map to two different regions of the WH2 motif. Arginine 438 is located along an amphipatic alpha helix that cups the barbed end of the actin monomer. Lysine 444 resides in an unstructured extended region of the verprolin domain following the core helix. Carlier and colleagues speculate that the positive charges of this extended region may form salt bridges with a negatively charged patch on the actin surface (Hertzog et al., 2004). However, because this region is unstructured in both the crystal and NMR structures, it is probably very flexible. It is possible that the WH2 domain

interacts weakly with polarization elements on the membrane. However, these interactions may be amplified when localized and restricted to the two-dimensional area of the membrane surface. Interestingly, while there is no experimental evidence demonstrating that WH2 domains can interact directly with actin filaments in the absence of actin monomers (see Chapter 3), Arginine 438 may disrupt the WH2 domain's ability to interact with both the barbed end of actin monomers and the barbed end of actin filaments.

Localization of N-WASP to the membrane-actin interface does not require interactions with the Arp2/3 complex. We initially hypothesized that the molecular interactions responsible for concentrating N-WASP molecules at the membrane-actin interface may also be responsible for physically attaching comet tails to the membrane. Therefore, we assumed that identification of a polarization domain within N-WASP would allow us to elucidate the molecular mechanism of this adhesion, and potentially provide insight into the mechanism by which a polarized actin structure is established and maintained on a symmetrical fluid membrane bilayer. It is commonly assumed that the interaction between the N-WASP CA domain and the actin filament bound-Arp2/3 complex was the source of the adhesion between the membrane surface and the growing actin network (Mogilner and Oster, 2003). However, there is no experimental evidence to support this assumption. The ability of N-WASP to localize to the membrane-actin interface independent of the CA domain but requiring the WH2 domain suggests a novel role for this domain in mediating membrane-actin adhesion.

At the initial stages of signal activation by PKC, N-WASP molecules are recruited by activated Cdc42 and stimulate Arp2/3-dependent nucleation. In our observations, the newly formed actin network can further recruit more N-WASP molecules from solution in a Cdc42-independent manner (B-$W_aW_b$ localization, Fig. 2.3) directly to sites of actin assembly. This model has two implications: first, directed recruitment prevents actin assembly at other sites of the membrane; second, it reinforces actin assembly and maintains a polarized actin network.

## Materials and Methods

### Protein expression, purification and fluorescent labeling.

N-WASP fragments were amplified by PCR from full length N-WASP and mini-N-WASP (BG-$W_aW_b$CA) and subcloned into plasmids pBH4 (Prehoda et al., 2000) or pVC54. A single influenza hemagglutinin (HA) tag was cloned into pBH4 following the $His_6$ tag to make pVC54. Subsequent PCR products were cloned into this HA tagged vector (pVC54). All constructs were verified by sequencing.

### N-WASP$^{151-501}$ expression and purification from *E. coli.*

A 50 ml culture of transformed BL-21 cells was grown to OD 0.6-1.0 at 37°C in LB + Amp/Chlor. BL21 cultures were kept in log phase (OD 0.2-1.0) at 37°C. N-WASP is induced at RT by IPTG (0.5 mM). The cultures are brought to

RT quickly by submerging flasks in an ice/water bath. Proteins are induced for 4-6 h at RT. Following induction, the cells are centrifuged at 3000xg, the supernatant discarded and the cell pellets resuspended in lysis buffer (20 mM Hepes pH 7.5, 200 mM NaCl, protease inhibitors) and flash frozen in liquid nitrogen. These cell slurries can be stored at -80°C for long-term storage. After thawing, PMSF and a leupeptin/pepstatin/chymostatin protease inhibitor cocktail are added to the cell lysates. Cells are lysed by sonication in an ice/water bath using 15 pulses at 50% power 3 times spaced by 1 min incubations on ice. The cell lysate was clarified by centrifugation at 12,000 rpm for 20 min at 4°C. The cell lysate was combined with Ni-NTA agarose and allowed to rotate at 4°C for 2-5 h. $His_6$-N-WASP was eluted with 1ml fractions of elution buffer (20 mM Hepes pH 7.5, 200 mM NaCl, 250 mM imidazole). The peak fractions are pooled and the $His_6$ tag was removed by incubation in TEV protease for 3 h at RT in TEV cleavage buffer (20 mM Hepes pH7.5, 200 mM NaCl, 1 mM DTT). N-WASP constructs were further purified using a heparin column (1 ml heparin HiTRAP from Amersham/Pharmacia) with a 0-1M NaCl gradient. Following chromatography, the peak fractions were pooled and dialyzed overnight in N-WASP storage buffer (20 mM Hepes pH7.5, 200 mM NaCl, 0.5 mM DTT).

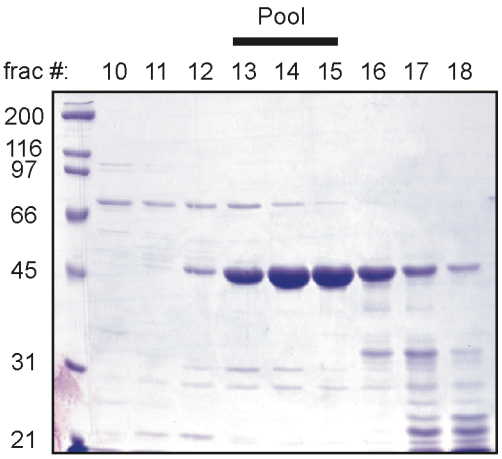


**Fig. 2.13 N-WASP$^{151-501}$ purification**

SDS-PAGE gel of the eluted fractions from the purification of N-WASP$^{151-501}$ using a heparin HiTRAP column (Invitrogen) (stained with Coomassie Blue).

Actin was purified from rabbit skeletal muscle (Pardee and Spudich, 1982). Actin was labeled on cysteine with pyrene iodoacetamide (Cooper et al., 1983), and for imaging experiments, on lysine with Alexa488-NHS or rhodamine-NHS (Molecular Probes) (Isambert et al., 1995). Arp2/3 complex was purified from bovine brain (Egile et al., 1999).

For fluorescent labeling of recombinant N-WASP fragments (containing one or two natural cysteines, Cys236 and/or Cys427), maleimide dyes (Molecular Probes) were added at a 20-fold molar excess and incubated either for 2 h at RT or overnight at 4°C. Labeling reactions were quenched by the addition of 5 mM β-mercaptoethanol for 15 min. Fluorescent proteins were subsequently purified over HiTRAP S, Q, or heparin columns. For fluorescence anisotropy assays,

Oregon Green-labeled WCA proteins were purified from free dye by S200 gel filtration chromatography. Labeling efficiency in all cases was 20-50%.

**Charging soluble bacterial Cdc42 with GTPγS.**

Cdc42 (100 μM) was dialyzed in 20 mM Hepes pH 7.5, 50 mM NaCl, 5 mM EDTA, 1 mM DTT for 1 h at RT. Cdc42 was charged with GTPγS (1 mM) at 30°C for 15 m. The reaction was quenched by the addition of $MgCl_2$ (10 mM). Unbound nucleotide was removed by dialysis in 20 mM Hepes pH 7.5, 50 mM NaCl, 2 mM $MgCl_2$, 1 mM DTT.

**Pyrene actin polymerization assays**.

Polymerization kinetics were measured using 2.5 μM purified rabbit skeletal muscle actin (5% pyrene labeled) and 20 nM bovine Arp2/3 complex, as described (Dueber et al., 2003). GTPγS-bound Cdc42 (nonprenylated, expressed in E. coli) was used at 6 μM to activate N-WASP constructs.

**Actin monomer binding assays.**

Fluorescence anisotropy was measured using an ANALYST AD fluorescence plate reader. WT and mutant Oregon Green-labeled $W_bCA$ (100 nM) were equilibrated with increasing concentrations of actin monomers for 30 min in G-buffer (5 mM Tris pH 8, 0.2 mM ATP, 0.2 mM DTT, 0.2 mM $CaCl_2$,

0.02% $NaN_3$). Anisotropy data were fit to a quadratic binding equation to determine the $K_d$.

**Polarization zone localization assays.**

Vesicle motility reactions were performed using Xenopus egg cytosol and a partially purified membrane fraction (Taunton et al., 2000). Labeled WT and mutant N-WASP fragments (50 nM) were added and vesicle motility initiated by the addition of phorbol ester (0.5 μg/ml). Under these conditions, rocketing vesicles are abundant (5-10 per microscope field with a 60X objective) and their actin comet tails easily visible with phase contrast optics. Red and green fluorescence and phase contrast images were acquired for ~50 rocketing vesicles 15-60 m after initiating the reaction (Olympus IX70 microscope; Olympus PlanApo 60X Oil PH3 objective lens; MetaVue software; Coolsnap HQ CCD camera), and image analysis was performed using ImageJ.

N-WASP localization assays were quantitated by performing a linescan along the longitudinal section of the vesicle. The relative fluorescence intensity along the linescan was plotted against the length of the linescan (length of vesicle) in Microscoft Excel.

**Vesicle motility assays.**

N-WASP immunodepleted-Xenopus egg cytosol was made by depleting high speed Xenopus supernatant, HSS (pre-spun at 75K prior to use), using anti-N-WASP antibodies and the absence of N-WASP was confirmed by western blot.

Rabbit antisera were raised (Cocalico Biologicals, Inc.) against full length rat N-WASP purified from baculovirus-infected Sf9 cells (Rohatgi et al., 1999), purified over an N-WASP Affigel-10 column (Bio-Rad, Inc.), eluted with 0.2 M glycine (pH 2.0), 0.15 M NaCl and dialyzed against TBS/50% glycerol. N-WASP was immunodepleted from HSS (200 μl) by treating with 2 μg affinity purifed antibodies for 1 h followed by 15 μl Protein A-conjugated agarose for 2 h, all at 4°C.

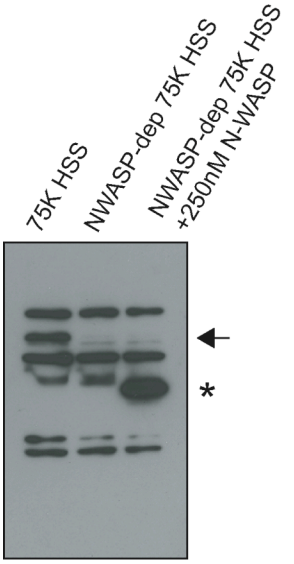


**Fig. 2.14 N-WASP-depleted high speed supernatant (HSS).**

Xenopus HSS was clarified at 75K for 15 min at 4°C. Endogenous N-WASP was immunodepleted with a rabbit anti-N-WASP antibody. N-WASP-depleted HSS was rescued with N-WASP $^{151-501}$ (250 nM). Supernatants were separated with SDS PAGE and N-WASP was probed using a rabbit anti-N-WASP antibody (1:1000). The arrow indicates endogenous N-WASP and the asterick indicates recombinant N-WASP $^{151-501}$. The other bands are nonspecific.

Vesicle motility was stimulated by the addition of phorbol ester (PMA) to a final concentration of 0.5 μg/ml. Actin was visualized by the addition of either Alexa488-actin or tetramethyl-5'-rhodamine actin to vesicle motility reactions. Reactions were incubated at RT for 15 min and examined under 60X magnification (Olympus IX70 microscope; Olympus PlanApo 60X Oil PH3 objective lens). Data were collected using a Photometrics Cool Snap HQ CCD camera.

Quantitation of vesicle motility was as follows: fluorescence or brightfield images were acquired with MetaVue software. Data analysis was performed using ImageJ software. For comet tail speed quantitation, instantaneous comet tail speeds were acquired under brightfield exposure at 10 s intervals for 1-2 min. Mean speeds were calculated from the acquired instantaneous speeds.

# Chapter 3

## Reconstitution of Cdc42/GDI-activated actin assembly on synthetic PIP2 lipid bilayers with pure proteins reveals a new mechanism for membrane-actin adhesion and a new mechanism of symmetry breaking.

**Abstract**

The movement and deformation of membranes in the cell are initiated by signaling cascades that localize from the cytosol to the membrane, leading to the formation and maintenance of force-generating, polarized actin structures. To dissect the mechanisms of signal-dependent actin assembly on membrane surfaces, we reconstituted a physiological signaling pathway on synthetic PIP2 lipid bilayers with pure proteins. We address two fundamental issues in cell biology: (1) How a polymerizing actin network maintains adherence to the membrane, (2) the mechanism of symmetry breaking on fluid membrane surfaces. This novel biomimetic system introduces a new mechanism of membrane-actin adhesion; a new mechanism of symmetry breaking, one that more physiologically mimics polarized actin assembly in the cell; and a new pure protein system to study signal transduction-dependent actin assembly on fluid membranes *in vitro*.

## Introduction

Actin assembly at the membrane surface is the final product of a complex signaling cascade that involves interactions between lipids and cytosolic proteins (Ho et al., 2004; Hussain et al., 2001; Rohatgi et al., 1999). Cytosolic signaling molecules required for actin polymerization are not constituitively active at the membrane; instead, they are soluble, inactive protein complexes such as the Cdc42/GDI complex, the WIP-N-WASP complex and the Arp2/3 complex that must be recruited to and activated at the membrane surface (Ho et al., 2004; Hoffman et al., 2000).

A major advance toward our understanding of the mechanistic details of actin assembly came with the reconstitution of this process on the surface of plastic beads in cell-free extracts (Cameron et al., 1999). These experiments showed that the Arp2/3 complex could be activated at the bead surface by constituitively active NPFs. Also, these experiments allowed for examination of the structure of the actin networks assembled *in vitro* relative to structures formed *in vivo* (Cameron et al., 2001). Further, four proteins, actin, capping protein, the Arp2/3 complex, and NPF were sufficient to reconstruct the movement of plastic beads by actin-based motility (Loisel et al., 1999). Previous work showed that the formation of a polarized actin comet tail occurred by a

mechanism of symmetry breaking. Specifically, a spherical actin shell formed around the entire bead which eventually ruptured, yielding an actin comet tail on one side of the bead (van der Gucht et al., 2005). Experiments with pure proteins also demonstrated that the comet tail was tightly associated with the bead surface (Marcy et al., 2004).

In spite of its advantages, the bead motility system fails to lend insight into the spatial regulation of NPFs and the Arp2/3 complex at the surface. In this system, beads are coated with NPFs nonspecifically, covalently attached to the surface, resulting in a heterogeneous mixture of molecules in various unfolded states. NPFs are not free to diffuse on the surface or to be regulated by cellular inputs. It has been shown that activators like PIP2 do not regulate bead-bound NPFs (Wiesner et al., 2003); instead, these important proteins are kept constituitively active. Thus, a system which allows for regulation of these proteins in their native state is necessary.

Experiments using N-WASP-coated beads suggest that the density of NPFs at the bead surface is a key component of force production: decreasing the NPF surface concentration by only two-fold induces a transition from salutatory to continuous motion of rocketing beads (Bernheim-Groswasser et al., 2002). This key observation demonstrates that the local concentration of proteins at the membrane-actin interface may be highly regulated and that this regulation plays an important role in the establishment and maintenance of polarized actin

networks. These experiments made it possible to systematically dissect the molecular mechanisms involved in actin assembly, but left out a critical component, the lipid bilayer. Therefore, the contribution of a fluid membrane surface remains unknown.

Characterization of actin assembly at a fluid membrane surface may offer new insights into our understanding of how actin assembly occurs in cells. NPFs are dynamic proteins whose activity must be regulated and who must interact with both membrane proteins and lipids in the plasma membrane (Papayannopoulos et al., 2005). NPFs localize to the membrane-actin interface: are they required for the physical attachment between the membrane and actin network? Does actin assembly on a membrane "break symmetry" by the same mechanism as on the surface of plastic beads? These are standing questions that can only be answered by the reconstitution of actin assembly on a membrane surface.

## Results

### Activation of the Cdc42/RhoGDI complex.

In cells, native Cdc42 is inactive in solution because it is bound to its inhibitor RhoGDI (Hoffman et al., 2000). Cdc42 is modified at its C-terminus by a geranylgeranyl moiety which allows it to either be bound to its inhibitor or be inserted into the membrane. The exchange of Cdc42 between these two states

marks a critical step in its activation. The other critical step in Cdc42 activation is the exchange of GDP for GTP by the guanine nucleotide exchange factors (GEFs) (Erickson and Cerione, 2004). While other systems use constituitively active and soluble Cdc42, our system allows for the physiological activation pathway.

Cdc42 activation at the membrane recruits N-WASP. Thus, we used the localization of fluorescent N-WASP to lipid-coated beads as our readout for Cdc42 activation. It has been demonstrated the GEF, intersectin, can activate Cdc42 in cells and in vitro (Hussain et al., 2001; Zamanian and Kelly, 2003). Therefore, we used intersectin in the activation of Cdc42 *in vitro*. In the presence of intersectin, GTPγS and PIP2, N-WASP was recruited to lipid-coated glass beads (Fig. 3.1). Omission of any of these components prevented N-WASP recruitment to the membrane. Therefore, we concluded that Cdc42 could be released from GDI and could be activated at the membrane by intersectin *in vitro*.

**Reconstitution of actin-based motility on lipid-coated glass beads.**

A breakthrough in the study of actin-based motility came with the reconstitution of actin assembly on polystyrene beads using pure proteins. This study showed that force generation by actin assembly could be driven by four pure proteins and also that myosin motor proteins were unnecessary for this movement (Loisel et al., 1999). We extend this system by introducing two

important variables: a completely soluble signal transduction pathway and a synthetic membrane motility substrate.

Because many (if not all) actin-dependent processes necessitate the presence of a membrane, we transformed this system to include a fluid lipid bilayer instead of polystyrene beads. Moreover, in cells, Cdc42 and N-WASP activation occurs at the membrane, where they can diffuse in two dimensions. By contrast, N-WASP immobilized to plastic beads as used in previous motility systems cannot diffuse. Experiments have shown that lipids can be supported on the surface of glass beads yielding a fluid membrane bilayer (Baksh et al., 2004). We used this system to assemble membrane-tethered actin comet tails so that we could study the mechanism of signal-dependent actin assembly, membrane-actin adhesion, and symmetry breaking in a more physiological context.

Following Cdc42/N-WASP activation with the active intersectin GEF (DH-PH domains) and GTP$\gamma$S, lipid-coated beads were added to a motility mix containing actin, the Arp2/3 complex, capping protein, and profilin. Cofilin, which is unnecessary for actin-based movement, was omitted in the motility medium to prevent the disassembly of actin comet tails. Polarized tails formed on 100% of the beads within 5 min, resulting in propulsive motility at 0.58 $\pm$ 0.20 $\mu$m/min, similar to previously published velocities with N-WASP-coated polystyrene beads (Fig. 3.2 B, Fig. 3.4 B) (Wiesner et al., 2003).

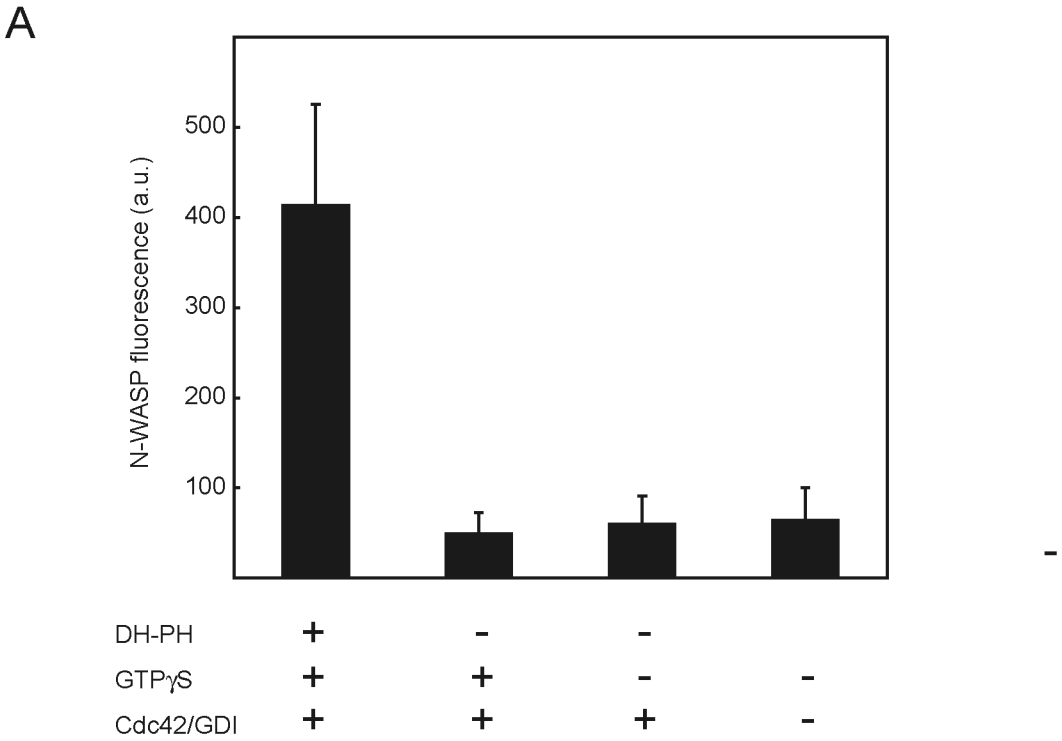
A
N-WASP fluorescence (a.u.)
500
400
300
200
100
DH-PH + - - -
GTPγS + + - -
Cdc42/GDI + + + -
B
Alexa594
N-WASP
Phase
Contrast

**Fig. 3.1 N-WASP translocation to lipid bilayer-coated glass beads is promoted by intersectin DH-PH, Cdc42/RhoGDI complex, and GTPγS.**
(A) Lipid bilayer-coated glass beads (1.6 μm diameter, Duke Scientific Corporation) were incubated for 30 minwith Alexa594 WT N-WASP (1 μM) and the indicated combinations of intersectin DH-PH (1 μM), GTPγS (50 μM), or the Cdc42/RhoGDI complex (1 μM) in 20 mM Hepes pH 7.5, 100 mM NaCl, 1 mM $MgCl_2$, 1 mM DTT, 2 mg/ml BSA. A circle (2.5 μm diameter) was drawn around the beads and the total integrated fluorescence, minus the background fluorescence, was calculated. Shown are fluorescence intensities (mean ± SD, n = 10 beads for each condition). (B) Representative fluorescence and phase contrast images of lipid-coated beads from (A). Bar = 2 μm.

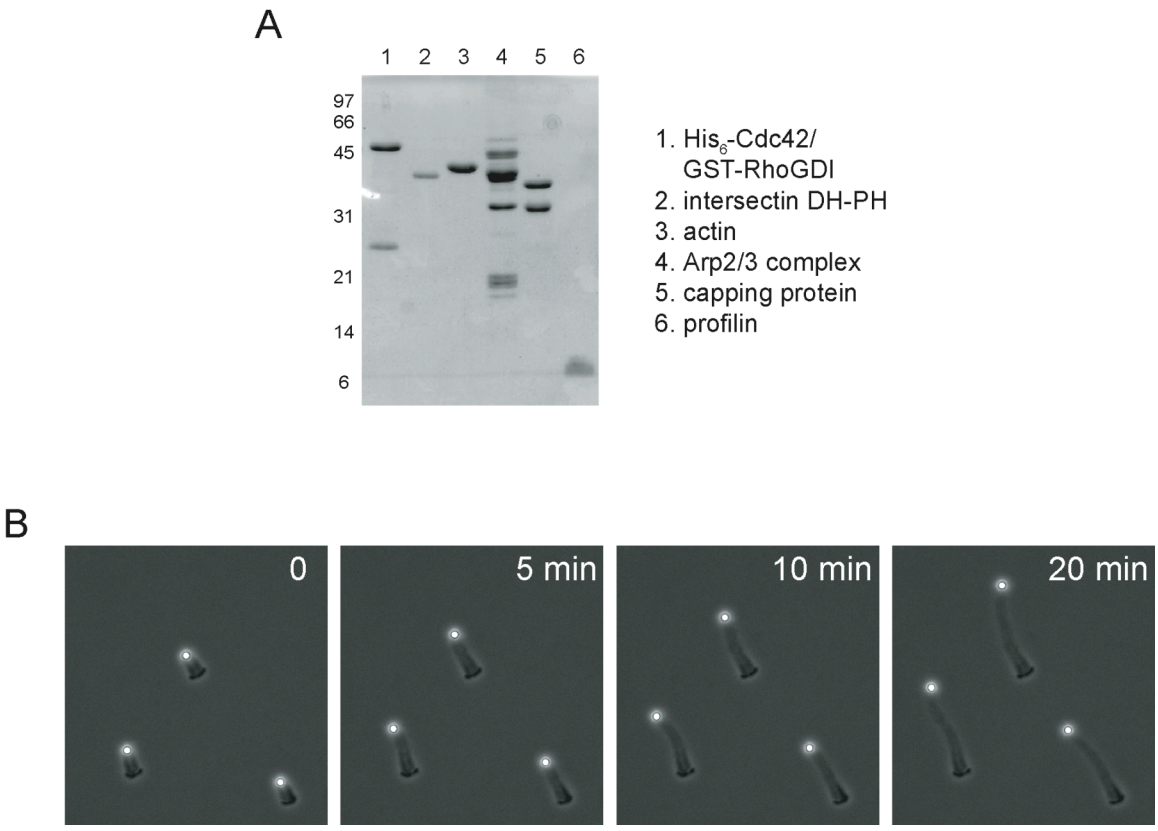


**Fig. 3.2 Reconstitution of membrane movement from pure components.**
(A) SDS-PAGE of purified proteins (stained with Coomassie blue) used to reconstitute motility of lipid bilayer-coated glass beads.
(B) Motility reactions were initiated by adding motility mix (actin, Arp2/3 complex, capping protein, and profilin) to lipid-coated beads that had been pre-activated with intersectin DH-PH, Cdc42/RhoGDI complex, GTPγS, and WT N-WASP, as described in the Materials and Methods.

**Symmetry breaking on lipid-coated glass beads.**

Reconstitution of PIP2/Cdc42-dependent-lipid bead motility allowed us to observe the formation of an asymmetric actin network at a membrane surface with pure proteins. In one experimental scenario, Cdc42 and N-WASP were recruited and activated to the lipid-bead surface prior to incubation with the motility medium (Fig. 3.3 A i, B). We observed that a symmetrical actin gel formed around the lipid-coated bead and ruptured at a specific point to form a single actin comet tail. This mechanism of symmetry breaking is similar to those observed with plastic beads (van der Gucht et al., 2005). In a second scenario, Cdc42 and N-WASP were mixed concurrently with the motility medium and lipid-coated beads were introduced into this mixture (Fig.3.3 A ii, C). In this case, we did not observe formation of a symmetrical actin shell. Interestingly, small bursts of actin assembly at the membrane occured at different regions of the surface. This observation is similar to the formation of actin comet tails in living prick-activated Xenopus eggs (Fig. 1D, (Taunton et al., 2000)). Ultimately, one main polarized comet tail became dominant and drove bead motility. Surprisingly, there was no symmetry breaking event. Nonetheless, spontaneous formation of a polarized network occurred apparently by a mechanism involving amplification of asymmetry. These experiments emphasize the unique properties of our system and allowed us to dissect a new mechanism of actin network formation.

**Characterization of polarization defective N-WASP mutants in a reconstituted medium.**

We initially hypothesized that the same interactions that regulated N-WASP localization to the membrane-actin interface are also responsible for tethering the actin network to the surface. Indeed, the polarization mutants (K444Q and R438A N-WASP) were defective in promoting robust vesicle motility (Fig. 2.9). Unfortunately, the Xenopus extract system had many experimental limitations. First, it was difficult to synchronize the formation of moving vesicles. Second, vesicles were hard to image due to size variability. Lastly, actin depolymerization factors rapidly disassembled actin comet tails as they formed, decreasing the probability of observing detachment events.

With the development of this novel lipid motility system, we could solve these issues and more carefully dissect the mechanisms of actin network formation and attachment on moving membranes utilizing our polarization mutants (K444Q and R438A in the WH2 domain). The formation of lipid-coated bead comet tails occurred relatively synchronously. All beads were uniform in size. And most importantly, we could vary the concentration of any protein or parameter or omit any protein from the motility medium (such as preventing actin depolymerization by omitting cofilin).

At early time points (5 min after mixing), there were no obvious differences between motility reactions containing WT, R438A, or K444Q N-WASP (Fig. 3.4 A). In fact, bead velocities with R438A and K444Q N-WASP were slightly faster

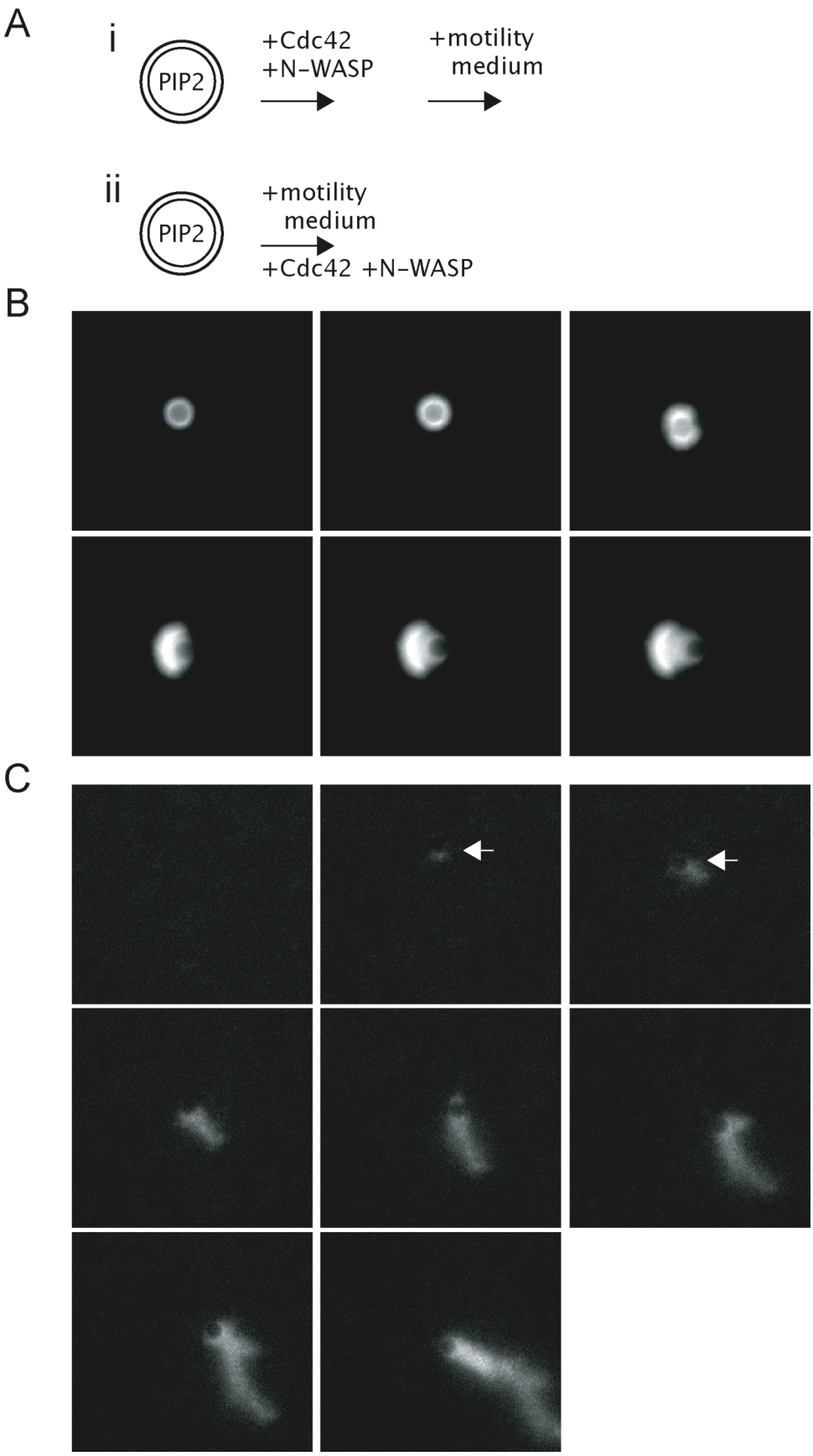
A
i
PIP2
+Cdc42
+N-WASP
+motility
medium
ii
PIP2
+motility
medium
+Cdc42 +N-WASP
B
C

**Fig. 3.3 Symmetry breaking or amplification of asymmetry, depending on the conditions.**

(A) Two experimental designs for comet tail formation delineating the order of addition of the signaling molecules N-WASP and Cdc42/GDI to PIP2 containing lipid-coated beads and standard motility medium. (i) N-WASP and Cdc42 are pre-activated prior to addition to motility medium containing Alexa488 actin. (ii) N-WASP and Cdc42 are activated in the presence of motility medium. (B) Shell formation and symmetry breaking in experimental design (i). (C) Symmetry breaking in experimental design (ii). Arrow points to the first sign of actin assembly on lipid-coated beads. In this experimental design, the actin network is already polarized. Note: In both experimental scenarios, the final concentration of all proteins is the same.

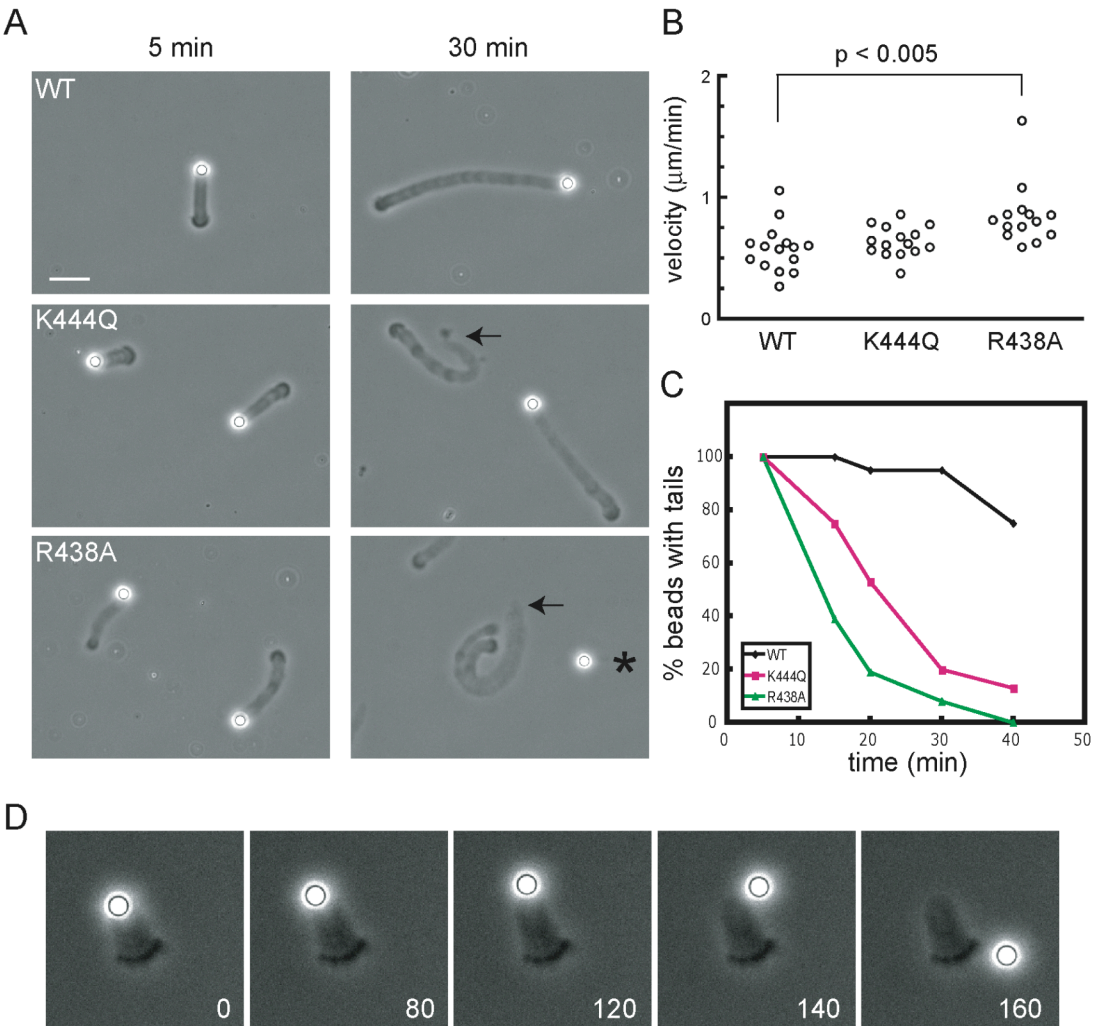


**Fig. 3.4 Catastrophic detachment of actin comet tails by polarization mutants.**

(A) Motility reactions were initiated by adding motility mix (actin, Arp2/3 complex, capping protein, and profilin) to lipid-coated beads that had been pre-activated with intersectin DH-PH, Cdc42/RhoGDI complex, GTPγS, and N-WASP (WT, K444Q, or R438A), as described in the Materials and Methods. Phase contrast images were acquired at the 5 and 30 min time points. Arrows indicate detached actin comet tails, and the asterisk indicates a detached lipid-coated bead. Bar = 10 μm.

(B) Quantification of bead velocities in motility reactions containing WT, K444Q or R438A N-WASP. Each point indicates the speed of a lipid-coated bead imaged 5-20 min after initiating the reactions. Mean speeds ± S.D.: WT = 0.58 ± 0.20, K444Q = 0.64 ± 0.12, and R438A = 0.85 ± 0.26 μm/min. For R438A vs. WT N-WASP, $p < 0.005$ by Student's T-test.
(C) Time course of comet tail detachment. Motility reactions containing WT, K444Q or R438A N-WASP were initiated and, at the indicated time points, aliquots were fixed with 1.5% glutaraldehyde. The percentage of beads with attached tails was quantified by phase contrast microscopy (n = 40 beads per time point).
(D) Time-lapse sequence (elapsed time in seconds) showing catastrophic detachment of a lipid-coated bead from its comet tail in a motility reaction containing R438A N-WASP.

A

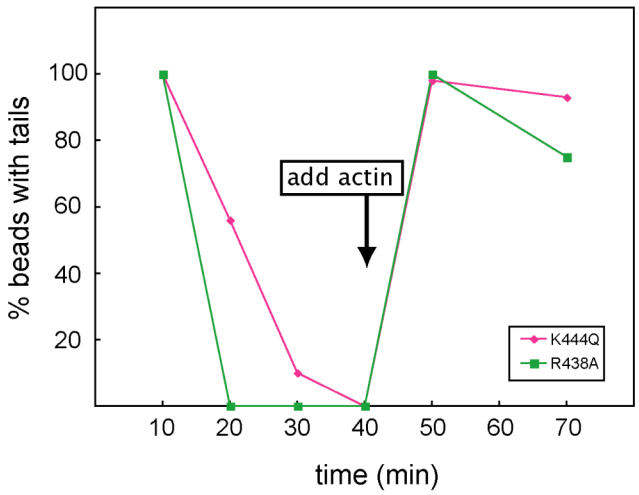
% beads with tails
100
80
60
40
20
add actin
K444Q
R438A
10
20
30
40
50
60
70
time (min)

B

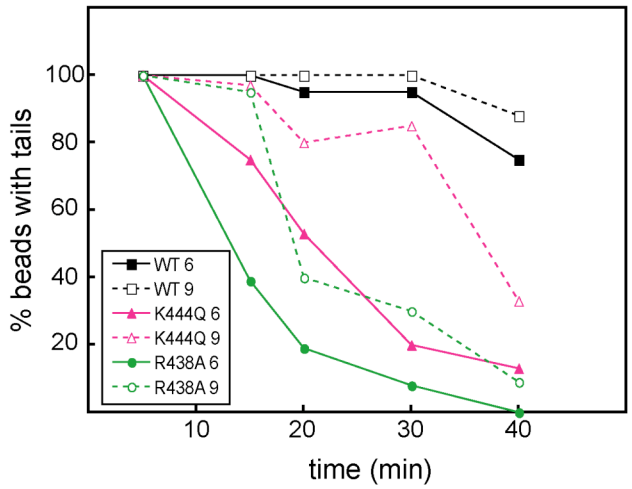
% beads with tails
100
80
60
40
20
WT 6
WT 9
K444Q 6
K444Q 9
R438A 6
R438A 9
10
20
30
40
time (min)

**Fig. 3.5 Comet tail detachment is dependent on actin monomer concentration.**

(A) Addition of fresh actin monomers to late-stage motility reactions resulted in comet tail re-formation on 100% of the lipid-coated beads. Actin monomers (2 μM) were added to motility reactions containing K444Q and R438A N-WASP at t = 40 min (denoted by arrow), after all of the lipid-coated beads had detached from their tails. At the indicated time points, aliquots were fixed with 1.5% glutaraldehyde and the percentage of beads with attached tails determined (n = 40 beads per time point). (B) Comet tail detachment can be delayed by increasing the initial actin monomer concentration, further suggesting that detachment is caused by actin monomer depletion. Motility reactions with WT, K444Q or R438A N-WASP were initiated by adding lipid-coated beads to motility mix containing either 6 or 9 μM actin. At the indicated time points, aliquots were fixed with 1.5% glutaraldehyde and the percentage of beads with attached tails quantified (n = 40 beads per time point).

than with WT N-WASP (R438A = 0.85 ± 0.26 μm/min, K444Q = 0.64 ± 0.12 μm/min, WT = 0.58 ± 0.20 μm/min) (Fig. 3.4 B).

However, within 30 min nearly all of the lipid-coated beads containing R438A or K444Q N-WASP had lost their comet tails, whereas beads containing WT N-WASP were still attached to their tails and continued to move (Fig. 3.4 A). Time-lapse movies revealed catastrophic comet tail detachment from most of the mutant N-WASP beads 10-30 min after initiating motility (Fig. 3.4 A, D). Quantification of fixed motility reactions demonstrated progressive tail detachment over time, with R438A-assembled comet tails detaching more rapidly than K444Q-assembled tails (Fig. 3.4 C). We hypothesized that the progressive loss of comet tails observed with the WH2 mutants is due to a steady decrease in the concentration of actin monomers over time and that comet tail tethering is strictly dependent on actin monomers (Fig. 3.5). Addition of fresh actin monomers to detached R438A and K444Q bead reactions resulted in reformation of actin comet tails, which eventually detached over time (Fig. 3.5 A).

Time course experiments with R438A and K444Q N-WASP provided further support for the dependence of comet tail tethering on the N-WASP WH2 domain, actin monomers, and barbed ends. With both of the WH2 domain mutants, tail detachment was delayed by simply increasing the initial actin monomer concentration from 6 μM to 9 μM (Fig. 3.5 B) or tail detachment was

exacerbated by reducing the initial actin monomer concentration from 6 to 3 μM (date not shown).

**Comet tail tethering is mediated by direct interactions between N-WASP WH2 domains, actin monomers, and the barbed ends of actin filaments.**

The inverse correlation between actin binding affinity (Fig. 2.8) and the rate of comet tail detachment (Fig. 3.4 C) observed with R438A, K444Q, and WT N-WASP suggested that interactions between the WH2 domain, actin monomers, and some part of the dendritic network might play a role in tethering. To address this, we acutely perturbed motility reactions by adding excess capping protein to block barbed ends and Latrunculin B (Lat B) to sequester actin monomers. We found that addition of excess capping protein (FC =1 μM) to motility mix promotes premature comet tail detachment (Fig. 3.6 A,C). Conversely, inhibition of actin polymerization and actin comet tail growth by Lat B (FC = 15 μM) does not promote premature comet tail detachment (Fig. 3.6 B,C).

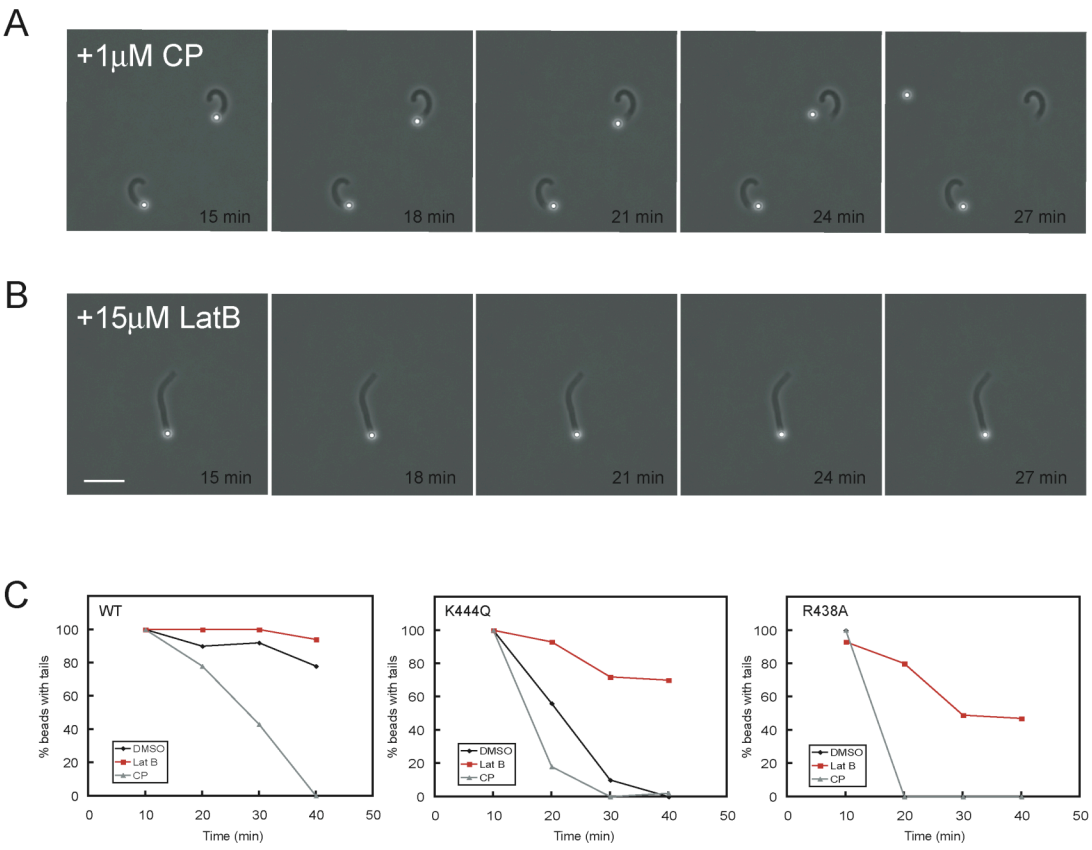


**Fig. 3.6 Perturbations of actin comet tail attachment by CP and Lat B.**
Lipid-coated beads that were pre-activated with Cdc42 and WT N-WASP were added to motility medium to initiate comet tail formation. At 15 min, CP (1 μM) or Lat B (15 μM) were added to the motility reactions.
(A) Time-lapse images of CP-induced detachment of actin comet tails. Phase contrast mages were acquired every 30 s. (B) Time-lapse images of an actin comet tail in the presence of Lat B (15 μM). Lat B does not cause comet tail detachment despite causing immediate cessation of bead motility. Phase contrast mages were acquired every 30 s. (C) CP exacerbates, whereas Lat B slows down the rate of comet detachment. Timecourse experiments of WT, K444Q and R438A comet tail detachment in the presence of DMSO (control), Lat B (15 μM) or CP (1 μM).

Addition of Lat B to pre-assembled comet tails caused a striking decrease in the rate of comet tail detachment with both mutants (Fig. 3.6 C), despite the immediate cessation of bead motility (data not shown). Under our standard motility conditions, 100% of the lipid-coated beads in the R438A N-WASP reaction lost their tails within 10 min, whereas fewer than 20% of the beads did so in the presence of 10 μM Lat B (Fig. 3.6 C). By contrast, addition of high concentrations of capping protein to pre-assembled tails dramatically accelerated tail detachment in motility reactions containing R438A, K444Q, or WT N-WASP (Fig. 3.6 C). We conclude that actin monomers promote, whereas capping protein antagonizes, comet tail tethering via mutually exclusive interactions with the barbed ends of actin filaments.

To confirm the importance of a direct actin monomer-WH2 domain interaction in tethering comet tails to the membrane, we added a cysteine-reactive cross-linker (bis-maleimidohexane, BMH) to motility reactions containing K444Q N-WASP. This protein has two cysteines, one of which (Cys427) is near the WH2 domain. When BMH was added 10 min after initiating the motility reaction, just at the point when K444Q N-WASP comet tails normally start to detach (Fig. 3.4 C), catastrophic tail detachment was completely suppressed; ~100% of the beads remained attached to their tails for at least 30 min (Fig. 3.7 A). Moreover, BMH had no apparent deleterious effects on the motility reaction, as the lipid-coated beads moved at similar velocities after BMH addition (data not shown). To test whether the WH2-proximal Cys427 was essential for BMH-

mediated rescue of K444Q N-WASP, we mutated this cysteine to alanine. The resulting C427A/K444Q mutant was indistinguishable from K444Q N-WASP, with the exception that BMH was unable to prevent progressive tail detachment; unlike the case with K444Q N-WASP, nearly all of the beads with C427A/K444Q N-WASP lost their tails within 20 min of adding BMH (Fig. 3.7 A). Immunoblot analysis of BMH-treated motility reactions demonstrated that actin was the only protein detectably cross-linked to K444Q N-WASP (Fig. 3.7 B). Importantly, cross-linking of actin to C427A/K444Q N-WASP was not observed, which explains the inability of BMH to suppress tail detachment with this mutant. BMH thus prevents catastrophic disruption of the comet tail-membrane interaction by covalent cross-linking of actin monomers to the WH2 domain of K444Q N-WASP. These results further argue that the comet tail detachment phenotype observed with K444Q N-WASP results from its decreased affinity for actin monomers.

These experiments corroborate the correlation between WH2-actin monomer affinity and membrane-actin attachment. Also, these experiments demonstrate that tethering can be uncoupled from actin polymerization as Latrunculin actually enhanced adhesion. Finally, these data suggest that comet tail tethering requires interactions with actin filament barbed ends.

The results suggest that in the presence of Lat B, WH2 domains remain stably associated with membrane-proximal barbed ends, thereby protecting them from high concentrations of capping protein. One plausible idea to explain this

observation is that Latrunculin prevents depletion of ATP-actin at the extreme barbed ends of actin filaments; and that WH2 domains may have higher affinity for the ATP-actin “caps” of actin filaments.

**Membrane-actin adhesion is maintained in the presence of inactive Arp2/3 complex.**

A popular mechanism to explain how the dendritic actin network remains tethered to the membrane surface is through the transient interaction between N-WASP CA domain and the filament-bound Arp2/3 (Mogilner and Oster, 2003). The addition of an actin monomer to the N-WASP-bound Arp2/3 complex results in the nucleation of a new branch and subsequent release of the WCA domain from the Arp2/3 complex. Thus, the N-WASP/Arp2/3/F-actin complex is extremely transient and its disruption by polymerization-competent actin monomers is essentially irreversible. The model of N-WASP release from the branch site is corroborated by fluorescent live imaging (Martin et al., 2006) and by the absence of NPFs from branch sites resolved by electron microscopy (Egile et al., 2005).

The results of our reconstituted motility experiments support the hypothesis that high-affinity actin binding by the WH2 domain plays a critical role in maintaining comet tail attachment (Figure 3.4, 3.7), but they do not rule out a

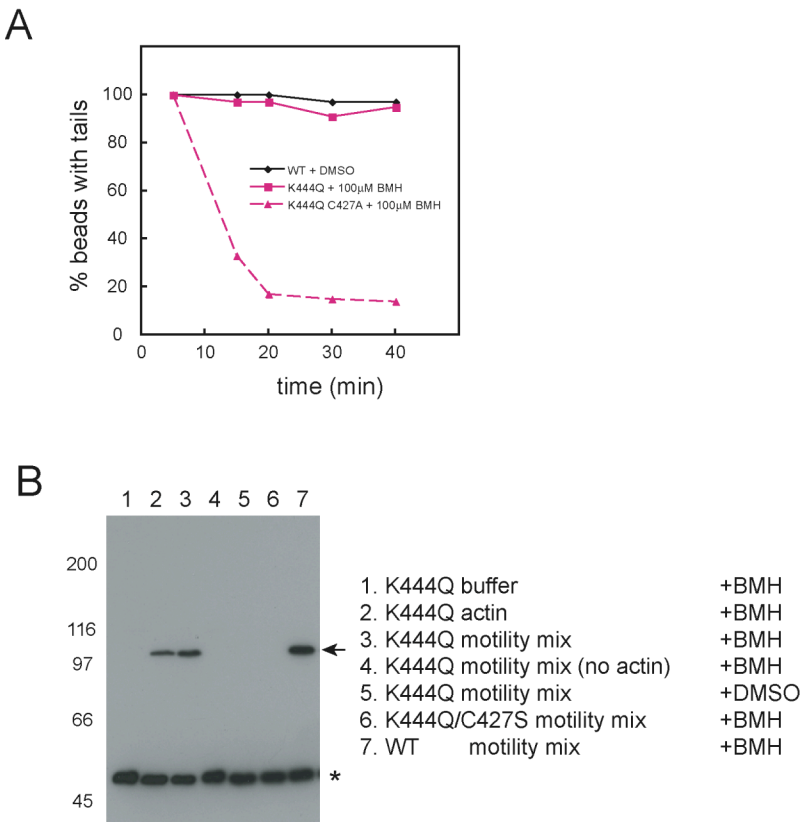


**Fig. 3.7 Cross-linking of actin monomers to the WH2 region suppresses comet tail detachment.**

(A) Cross-linking of actin monomers to Cysteine 427 by BMH (100 μM) prevented catastrophic comet tail detachment. 100 μM BMH or DMSO was added to motility reactions at the 10 min time point. The % of beads with tails was quantified over time. K444Q/C427A N-WASP was resistant to the effects of BMH addition.

(B) BMH addition to motility reactions resulted in the preferential cross-linking of actin monomers to Cys427 of N-WASP. 100 μM BMH or DMSO was added to the indicated reactions. Reactions were analyzed by SDS-PAGE and immunoblotting using an antibody (12CA5) against HA-tagged-N-WASP. The asterick marks the N-WASP monomer and the arrow marks the cross-linked actin monomer-N-WASP heterodimer.

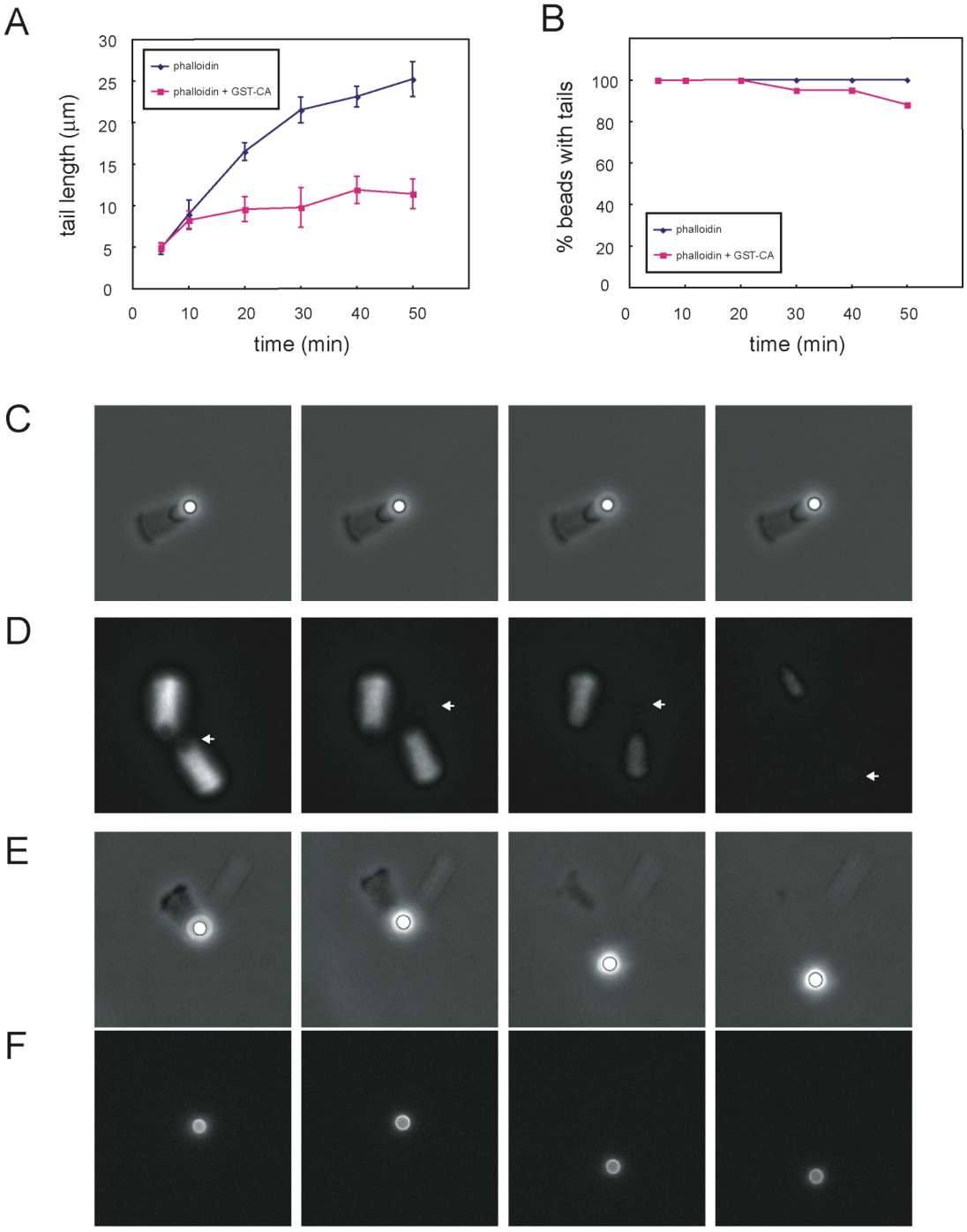
A
tail length (µm)
30
25
20
15
10
5
0
phalloidin
phalloidin + GST-CA
0
10
20
30
40
50
time (min)
B
% beads with tails
100
80
60
40
20
0
phalloidin
phalloidin + GST-CA
0
10
20
30
40
50
time (min)
C
D
E
F

**Fig. 3.8 Arp2/3 complex sequestration by GST-CA arrests comet tail growth, but has no effect on comet tail attachment.**

(A) In these experiments, phalloidin was added immediately before GST-CA to stabilize Arp2/3-containing branch junctions in the comet tails (Blanchoin and Pollard, 2002), as GST-CA alone caused rapid and complete disappearance of all actin comet tails. GST-CA (5 μM) plus phalloidin (3 μM) or phalloidin alone was added 5 min after initiating motility reactions with WT N-WASP. At the indicated time points, aliquots were fixed with 1.5% glutaraldehyde. Comet tail lengths were measured (mean ± S.D., n = 10 tails per time point), and the percentage of beads with attached tails was determined (B) (40-50 beads per time point were counted). With R438A and K444Q N-WASP, the rate of comet tail detachment was not significantly affected by phalloidin or GST-CA/phalloidin (data not shown). (C) Time-lapse images of GST-CA in the presence of phalloidin. Comet tails are stable and remain attached to lipid-coated beads. (D,E) The actin comet tail is disassembled in the presence of GST-CA alone. (D) Actin comet tail is labeled with Alexa594 actin. Arrow indicates the lipid-coated bead. (F) GST-CA does not dissociate Alexa488 WT N-WASP from the bead surface.

role for filament side-binding by the Arp2/3 complex. We asked whether inhibition of the Arp2/3 complex would promote detachment of membrane-tethered actin networks. N-WASP CA fragment has previously been shown to potently inhibit Arp2/3-mediated actin nucleation (Hufner et al., 2001; Rohatgi et al., 1999) and *Listeria monocytogenes* motility (Brieher et al., 2004). We first determined that the N-WASP CA domain could inhibit Arp2/3-dependent motility in our reconstituted motility medium, as SCAR CA domain could not (data not shown). In the present experiments, phalloidin was added to stabilize Arp2/3-containing branch junctions in the comet tails (Blanchoin et al., 2000), as GST-CA alone induced rapid and complete disappearance of all actin comet tails (Fig 3.8 D, E). Consistent with the ability of GST-CA to sequester the Arp2/3 complex and compete with membrane-bound N-WASP, addition of GST-CA/phalloidin to motility reactions rapidly arrested comet tail growth and bead movement (Fig. 3.8 A, C). Importantly, GST-CA failed to induce comet tail detachment (Fig. 3.8 B), and phalloidin alone had no effect on either comet tail attachment or growth (Fig. 3.8 A, B). With R438A and K444Q N-WASP, comet tail detachment was not significantly affected by either phalloidin or GST-CA/phalloidin (data not shown). In addition, GST-CA did not dissociate N-WASP from the membrane (Fig. 3.8 F). Collectively, these results largely exclude a direct role for the Arp2/3 complex in maintaining comet tail attachment to the membrane.

**Actin filament barbed end capture by N-WASP WH2 domains.**

We sought direct evidence for ternary complex formation between the N-WASP WH2 domain, actin monomers, and actin filament barbed ends outside the context of Arp2/3-assembled comet tails (in the absence of the Arp2/3 complex, capping protein, and profilin). Because comet tail tethering is likely governed by multivalent, low-affinity (high-avidity) interactions, and standard co-sedimentation assays have failed to reveal a stable interaction between F-actin and WASP-family WH2 domains (our unpublished data, (Higgs et al., 1999)), we adapted an F-actin capture assay (Bear et al., 2002; Samarin et al., 2003) using N-WASP-coated polystyrene beads and Alexa488 phalloidin-stabilized actin filaments (Alexa488 F-actin). We quantified Alexa488 fluorescence on the surface of individual beads as a function of increasing concentrations of rhodamine-labeled, Lat B-stabilized actin monomers.

Whereas Alexa488 F-actin (4 μM) alone did not detectably associate with the N-WASP-coated beads, actin filaments were robustly captured in the presence of increasing concentrations of rhodamine-labeled actin monomers (Fig. 3.9 A). That the rhodamine-labeled actin monomers were prevented from polymerizing by excess Lat B was confirmed by fluorescence microscopy; Alexa488 actin filaments extended up to 10 μm away from the beads, whereas rhodamine actin fluorescence was confined to the bead surface (Fig. 3.9 B). Maximal binding of Alexa488 filaments to N-WASP-coated beads occurred in the presence of 1 μM actin monomers and was blocked by 250 nM capping protein.

Importantly, actin capture was abrogated by the R438A and K444Q mutations in a manner that correlated with their actin monomer binding affinities (Fig. 3.9 B). Equal amounts of the three N-WASP constructs were adsorbed to the beads (Fig. 3.9 C). Quantitation of bead-associated rhodamine fluorescence provided actin binding curves for WT, R438A, and K444Q N-WASP that were qualitatively consistent with fluorescence anisotropy assays carried out with labeled $W_bCA$ fragments (Fig.2.8). We corroborated these data by comparing the Cdc42-binding BG fragment with the WH2-containing BG-$W_aW_b$ (BG-W) fragment (Fig. 3.10) in the same assay. The BG-W fragment captured actin filament barbed ends in the presence of increasing Lat B/actin monomers, whereas the BG fragment did not (Fig. 3.10). These data indicate that actin monomers can link actin filament barbed ends to immobilized N-WASP WH2 domains. Moreover, the actin monomer binding affinities of the three WH2 domains correlated with their ability to capture actin filaments and tether comet tails to lipid-coated beads.

Finally, we asked whether the interactions between WH2 domains, actin monomers and actin filament barbed ends are functionally relevant in the context of an actual dendritic actin network. Our lipid-coated bead system is more physiological than previous protein-coated bead systems in that NPFs are not permanently fixed to the bead surface. This advantage allowed us to introduce soluble N-WASP derivatives to “replace” membrane-bound N-WASP molecules at any time during an ongoing reaction as illustrated in Figure 6C. Using this system, we devised an experimental strategy to test

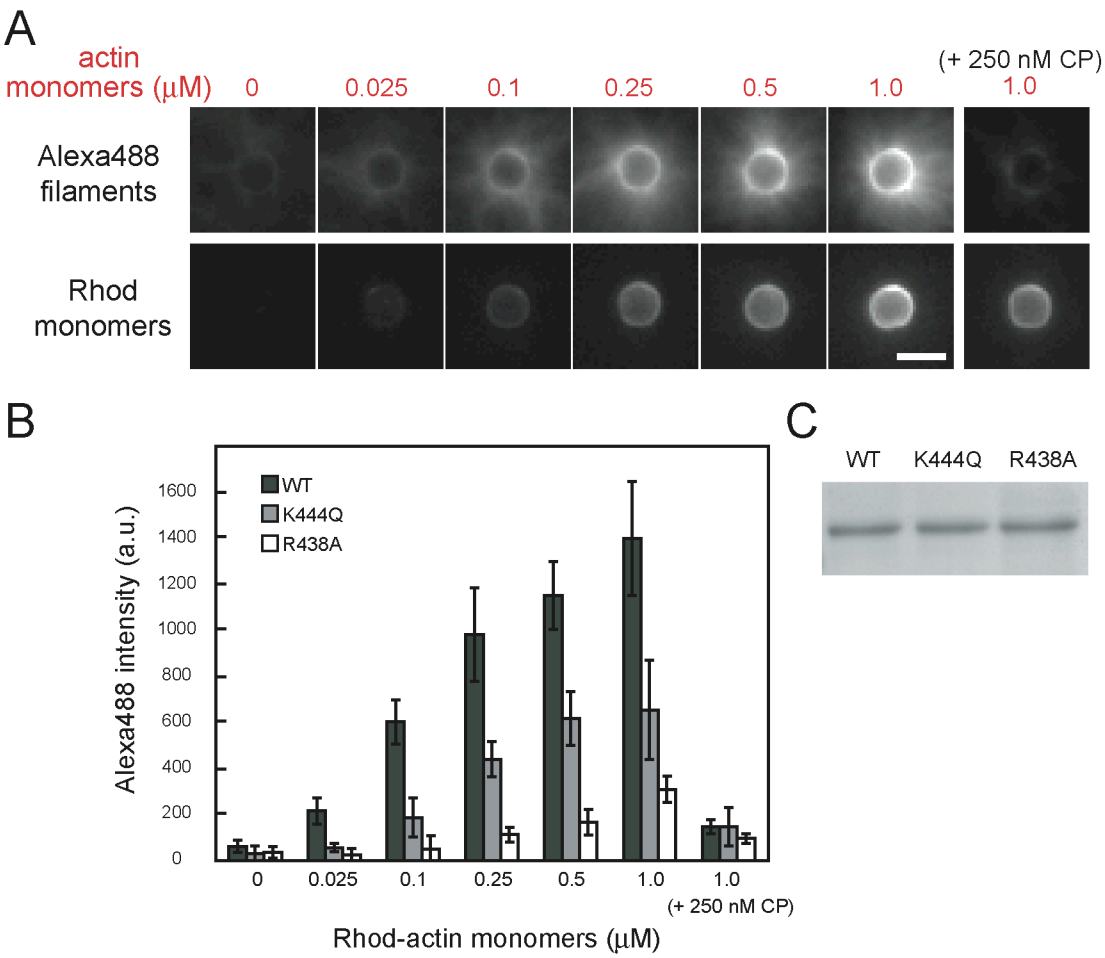
A
actin monomers (μM)
0
0.025
0.1
0.25
0.5
1.0
(+ 250 nM CP)
1.0
Alexa488 filaments
Rhod monomers
B
WT
K444Q
R438A
Alexa488 intensity (a.u.)
1600
1400
1200
1000
800
600
400
200
0
0
0.025
0.1
0.25
0.5
1.0
1.0
(+ 250 nM CP)
Rhod-actin monomers (μM)
C
WT
K444Q
R438A
D
WT
K444Q
R438A
Rhod fluorescence (a.u.)
600
500
400
300
200
100
0.2
0.4
0.6
0.8
1
Rhod actin monomers (μM)

**Fig. 3.9 Immobilized N-WASP captures actin filament barbed ends in a WH2-dependent manner.**

(A) Polystyrene beads were coated with N-WASP (WT, K444Q, and R438A) as described in the Materials and Methods and incubated for 10 min with Alexa488 phalloidin-stabilized actin filaments (4 μM pre-polymerized filaments, 3 μM Alexa488 phalloidin) and increasing concentrations of Lat B-stabilized actin monomers (17% rhodamine labeled). After 5-fold dilution into buffer containing 1 mg/ml BSA, beads (15-20) were chosen at random by phase contrast microscopy and imaged by two-color fluorescence microscopy. Shown are images of WT N-WASP beads with bound Alexa488 filaments (upper panels) and rhodamine actin monomers (lower panels). Actin filament capture was abolished by co-incubation with 250 nM capping protein. Bar = 2 μm.

(B) Quantification of Alexa488 filaments captured by WT, K444Q and R438A N-WASP beads. A circle (2.3 μm diameter) was drawn around the beads and the total integrated fluorescence, minus the background fluorescence, was calculated. Shown are mean fluorescence intensities ± S.D., n = 15 - 20 beads for each condition.

(C) Equivalent amounts of N-WASP (WT, K444Q and R438A) are absorbed to polystyrene beads. SDS-PAGE gel of N-WASP proteins denatured from polystyrene beads used in (A).

(D) Binding of rhodamine-labeled, Lat B-stabilized actin monomers (17% rhodamine labeled) to bead-immobilized N-WASP (WT, K444Q, and R438A). Bead-associated rhodamine fluorescence was quantified for the experiment shown in (A,B). A circle (2.3 μm diameter) was drawn around the beads and the total integrated fluorescence, minus the background fluorescence, calculated. Shown are mean ± S.D. fluorescence intensities, n = 15 - 20 beads for each condition.

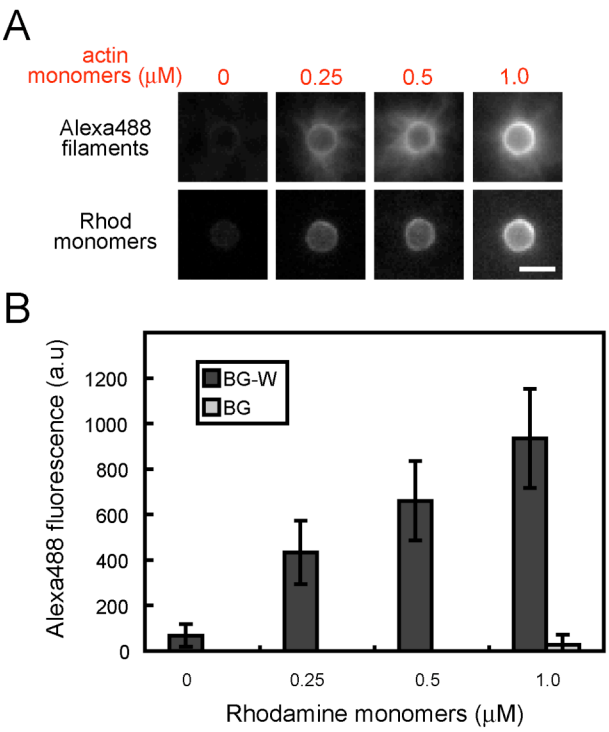


**Fig. 3.10 Actin filaments are captured by immobilized BG-W, but not BG.**
(A) Polystyrene beads saturated with BG or BG-W fragments were incubated for 30 min with Alexa488 phalloidin-stabilized actin filaments (4 μM filaments, 3 μM Alexa488 phalloidin) and increasing concentrations of Lat B-stabilized actin monomers (17% rhodamine labeled). Shown are images of BG-W beads with bound actin filaments (Alexa488 phalloidin, upper panels) and actin monomers (rhodamine, lower panels). Actin filament capture was abolished by co-incubation with 250 nM capping protein, and equivalent amounts of BG and BG-W were adsorbed to the beads (data not shown). Bar = 2 μm.
(B) Quantification of Alexa488 filaments captured by BG and BG-W. Bead-associated Alexa488 fluorescence was quantified using a circle (2.3 μm diameter) region of interest. Shown are background-subtracted mean ± S.D. fluorescence intensities (n = 15 - 20 beads for each condition).

whether WH2 domains were sufficient to maintain adhesion between the membrane and a more complex dendritic network.

We first formed actin comet tails by pre-loading lipid-coated beads with Cdc42 and fluorescent N-WASP (5% labeled with Alexa488). At 12 min following the start of the reaction, either BG or BG-W was introduced into the system to replace the membrane-bound N-WASP. By monitoring the fluorescence levels of membrane-bound N-WASP, we demonstrated that BG and BG-W were equally efficient at replacing N-WASP on the beads (Fig. 3.11 B). Addition of either BG or BG-W (2 $\mu$M) caused rapid disappearance of N-WASP from the beads ($t_{1/2}$ ~ 5 min, Fig. 3.11 B), whereas buffer alone resulted in a slight increase in N-WASP fluorescence. As expected, replacement of N-WASP by BG caused 100% of the comet tails to detach within 15 min (Fig. 3.11 C). Remarkably, comet tails remained attached for up to 45 min after addition of BG-W, despite depletion of N-WASP from the membrane. These results were also observed at various concentrations of BG and BG-W (Fig. 3.12). We conclude that the minimal requirements for attaching actin comet tails to the membrane are (1) the BG domain, which binds PIP2 and Cdc42 and (2) the WH2 domain, which binds the barbed ends of actin filaments. Notably, interactions between the CA domain and the Arp2/3 complex are not required. Despite the stable connections between the membrane and the dendritic actin network, comet tail growth was completely inhibited by BG-W. By contrast, control comet tails (buffer added at t = 12 min) grew steadily during the entire observation period (Fig. 3.11 D). These

results suggest that WH2-mediated elongation or elongation by profilin/actin does not generate sufficient force to sustain forward movement and that Arp2/3-mediated branching/ nucleation is required.

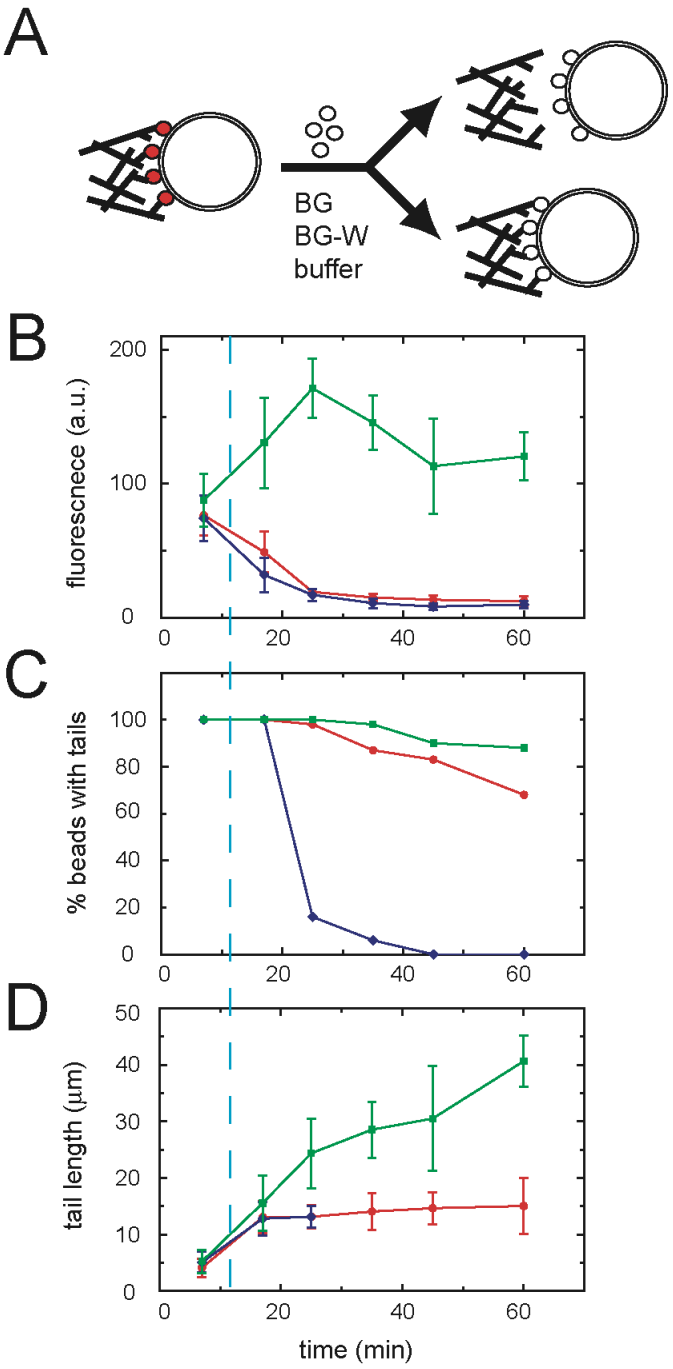
A
BG
BG-W
buffer
B
fluorescnece (a.u.)
200
100
0
0
20
40
60
C
% beads with tails
100
80
60
40
20
0
0
20
40
60
D
tail length (μm)
50
40
30
20
10
0
0
20
40
60
time (min)

**Fig. 3.11 WH2 domains are sufficient to maintain actin network attachment.**
(A) N-WASP replacement experiment. Actin comet tails were assembled in standard motility reactions containing WT N-WASP (150 nM final concentration, 5% labeled with Alexa488). After 12 min, N-WASP fragments (BG or BG-W, 2 μM final concentration) or buffer was added to displace WT N-WASP from the lipid-coated beads. At the indicated time points, aliquots were fixed and analyzed as shown in (B)-(D).
(B) Bead-associated Alexa488 N-WASP was quantified by fluorescence imaging. A circle (3 μm diameter) was drawn around the beads and the total integrated fluorescence, minus the background fluorescence, was calculated. Shown are mean fluorescence intensities ± S.D. (n = 10 beads per time point).
(C) The percentage of beads with attached tails was quantified (n = 40 beads per time point). Lipid-coated beads containing the BG-W fragment mediated actin comet tail attachment almost as well as WT N-WASP, whereas beads containing the BG fragment rapidly lost their tails.
(D) Actin comet tail lengths were measured (mean ± S.D., n = 10 - 15 tails per time point). Bead movement was arrested by the BG-W and BG fragments.

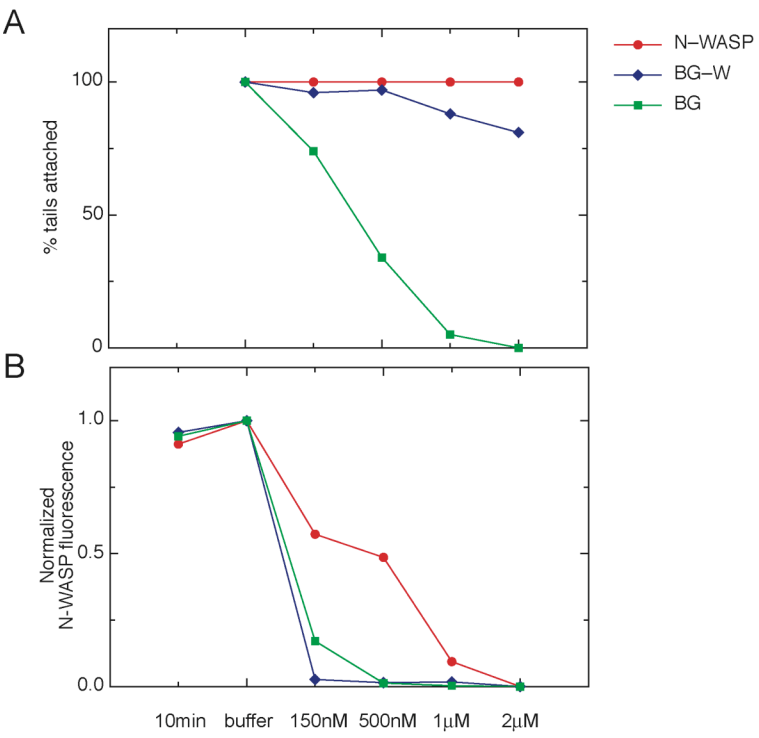


**Fig. 3.12 Concentration dependence of WH2 domains in maintenance of actin network attachment.**

Replacement experiment varying the concentration of BG, BG-W and WT N-WASP and assessing their ability to maintain actin comet tail attachment. Experiment was performed as in Fig. 3.11 A except that only one time point was taken 30 min after addition of replacement constructs.

(A) % beads with tails attached at 30 min after addition of increasing concentrations of BG, BG-W or WT N-WASP.

(B) Remaining Alexa488 N-WASP fluorescence on the bead after incubation with increasing concentrations of BG, BG-W or WT N-WASP, from experiment in (A).

## Discussion

We successfully reconstituted, using pure components, a physiological signaling pathway leading to actin polymerization propelled-membrane movement. This biomimetic system is novel in several ways: first, our substrate is a fluid membrane bilayer that includes PIP2; second, actin polymerization is activated by a signaling cascade comprised entirely of components that are inactive and must be recruited from solution to the membrane. The development of this system has allowed us to dissect a mechanism that describes how the actin network is attached to the membrane surface and how soluble signaling molecules coordinate with the membrane surface and actin machinery to generate polarized actin networks.

Signal transduced-actin assembly in the cell is activated by RhoGTPase-switch-like cascades (Welch and Mullins, 2002). In our system, the RhoGTPase, Cdc42 is prenylated and bound to its inhibitor RhoGDI which keeps it in solution. Cdc42 is activated at the membrane by intersectin which exchanges GDP for GTP$\gamma$S. The precise order of events, which is still unresolved, may be solved by experiments in this system. Preliminary experiments in our system have already shown that increased PIP2 levels enhance the activation of the Cdc42/GDI complex (unpublished data). These *in vitro* experiments corroborate experiments *in vivo* (Heo et al., 2006).

Symmetry breaking and formation of polarized actin networks occurs by a different mechanism on membrane surfaces than on plastic bead surfaces (van der Gucht et al., 2005) when driven by signal transduction from solution. The development of this biomimetic system has allowed us to distinguish between two mechanisms of symmetry breaking on surfaces. In one mechanism, a shell encases the bead, ruptures and initiates polarized tail formation. In the other mechanism, a spherical shell around the bead does not form. Rather, actin polymerization occurs stochastically on the membrane surface until a dominant polar actin network is sufficient to produce enough force to drive bead movement. Rather than breaking symmetry, the mechanism involves amplification of spontaneous asymmetry. We often observe that actin network formation occurs on different parts of the spherical surface; multiple, mini-comet tails appear to diffuse in the plane of the membrane and merge to eventually form one polarized actin network as seen on moving vesicles in PMA-stimulated extracts and in prick-activated Xenopus eggs (Svitkina et al., 2003; Taunton et al., 2000). The spontaneous formation of localized actin networks that intensify and merge with neighboring networks is reminiscent of the highly complex behavior of lamellipodia in motile cells (Svitkina et al., 2003). These results emphasize that the order of component addition is critical to membrane motility *in vitro*.

**Mechanism of actin network attachment to moving membranes by N-WASP WH2 domain capture of actin filament barbed ends.**

Conventionally, it is thought that the interaction between membrane-bound N-WASP and the actin filament-bound Arp2/3 complex defines the molecular unit that tethers the actin network to the membrane surface and ultimately generates the "pulling" force that retards propulsive movement (Giardini et al., 2003; Mogilner and Oster, 2003). However, our finding that N-WASP WH2 domain can bind the actin network independent of the Arp2/3 complex, has forced us to construct alternative models of how N-WASP molecules interact with the actin network during vesicle motility.

We have devised an actin-tethering model of how a membrane-tethered WH2 domain acts at the membrane-actin interface. Several lines of evidence have led us to this model. WH2 domains localize to membrane-actin interface independent of the CA domain of N-WASP. This demonstrates that the Arp2/3 complex is not required for N-WASP localization to the membrane-actin interface. WH2 domains interact with the barbed ends of actin filaments. Excitingly, this lends support to a recent study by Chereau and colleagues (2005) which argues that WH2-actin contacts are fully compatible with intersubunit contacts between actin subunits in the Holmes model of an actin filament (Chereau et al., 2005).

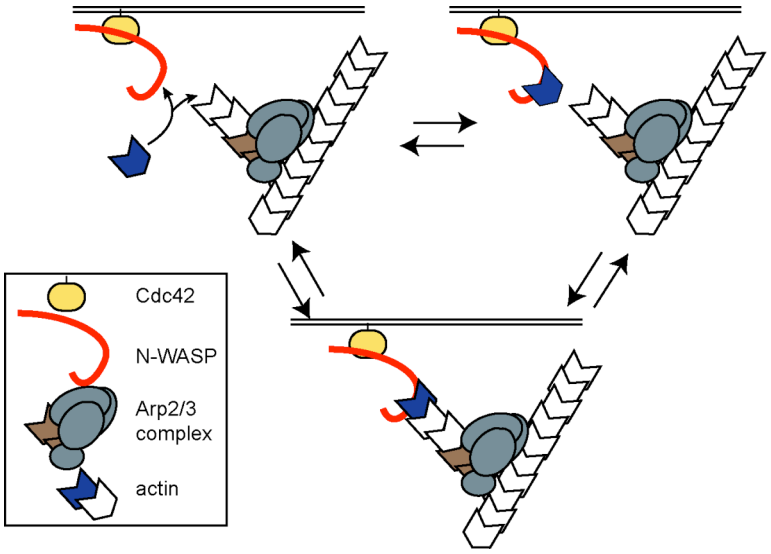


**Fig. 3.13 Model of actin filament capture by membrane-tethered WH2 domains**

Membrane-proximal barbed ends encounter a high local concentration of N-WASP WH2 domains/Cdc42 and enter a reversible elongation/attachment/ release cycle: ATP-actin monomers associate with membrane-associated N-WASP WH2 domains or with free barbed ends; WH2-ATP-actin monomer complexes capture actin filament barbed ends and can add the actin monomer to the filament barbed ends; filaments (elongated by one actin subunit) dissociate from WH2 domains. Attachment of the dendritic network occurs when a critical number of filament barbed ends interact with WH2/ATP-actin monomers or free WH2 domains. Upon dissociation of the attachment complex, rapid rebinding to either WH2 or WH2/ATP-actin can occur due to the high local concentration of barbed ends and N-WASP and the inability of actin filaments in the dendritic network to rapidly diffuse away from the membrane.

We propose that the interaction between actin filament barbed ends and N-WASP WH2 domains ensures polarized and persistent actin assembly during vesicle motility by recruiting and trapping NPFs at sites of actin assembly. This interaction also ensures that the polarized network remains constantly attached to the membrane during actin assembly. We identified three crucial components that collectively mediate this tethering mechanism: the C-terminal WH2 motif of N-WASP, ATP-actin monomers and actin filament barbed ends. We propose that the actin network is connected dynamically to the membrane surface during rapid WH2-mediated filament capture, elongation and release: (1) an ATP-actin monomer binds to the C-terminal WH2 domain; (2) the WH2/ATP-actin monomer complex or WH2 domain alone captures a nearby filament via its barbed end; barbed ends that are not in close proximity to membrane-tethered WH2 domains become capped; (3) the actin monomer incorporates into the filament, which leads to release of WH2 from the filament. A key property of this system that remains to be experimentally resolved is the probability that WH2 domains recognize the ATP-actin terminal ends of actin filaments. Actin network tethering appears to be the transient step in which all three components form a ternary complex. The dendritic network of individual tethering events contributes to the overall movement of vesicles.

## Materials and Methods

### Proteins used in motility assays

Cdc42/GDI complex was purified from SF9 cells and *E.coli.* Capping protein was expressed in *E.coli*. Arp2/3 complex was purified from bovine brain. Intersectin DH-PH was purified from *E.coli,* (Zamanian and Kelly, 2003). Profilin (purified from *Acanthamoeba castellanii*) was a gift from Mark Dayel and Dyche Mullins (UCSF). GST-CA (derived from human N-WASP and expressed in *E. coli*) was a gift from Bill Brieher (Harvard Medical School).

### Cdc42/GDI exression and purification

The Cdc42/GDI complex was expressed and purified as described in (Hoffman et al., 2000) (Cdc42 baculovirus and RhoGDI plasmid from Rick Cerione, Cornell University). Briefly, $His_6$-Cdc42 was expressed in insect cells using a baculovirus expression system. GST-RhoGDI was expressed in *E.coli* BL-21 cells. Lysates from insect cells and *E.coli* cells were combined and incubated for 1 h at 4°C to allow complex formation. The complex was purified sequentially by binding and elution from Ni-NTA agarose and glutathione agarose columns.

### Capping protein expression and purification

Capping protein was purified as described (Palmgren et al., 2001).

The plasmid for the expression of mouse capping protein a1 and b2 subunits were a gift from Dyche Mullins. Briefly, transformed BL-21 cells were induced by addition of IPTG to 1 mM at 37°C for 3 h. Cells were harvested by centrifiguation (3000 x g for 15 min), resuspended in and washed in 40 mM Tris pH 8, 40 mM EDTA and 140 mM NaCl. The cell pellet was resuspended in 100 mL 50 mM Tris pH 8, 1 mM EDTA, 1 mM DTT and 1 mM PMSF and sonicated on ice. The cell lysate was centrifuged at 35K for 1 h at 4°C. A 50-70% ammonium sulfate fraction was obtained from the high-speed supernatant and the precipitate obtained by centrifugation at 32,000 x g for 20 min at 4°C. CP was purified by hydroxapatite, Mono Q, Mono S and finally dialyzed against CP storage buffer (10 mM TrisCl pH 8, 40 mM KCl, 0.5 mM DTT and 50% glycerol) for storage at -80°C.

**Preparation of $His_6$-WA column for Arp2/3 purification**

$His_6$-WA is a gift from Dyche Mullins. $His_6$-WA was induced with 1 mM IPTG in BL-21 cells at 37°C for 3-6 h. Induced cells were spun at 3000g and cell pellets were resuspended in 4M Urea and rotated at RT overnight. The cell lysate was clarified and added to Ni-NTA for 2-4 h at RT. Ni-NTA beads were washed with 20 mM Hepes, 100 mM NaCl and eluted with 20 mM Hepes, 100 mM NaCl, and 250 mM imidazole. Eluted $His_6$-WA was dialyzed in 20 mM Hepes, 100 mM NaCl, 0.5 mM DTT and frozen in liquid nitrogen.
$His_6$-WA was immobilized to pre-activated CH4B Sepharose (Pharmacia). CH4B Sepharose is activated with 1 mM HCl pH 2.0. Swelled sepharose was added

directly to $His_6$-WA and allowed to incubate rocking for 1-2 h at RT. The resin was then washed with 1 mM HCl pH 2.0, 4 M Urea to remove any unbound $His_6$-WA and 20 mM Hepes, 100 mM NaCl and stored in the same buffer with 0.2% $NaN_3$ until use.

**Arp2/3 complex purification from Bovine brain**

Arp2/3 complex was purified as described with minor modifications (Egile et al., 1999). Briefly, thawed de-membraned brains (Pelfreez) were combined with equal volume Arp2/3 buffer (50 mM PIPES pH 6.8, 5 mM EGTA, 2 mM $MgCl_2$, 1 mM DTT, 0.1 mM PMSF, 0.2 mM ATP) and blended at 4°C until smooth. The brain lysate was centrifuged at 10,000 rpm for 1 h at 4°C. The supernatant was removed and the lysate was centrifuged for an additional 10 min. Brain supernatant was batch bound with S-sepharose with slow stirring at 4°C for 1 h and washed Arp2/3 buffer. Arp2/3 complex was eluted with Arp2/3 buffer containing 100 mM KCl. The eluted slurry was applied to a pre-equilibrated WA column and the Arp2/3 complex was eluted with Arp2/3 elution buffer (10 mM imidazole pH 7.5, 200 mM $MgCl_2$, 150 mM NaCl, 0.2 mM ATP, 1 mM DTT). The peak fractions were pooled and dialyzed into Arp2/3 storage buffer (10 mM imidazole pH 7.5, 0.2 mM MgCl2, 150 mM NaCl, 0.2 mM ATP, 1 mM DTT, 10% glycerol) and freeze in liquid nitrogen.

**Lipid Preparation**

Phosphatidyl Choline (egg yolk), Phosphatidyl Serine (brain) and $PI(4,5)P_2$ (brain) were purchased from Avanti lipids. Large vesicles were prepared as previously described with modifications (Klopfenstein et al., 2002): mixed lipids were dried over an argon stream, placed under vacuum for 3 h, and resuspended in vesicle buffer (20mM Hepes pH 7.5, 100mM NaCl, 250mM sucrose). Hydrated lipids were sonicated in a water bath, followed by at least 6 cycles of freeze/ thawing in liquid nitrogen. Hydrated lipids were stored at -80°C for long-term storage.

**Actin-based motility of lipid-coated glass beads**

A suspension containing 5 μl liposomes (5 mM total lipids), 3 μl glass beads (Bangs laboratories, 2.3 μm diameter, 10% solids w/v, cat.# SS04N), and 27 μl vesicle buffer (20 mM Hepes pH 7.5, 100 mM NaCl, 250 mM sucrose) were mixed, bath sonicated twice for 20 s, and rotated for 15 min at RT. Under these conditions, liposomes fuse with the glass beads to create a membrane bilayer (Baksh et al., 2004). Lipid-coated glass beads were collected by brief, low-speed (< 200 rpm) centrifugation, washed, and resuspended in vesicle buffer. Lipid-coated beads ($6.25 \times 10^8$ beads/ml) were stored rotating at room temperature and used within 2 weeks of preparation.

For motility reactions, lipid-coated glass beads (2.3 μm diameter) were diluted 10-fold into Cdc42 charging buffer (10 mM imidazole pH 7, 0.05 M KCl, 1 mM $MgSO_4$, 1 mM EGTA, 1 mM DTT) and incubated with 1.5 μM Cdc42/RhoGDI

complex, 2 μM intersectin DH-PH, and 100 μM GTPγS for 10 min at room temperature, followed by addition of 1.5 μM N-WASP for 10 min. Motility reactions were initiated by diluting the suspension of N-WASP/Cdc42/lipid-coated glass beads 10-fold into motility buffer (10 mM imidazole (pH 7.0), 50 mM KCl, 1 mM $MgSO_4$, 1 mM EGTA, 5 mg/ml BSA, 0.2% methylcellulose, 5 mM TCEP, 1 mM ATP, 7.5 mM creatine phosphate, 1.25 mM DABCO) containing the motility proteins at the following optimal concentrations (unless otherwise stated): 6 μM actin monomers, 0.075 μM Arp2/3, 0.05 μM capping protein, 2 μM profilin. "Optimal concentrations" of capping protein and the Arp2/3 complex varied somewhat from preparation to preparation. For quantification of percent comet tail attachment and tail length, 0.75 μl aliquots were fixed by pipetting into 0.75 μl 3% glutaraldehyde on a microscope slide, sealed with VALAP (vaseline, lanolin, paraffin 1:1:1), and observed within 2 h. To measure speeds, 5 min time-lapse sequences were recorded for each lipid-coated bead (n = 14 – 15 for WT, K444Q, and R438A N-WASP). For the Alexa594 N-WASP translocation experiment in Fig. 3.1, 1.6 μm glass beads (Duke Scientific Corporation, 2% solids w/v, cat.# 8150) were used in the preparation of lipid-coated beads, as described above.

**Actin filament capture assay**

Polystyrene beads (2.0 μm, Polysciences, Inc., cat.# 18327) were coated with 1 μM N-WASP in F-buffer (10 mM imidazole pH 7, 0.05 M KCl, 1 mM $MgCl_2$, 1 mM EGTA) at RT for 1 h. Coated beads were spun at 10,000*g* for 10 m and the supernatant was removed. BSA (1 mg/ml in F-buffer) was added to block the

beads for 1 h at RT. N-WASP beads were washed and stored in 1 mg/ml BSA at 4°C. Actin (8 μM) was polymerized in F-buffer for 2 h and stabilized with 6 μM Alexa488 phalloidin to give "Alexa488 filaments". N-WASP beads ($5.73 \times 10^8$ beads/ml) were gently rotated with Alexa488 filaments (4 μM) in the presence of varying concentrations of rhodamine actin monomers (stabilized with a 10-fold molar excess of Lat B). After 10 min, the suspension was diluted 5-fold into F-buffer containing 1 mg/ml BSA. An aliquot (2 μl) was placed on a microscope slide, gently sealed under a coverslip with VALAP, and imaged by fluorescence microscopy. In some experiments, Alexa488 filaments were treated with 250 nM capping protein prior to mixing with the beads.

# Chapter 4

## N-WASP regulates the formation of large podosome structures in cells.

**Abstract**

N-WASP promotes the formation of podosomes (invadopodia) in transformed cells (Mizutani et al., 2002; Yamaguchi et al., 2005). Podosomes are actin structures that form at the membrane and protrude from the ventral surface of cells. Podosomes contain extracellular matrix-degradative activity and have been implicated in the invasivity of carcinoma cells and the bone-resorbing function of osteoclasts (Jurdic et al., 2006; Yamaguchi et al., 2006). Their formation requires N-WASP in cancerous cells and WASP in macrophages and osteoclasts (Linder et al., 1999). We tested whether WH2 domain mutations, which result in membrane attachment defects *in vitro,* affect the formation, organization and dynamics of podosome structures *in vivo*.

## Introduction

Cancerous cells use various polarized membrane-actin structures to invade their surroundings. The invasion process can be broken down into three steps. First, actin-rich structures called podosomes form at the base of the membrane. Second, these podosomes degrade the surrounding extracellular matrix (ECM). Finally, these cells migrate through the holes in the ECM (Yamaguchi et al., 2006).

Despite their interesting ability to facilitate invasion of cancerous cells, podosomes and the molecular details of their formation and organization have not been well studied. Two key discoveries illuminated molecular pathways that drive podosome formation. In 1989, scientists discovered that Rous Sarcoma Virus transformed-cells form actin-rich protrusions at their basal membrane as they migrated across ECM proteins (Chen, 1989). Interestingly, these cells left behind holes in the ECM where the actin-rich structures were formed, indicating that these structures contained a degradative activity. Similarly, osteoclasts also contain podosomes, required for bone-resorption, another degradative process (Jurdic et al., 2006). A breakthrough in our understanding of the molecular details of podosome formation occurred when it was discovered that the macrophages of WAS patients were unable to form podosomes (Linder et al., 1999). This discovery created the first link between the Wiskott Aldrich Syndrome gene and a physiological process in cells.

Two distinct aspects of podosome formation have been described: the signaling cascades which determine podosome formation and the morphological organization of these structures (Destaing et al., 2003; Evans et al., 2003; Yamaguchi et al., 2005). Given the deficiency in podosome formation in WAS patients, we were interested in determining the precise role of N-WASP in these two processes.

The signaling cascades described for podosome formation is similar to the signaling cascade described for intracellular vesicle motility. First, an upstream kinase must be activated. Downstream, the RhoGTPase, Cdc42, is required. Cdc42 activates N-WASP, which activates the Arp2/3 complex (Spinardi et al., 2004). Recently, these two pathways have been linked showing that they may function simultaneously during podosome formation (Baldassarre et al., 2006).

The molecular mechanisms governing the formation and organization of podosomes in cellular models of cancer are not fully understood. In normal cells including macrophages and osteoclasts, chemotactic signals like EGF initiate signaling events that lead to the formation of punctate podosome structures (Destaing et al., 2003; Evans et al., 2003; Luxenburg et al., 2006; Yamaguchi et al., 2006). Over time, larger podosome structures form and organize into distinct patterns like bars and rings. In osteoclasts, the formation of larger structures appears to be a step-wise process, where punctate structures form rings and rings cluster to form large belts (Jurdic et al., 2006). On the other hand, macrophages contain podosome structures that exist solely as punctate

structures (Evans et al., 2003). Given its role in the adhesion of the actin network to membranes in vitro, we wanted to investigate if N-WASP is required for the formation and organization of podosome structures in vivo.

## Results

To study the possible role of WH2-membrane-actin interactions in podosome formation and/or organization, we utilized a podosome model system that requires N-WASP. We transformed N-WASP$^{-/-}$ fibroblasts with two retroviruses: a v-Src retrovirus and a retrovirus containing WT or a mutant GFP-N-WASP, in which both arginine residues in the WH2 domains have been mutated to alanine (hereafter referred to as RA/RA N-WASP). These arginine residues are critical for tethering of actin filaments to membranes (see Chapter 3).

To compare the abilities of WT and RA/RA GFP-N-WASP to form podosome structures, we used Fluorescence Activated Cell Sorting (FACS) to purify cells which expressed equivalent levels of WT and RA/RA GFP-N-WASP. The FACS-sorted cells expressed equal amounts of GFP-NWASP, v-Src and VASP, which also contains a WH2 domain and has been implicated in podosome formation (Fig. 4.1 A)(Spinardi et al., 2004). In vitro, *E.coli* expressed-WT and RA/RA N-WASP151-504 nucleated actin polymerization similarly (Fig. 4.1 B).

Consistent with previous dominant negative and siRNA experiments (Mizutani et al., 2002; Yamaguchi et al., 2005), v-Src$^{+}$/N-WASP$^{-/-}$ cells were devoid of podosomes, whether left untreated or transduced with a control GFP retrovirus (data not shown). By contrast, we observed podosomes in both the WT (50 ± 6%) and RA/RA cells (38 ± 7%, mean ± S.D., three independent experiments; essentially all cells from two coverslips [40X objective, 150 microscope fields per coverslip] were quantified in each experiment) (Fig. 4.3 A).

Live imaging of v-Src$^{+}$/N-WASP$^{-/-}$ cells transduced with WT and RA/RA GFP-N-WASP demonstrated that podosomes are heterogeneous in structure and dynamic (Fig. 4.2). We made several observations. First, localization of GFP-N-WASP to podosomes dynamically requires v-Src kinase activity. Addition of the Src kinase inhibitor PP1 (10 μM) to cells resulted in the rapid disappearance of podosome localized-GFP-N-WASP (Fig. 4.4). Following washout of PP1, cells re-formed podosomes (data not shown). Second, podosomes in v-Src$^{+}$/N-WASP$^{-/-}$ cells transduced with WT and RA/RA GFP-N-WASP existed as a diverse array of heterogeneous structures that we broadly classified into 3 groups: punctate structures, more extended bar-like structures, and arrays of podosomes in ring-like structures reminiscent of those found in osteoclasts (Fig. 4.2, 4.3).

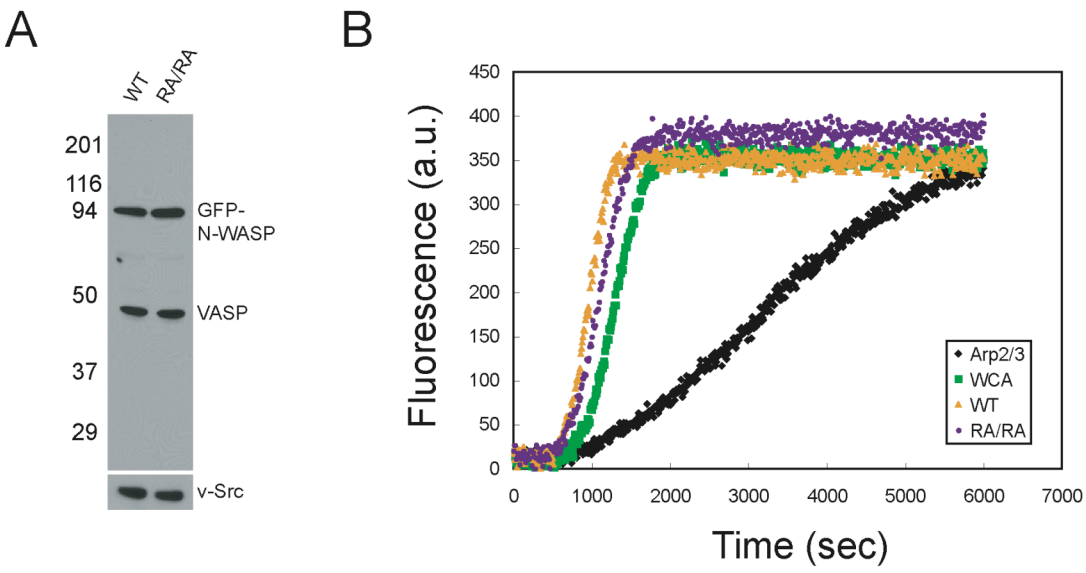


**Fig. 4.1 Characterization of RA/RA mutant.**

(A) Western blot of FACS-sorted v-Src-transformed N-WASP$^{-/-}$ fibroblasts rescued with full-length WT or R410A/R438A (RA/RA) GFP-N-WASP. WT and RA/RA cells show similar expression levels of GFP-N-WASP, v-Src, and VASP. (B) Pyrene actin polymerization assays comparing constitutively active $W_aW_bCA$ (WCA) fragment, WT N-WASP$^{151\text{-}501}$ and RA/RA N-WASP$^{151\text{-}501}$. N-WASP amino acids 1-150 (EVH1 domain) were deleted to facilitate expression in *E. coli*. N-WASP proteins (200 nM) were combined with 6 μM Cdc42/GTPγS (except for WCA), 20 nM Arp2/3 complex, and 2 μM actin (5% pyrene-labeled). Fluorescence was monitored as described in Fig. 2.7. Note that this experiment was performed with a different batch of actin and Arp2/3 complex from that shown in Fig. 2.7, which explains the slightly increased $t_{1/2}$ values. Due to the slight batch-to-batch variability of actin and Arp2/3 complex, comparisons between different N-WASP constructs are only valid when performed in parallel.

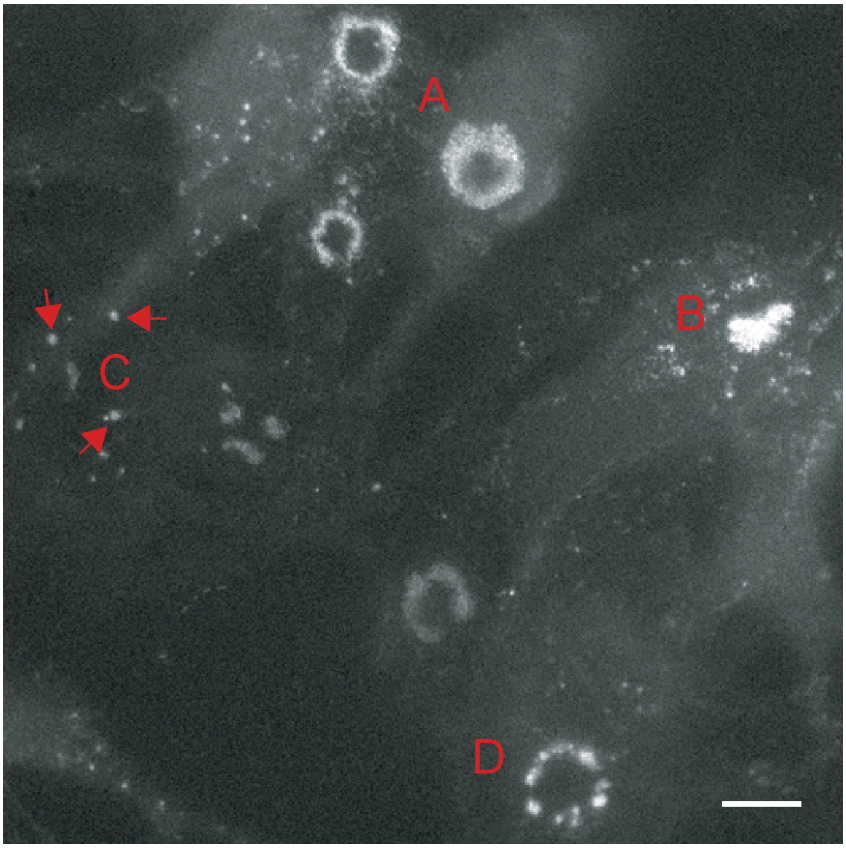


**Fig. 4.2 Podosome structures in v-Src$^{+}$/N-WASP$^{-/-}$ cells transduced with WT GFP-N-WASP.**

WT GFP-N-WASP cells were plated on fibronectin-coated glass bottom 35 mm dishes (Mattek) and incubated overnight at 37°C. GFP-N-WASP localization to podosomes was visualized by fluorescence microscopy (60X).

(A) Circular array of podosomes; (B) extended, bar-like podosome; (C) punctate podosomes; arrows point to punctuate structures; (D) circular array of punctate podosomes that are likely precursors to ring-like podosomes. Scale bar = 10 μm.

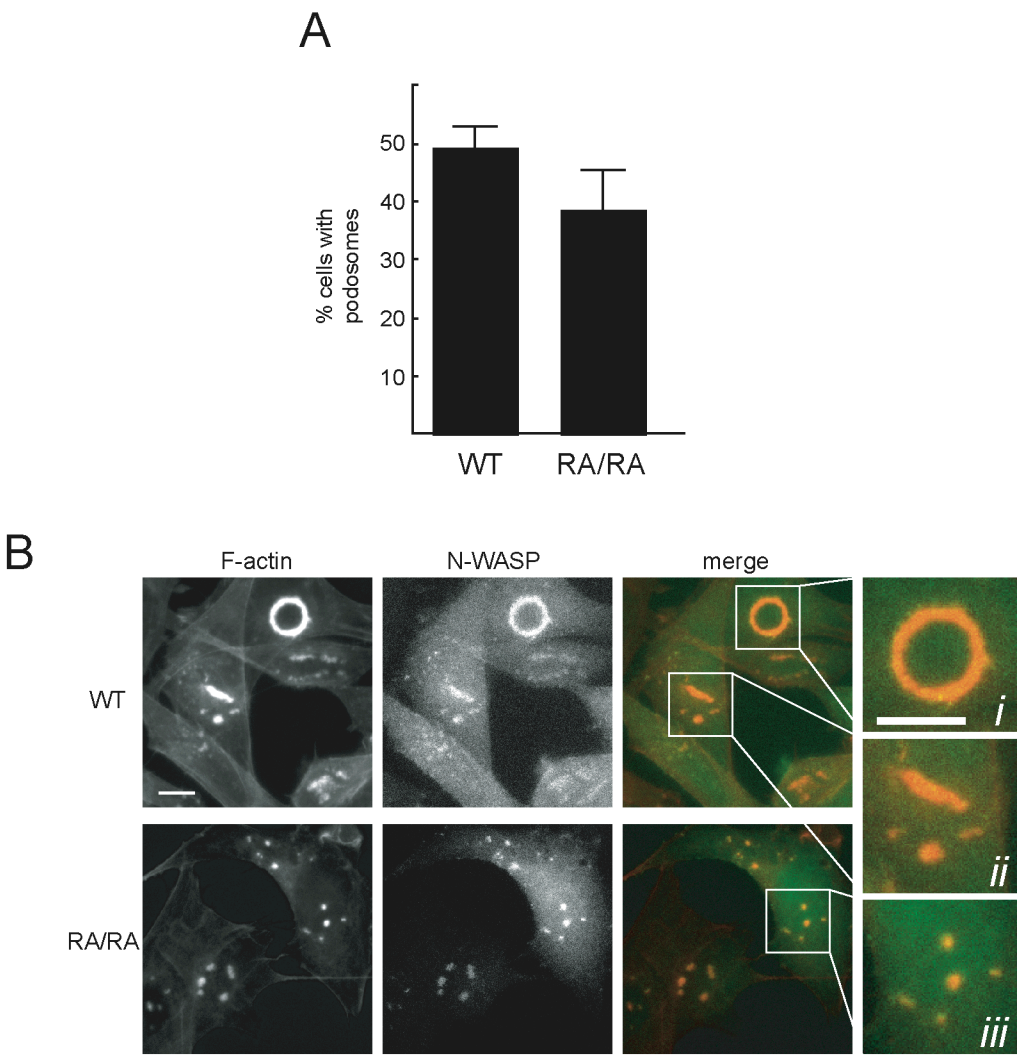


**Fig. 4.3 Podosome formation and structures in v-Src$^{+}$/N-WASP$^{-/-}$ cells rescued by WT and RA/RA GFP-N-WASP.**

(A) Percentage of podosome-positive cells. WT and RA/RA GFP-N-WASP cells were plated on fibronectin-coated coverslips. After 24 h, cells were fixed and stained with Alexa594-phalloidin. In each experiment (performed on different days), complete image datasets were obtained from two coverslips for each construct (150 microscope fields, 2300-5300 cells, per coverslip) and the entire dataset was analyzed blind. Data shown are mean ± S.D. from 3 independent experiments.

(B) Representative images of WT and RA/RA GFP-N-WASP cells 24 h after plating on fibronectin-coated coverslips. Cells were fixed, stained with Alexa594-phalloidin (red) and visualized by fluorescence microscopy. Boxed regions are magnified to display three podosome classes: (i) rings, (ii) bars, and (iii) puncta. Bar = 10 μm.

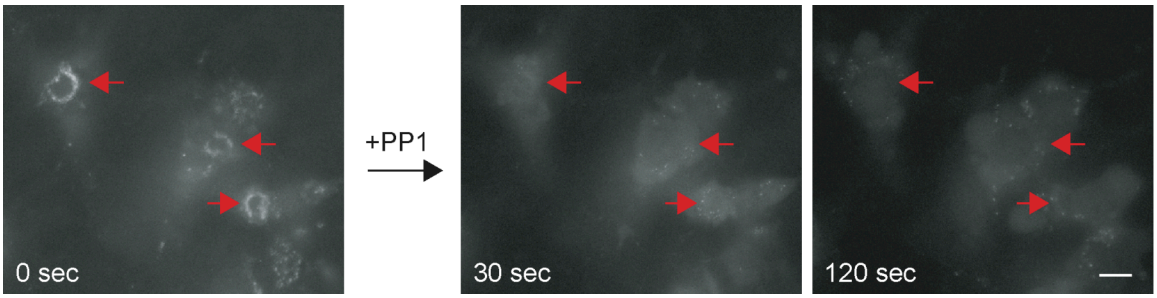


**Fig.4.4 GFP-N-WASP localization to podosomes requires Src kinase activity.**

WT GFP-N-WASP cells were plated on fibronectin-coated glass bottom 35mm dishes (Mattek) and incubated overnight at 37°C. GFP-N-WASP localization to podosomes was visualized by fluorescence microscopy (60X). 10 μM PP1 was added to the growth medium. Images were acquired every 30 s. Arrows denote sites of podosome structures. Scale bar = 10 μm.

Live imaging of these cells showed that large podosome arrays were highly dynamic--these structures fused, fragmented, assembled *de novo* and dissolved over time. This is consistent with live imaging of podosome structures in macrophages and osteoclasts (Destaing et al., 2003; Evans et al., 2003). We observed that podosomes in v-Src transformed cells undergo a maturation process. Punctate podosomes were often patterned in a circular array (Fig. 4.2 D). These arrays may be precursors to the circular podosomes we also observed in cells (Fig. 4.2 A). We observed bar-like arrays that extended and fused to form circular podosome arrays (Fig. 4.5). Although these maturation events occurred within minutes (osteoclastogenesis occurs over days), these large scale podosome rearrangements are reminiscent of the re-organization of podosome structures in osteoclasts, where podosomes evolve from punctate clusters to rings and finally to belts as cells undergo osteoclastogenesis (Jurdic et al., 2006). We conclude that podosomes are highly dynamic structures, whose organization might be affected by interactions between the actin network and membrane-associated N-WASP.

To test for differences in podosome size and organization between WT and RA/RA cells, we focused on the podosome-containing cells from three independent datasets (quantification was performed blind). We quantified the percentage of these cells that contained large podosome structures, defined as those containing "bars" (podosome arrays with length/width ≥ 3; Fig. 4.3 (ii)) and

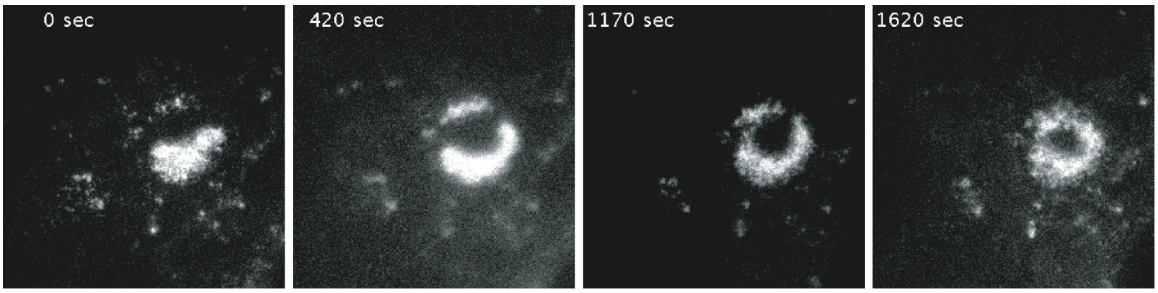


**Fig. 4.5 Maturation of extended, bar-like podosomes into ring podosome structures.**

WT GFP-N-WASP cells were plated on fibronectin-coated glass bottom 35mm dishes (Mattek) and incubated overnight at 37°C. GFP-N-WASP localization to podosomes was visualized by fluorescence microscopy (60X). Images were acquired every 30 s.

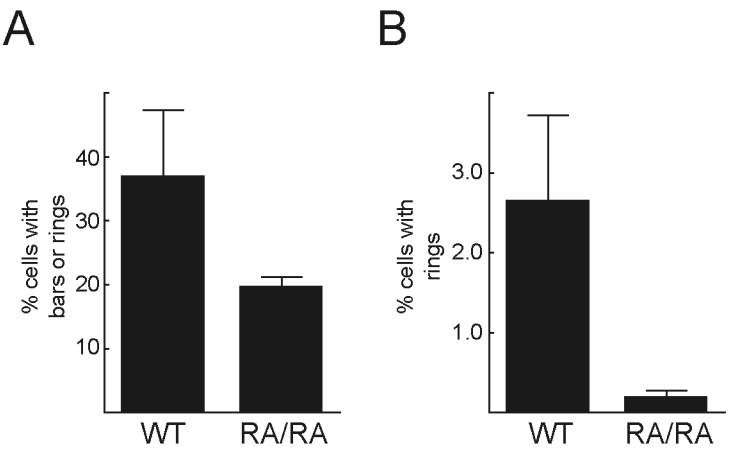


**Fig. 4.6 RA/RA GFP-N-WASP cells are defective in the formation of large and ring podosome structures.**

(A) Percentage of podosome-positive cells with bars and/or rings (see main text for definition). WT and RA/RA GFP-N-WASP cells were plated on fibronectin-coated coverslips. After 24 h, cells were fixed and stained with Alexa594-phalloidin. In each experiment (performed on different days), complete image datasets were obtained from two coverslips for each construct (150 microscope fields, 2300-5300 cells, per coverslip) and the entire dataset was analyzed blind. Data shown are mean ± S.D. from 3 independent experiments, $p < 0.03$ by Student's T-test.

(B) Percentage of podosome-positive cells with rings determined as described in (A). Data shown are mean ± S.D. from 3 independent experiments, $p < 0.01$.

"rings" (defined as a circular array of contiguous podosomes; Fig. 4.3 (i)). Compared to the RA/RA cells, twice as many WT cells had podosome bars or rings (Fig. 4.6 A, $p < 0.03$, T-test). Moreover, WT cells were ~10 times more likely than RA/RA cells to assemble a ring of contiguous podosomes (Fig. 4.6 B, $p < 0.01$). We obtained similar results with a second batch of FACS-sorted cells that expressed higher levels of both WT and RA/RA GFP-N-WASP (data not shown).

To further characterize the differences between WT and RA/RA GFP-NWASP in podosome formation, we quantified the size of podosomes formed in both cells as well as their dynamics over time using live imaging. We measured the size (area) of individual bars, rings, and puncta, restricting our analysis to WT and RA/RA cells that had at least one podosome bar or ring (thus, we excluded from this analysis the large fraction of RA/RA cells that lacked podosomes entirely or had only very small puncta). These data revealed a population of large podosomes (> 20 $\mu m^2$) that were ~5 times more abundant in the WT cells (Fig. 4.7 B), although the average number of podosomes per cell was similar for WT and RA/RA cells.

To determine whether podosome dynamics are affected in RA/RA cells, we measured the change in podosome size and fluorescence over time in both cell types. Using live imaging, we qualitatively compared podosome size and fluorescence in WT and RA/RA cells. In these preliminary experiments, WT

podosomes maintained their overall structure (Fig. 4.8 A: eg. three rings maintain their circular structure over many minutes), whereas RA/RA podosomes disassembled over similar time periods (Fig. 4.8 A: in RA/RA images, top right bar-like podosomes decrease in fluorescence intensity). It will be interesting to investigate these dynamics at shorter time intervals to assess the differences between WT and RA/RA podosomes. Nonetheless, these preliminary results in live cells may reflect the membrane-actin interactions that have been disrupted in RA/RA cells and also corroborate our data in fixed cells. We conclude that RA/RA N-WASP is defective in the assembly of large podosome arrays in v-Src-transformed fibroblasts.

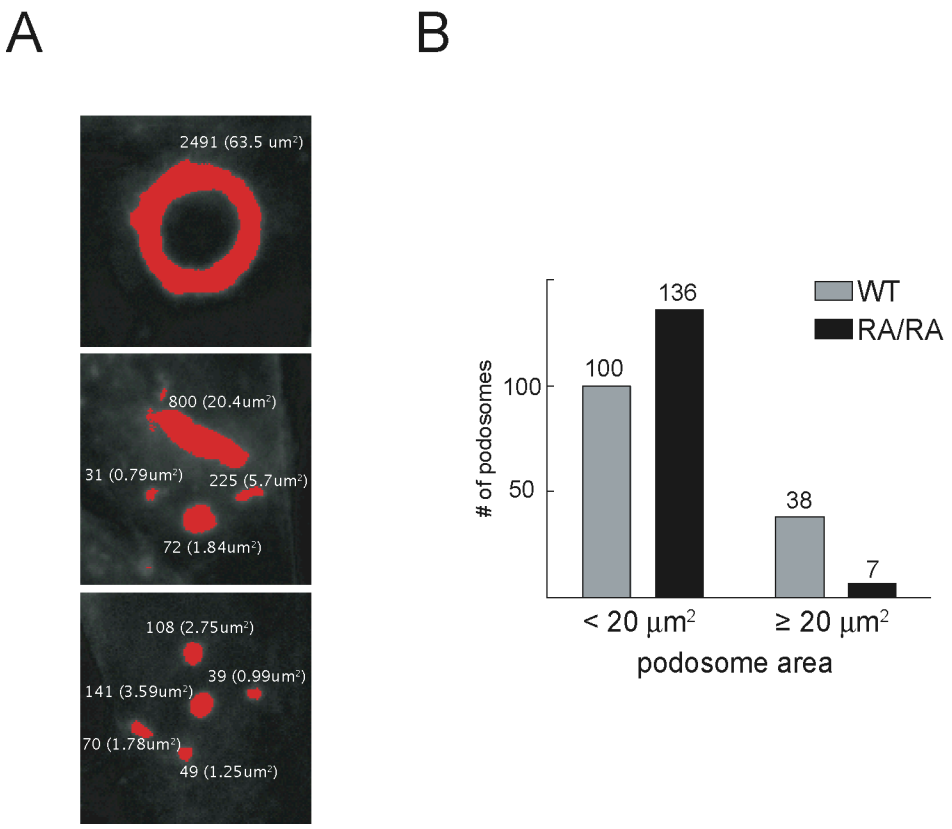


**Fig. 4.7 Quantification of podosome sizes in WT and RA/RA GFP-N-WASP cells.**

(A) Thresholded images of podosomes from representative podosome positive cells (note: (A) is same as magnified inset in Fig. 4.3 B). Thresholding was performed in ImageJ. The size in pixels and in corresponding $\mu m^2$ conversion is listed next to each podosome structure.

(B) Areas of podosome rings, bars, and puncta were measured in 50 randomly selected WT and RA/RA cells, all of which contained at least one podosome bar or ring. Podosome structures were classified as "small" (< 20 $\mu m^2$) or "large" (> 20 $\mu m^2$) (for reference, the ring in the upper panel of (A) is ~64 $\mu m^2$, whereas the bar in the middle panel in (A) is ~20 $\mu m^2$).

A

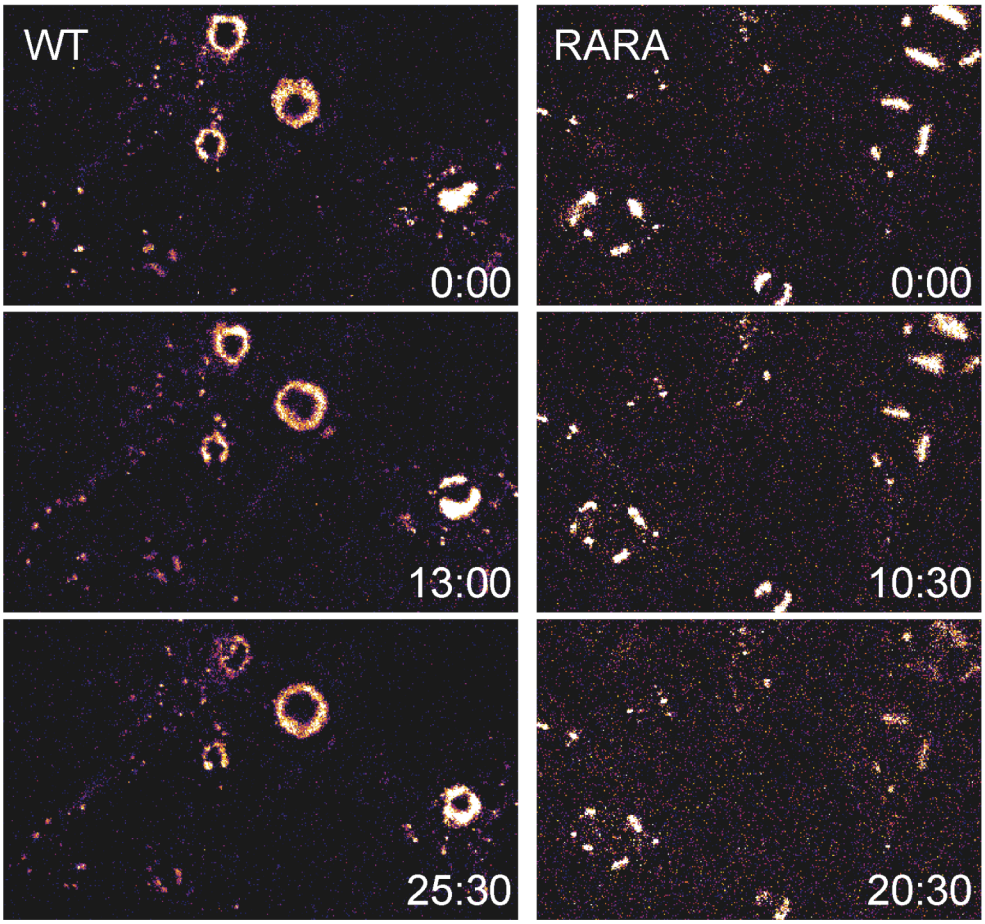
WT
RARA
0:00
0:00
13:00
10:30
25:30
20:30

B

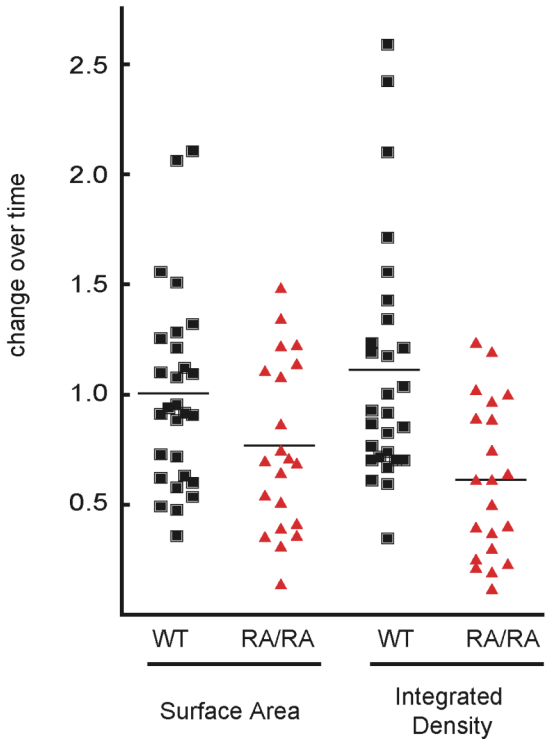
change over time
2.5
2.0
1.5
1.0
0.5
WT
RA/RA
WT
RA/RA
Surface Area
Integrated Density

**Fig. 4.8 Podosome dynamics in WT and RA/RA GFP-N-WASP cells.**
(A) Timelapse images of WT and RA/RA GFP-N-WASP podosomes. RA/RA podosome structures seem to dissolve over time. GFP fluorescence images are pseudocolored in ImageJ to emphasize changes in fluorescence intensity over time. Fluorescence images were taken every 30 s. Elapsed time is in seconds. (B) Quantification of the change in podosome surface area and integrated density (fluorescence x surface area) over time. Graph represents the relative change in surface area and integrated fluorescence between the first and last image of the timelapse. A value of 1 indicates that there is no change in podosome size or intensity. A value higher than one suggests that podosomes grew over time, while a value less than 1 indicates the podosome decreased in size and/or fluorescence over the length of the timelapse.

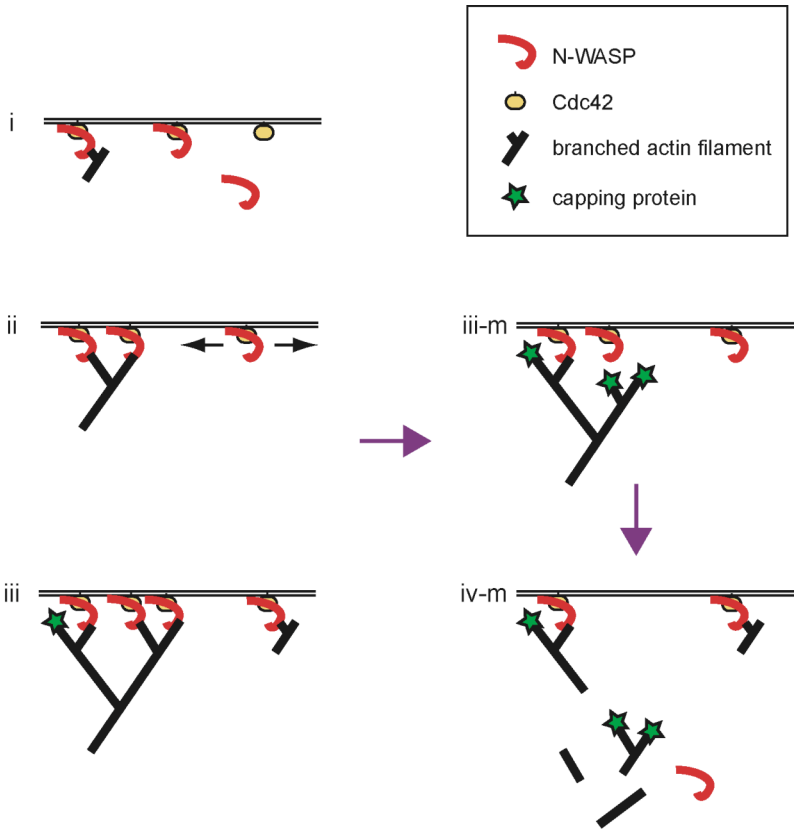


**Fig. 4.9 Model of WH2-mediated podosome organization in WT and RA/RA cells.**

A nascent actin network (i) can capture neighboring, diffusing N-WASP molecules (ii) through the interactions of available barbed ends and the N-WASP WH2 domains. Subsequent nucleation and branch formation locally generate more available barbed ends, which in turn can cluster and concentrate more N-WASP molecules and create extended, highly cross-linked actin networks and podosomes (iii).

RA/RA molecules are defective in capturing actin filament barbed ends and in podosome organization. Filament barbed ends that are not captured or protected are capped by capping protein (iii-m). Subsequently, the unorganized actin networks are disassembled or remain as smaller, punctate structures (iv-m).

## Discussion

The formation, organization and dynamics of podosome structures were unknown in v-Src transformed fibroblasts. How do podosomes assemble? How do larger order podosome arrays organize? The striking phenotype comparison of WT and RA/RA GFP-N-WASP v-Src$^{+}$/N-WASP$^{-/-}$ cells suggest that interactions between N-WASP and the actin filament network may play an essential role in the establishment and maintenance of larger-ordered podosome structures.

Although the precise mechanisms that determine podosome size and organization remain unknown, a recent four-dimensional imaging study of macrophage podosomes revealed complex dynamic behavior, including *de novo* assembly of small puncta, fusion of individual puncta to make clusters, and fragmentation of large podosome clusters (Evans et al., 2003). Our preliminary live imaging experiments corroborate these podosome events in v-Src transformed cells. However, in contrast to macrophages, which only contain punctate-like podosomes, we observe much larger and complex organization of podosomes in v-Src transformed cells (ie. extended bar and circular podosome arrays). Importantly, we observed that mutations that affect membrane-actin interactions lead to a decreased ability to form and/or maintain these larger podosome arrays. We propose that N-WASP clustering, mediated by

WH2/barbed end interactions, plays a role in the propagation and/or stabilization of extended podosome networks (Fig. 4.9).

Live imaging of v-Src transformed cells revealed that larger podosome structures are highly dynamic. The maintenance of constantly changing structures requires the continual assembly, disassembly, and reassembly of the actin network. Our model indicates that the capture of actin filaments by membrane-tethered WH2 domains is required for these observed changes. Our *in vitro* and *in vivo* experiments both support this model. Defects in membrane-actin attachment *in vitro* result in formation of actin comet tails but defective maintenance. Similarly in cells, formation of podosomes is not affected in RA/RA mutants, but maintenance of larger podosome structures especially ring-like structures is defective. In other work, actin polymerization dynamics plays a role in this process. RNAi knockdown of the actin disassembly factor, cofilin, results in podosomes that are smaller (Yamaguchi et al., 2005). Given the potential involvement of podosomes in metastasis, it will be interesting to compare the invasivity of WT and RA/RA cells.

## Materials and Methods

### Construction of WT and RA/RA GFP-N-WASP retroviral vectors.

Full-length GFP-N-WASP from pCDNA3.1 (Papayannopoulos et al., 2005) was cloned into the pMXs-puro retroviral vector (a gift from Orion Weiner, UCSF), (Kitamura et al., 1995). For the N-WASP RA/RA mutant, R410A and R438A mutations in each of the WH2 domains were introduced by Quikchange mutagenesis (Stratagene) and were verified by DNA sequencing. WT and RA/RA GFP-N-WASP in pMXs-puro were transiently transfected into Phoenix retrovirus packaging cells by the calcium phosphate transfection method (Pear et al., 1993). Culture medium containing retroviruses was harvested 5 days after transfection.

### Cell lines

Cells were grown in Dulbecco's modified Eagle's medium (DMEM) supplemented with 10% fetal bovine serum at 37°C and 5% $CO_2$. v-Src-transformed N-WASP $^{-/-}$ fibroblasts were created by infecting N-WASP$^{-/-}$ fibroblasts (Snapper et al., 2001) with a v-Src retrovirus (Cohen et al., 2005). Selection for v-Src-positive cells was performed in growth media containing 1.8 μg/ml puromycin (InvivoGen) as previously described (Shah and Shokat, 2002). v-Src-transformed N-WASP$^{-/-}$ fibroblasts were subsequently infected with WT or RA/RA GFP-N-WASP retroviruses in the presence of polybream (4 μg/ml). 3 h after infection, the viral supernatant was removed and replaced with fresh

medium (10% fetal bovine serum/DMEM). WT and RA/RA cells were FACS-sorted to obtain cells that express similar levels of GFP-N-WASP. Cells were maintained in 1.8 μg/ml puromycin.

**FACS sorting.**

To ensure a more homogeneously N-WASP-expressing population of cells, we FACS-sorted cells for equal fluorescence levels of WT and RA/RA GFP-N-WASP. Because we could not predict the behavior of podosome forming cells based on their levels of expression, we FACS-sorted for four populations of cells: first, we sorted for the all GFP-expressing cells. These cells were expressed heterogeneous levels of GFP fluorescence. Second, we FACS sorted this GFP+ population for cells expressing low, medium and high expressing cells as gated by their GFP fluorescence intensity levels. We ultimately chose to test two populations of FACS sorted cells: the low and medium expressing GFP-N-WASP cells. The cells expressed similar levels of GFP-N-WASP, v-Src, and VASP, which has a related-WH2 domain and has been localized to podosomes (Fig. 4.1 A).

**Live imaging of podosomes**

Cells were plated onto 35 mm fibronectin-coated (10 ug/ml) glass bottom dishes (Mattek) and grown at 37°C overnight. 10 mM Hepes pH 7.0 was added to the growth medium and cells were imaged at RT through a 60X oil immersion

objective using an inverted Olympus microscope. GFP-N-WASP fluorescence images were acquired every 30 s. Image stacks were processed using ImageJ.

**Podosome assay**

Round coverslips (11 mm) were coated with 150 μl of 10 μg/ml fibronectin (Sigma) at room temperature for 1 h and washed thoroughly with PBS. Cells were seeded onto fibronectin-coverslips and grown for 24 h, fixed with 4% formaldehyde in PBS, permeabilized with 0.5 % Triton-X-100 in cytoskeleton buffer (10 mM MES pH 6.1, 138 mM KCl, 3 mM MgCl2, 2 mM EGTA, 0.32 M sucrose), and stained with DAPI (1 μg/ml) and Alexa594-phalloidin (Molecular Probes). Coverslips were mounted using Vectashield (Vector Laboratories) and imaged by fluorescence microscopy using a 40X dry objective.

Cells from three independent experiments (plated and stained on different days), two coverslips per experiment, were analyzed. For each coverslip, 150 fields covering the entire coverslip were digitally recorded, and the images were analyzed blind. Podosome structures were defined by colocalization of GFP-N-WASP and Alexa594-phalloidin. Podosome morphologies were categorized as puncta, bars, and rings. Contiguous podosome arrays forming a complete circle were classified as "rings", whereas linear and curved podosome arrays with lengh/width t ≥ 3 were classified as "bars" (see Fig. 4.3 B). Comparisons were analyzed by Student's T-test.

# Chapter 5

# Discussion and Future Directions

Actin assembly at the membrane surface is governed by the coordinated regulation of NPFs, which are recruited from the cytoplasm to the membrane via signaling cascades. In the case of intracellular vesicle motility, cytosolic N-WASP is recruited to endosomes and lysosomes by a signaling pathway involving Cdc42 and PIP2, to form polarized force-generating actin networks (Papayannopoulos et al., 2005; Taunton et al., 2000). We have used a combination of experiments in extracts, a pure protein system, and mammalian cells to propose how N-WASP ensures persistent and robust actin assembly on fluid membrane surfaces and, further, how this may lead to the organization of more complex actin structures in cells. Our findings are three-fold: first, we identified a new mechanism to explain how a growing actin network remains bound to the membrane surface; second, we developed a novel biomimetic system to study actin-based motility at the membrane. Third, our data suggest that actin/WH2 interactions play a critical role in podosome organization.

Our identification of a novel mechanism of adherence of the actin network to the membrane involves the WH2 domain, which was previously known only to bind actin monomers for nucleation (Kelly et al., 2006; Marchand et al., 2001). In its new role as a critical determinant in the localization of N-WASP molecules to the membrane-actin interface of rocketing vesicles, WH2 domains tether the actin network to the membrane surface by interacting with actin filament barbed ends. We demonstrated that this interaction is essential for the adhesion of comet tails to membranes *in vitro* and for the organization of large podosome

structures in cells. Based on these collective findings, we posit a model in which N-WASP molecules interact weakly with a dendritic array of actin filament barbed ends to maintain adhesion of the fast-growing actin network. Because N-WASP binds to many other molecules via its EVH1 domain and proline-rich domain, the interaction between barbed ends and N-WASP suggests that barbed ends may recruit other signaling molecules to the membrane surface.

Our development of a novel biomimetic system extends the platform initially created by Carlier and colleagues (1999) by inserting two new parameters that more physiologically reflect actin assembly in the cell (Bernheim-Groswasser et al., 2002). First, actin assembly is activated by a signaling cascade with all soluble components that must be recruited to the membrane. Second, our substrate is a synthetic fluid PIP2 lipid bilayer that can modified to contain any lipid component.

**The role NPF capture by barbed ends in membrane motility.**

The direct interactions between actin filament barbed ends and NPFs at the membrane surface plays several roles in actin-based membrane motility. The capture of NPFs by barbed ends ensures that nucleation occurs at already enriched polymerization areas. This maintains persistent and localized actin assembly. Indirectly, this mechanism restricts polymerization to one side of the membrane. Thus, capture of NPFs by filaments at the membrane is a form of

reinforcement. Also, the affinity of actin filament barbed ends for N-WASP molecules can drive the formation larger actin structures. Separate, diffusing actin networks on the membrane surface may cluster and merge due to N-WASP's ability to interact with actin filaments directly (Fig. 4.9). This is a form of self-organization. We propose that this mechanism plays a role in the formation and maintenance of larger actin structures, such as the ring and bar-like podosomes of v-Src transformed cells. Large podosome structures are required *in vivo*. Experiments have demonstrated that larger podosome structures are required for the robust degradative activity of cancerous cells (Brabek et al., 2004).

The organization of actin filaments and NPFs at the membrane surface are critical to formation and maintenance of polarized, force-producing actin networks. Actin filaments exist at the membrane surface of moving vesicles not as individual filaments but as part of a dendritic network (Mogilner, 2006; Mogilner and Oster, 2003). The architecture of the membrane-actin interface is such that membrane-bound N-WASP molecules are within close proximity to the dendritic array of actin filament barbed ends pointing towards them (Fig.1). Once a new daughter filament has been nucleated by the Arp2/3 complex, this filament barbed end has limited potential interactions because its pointed end is relatively fixed in space. These potential interactions include: (1) additional Arp2/3 complex binding near the barbed ends of filaments, mediated by the WH2 interactions between filaments and the Arp2/3 complex. This may explain how

Arp2/3-dependent branching can occur near the barbed end (Laurent et al., 1999; Pantaloni et al., 2000) and how this mechanism is employed to control localized nucleation; (2) the filament barbed end can encounter an actin monomer. This event relies on the random collision and correct positioning of an actin monomer to the filament barbed end; (3) the barbed end can be capped by capping protein. However, at the membrane-actin interface, WH2-ATP-actin monomer complex or WH2 interactions with actin filament barbed ends suggest that the WH2 domain reduces the probability of filament capping at the membrane;(4) the WH2 domain, bound to an ATP-actin monomer, captures a filament barbed end and extends the filament by at least one actin monomer. A WH2-mediated capture, elongation and release mechanism guarantees that filament nucleation and elongation occurs towards the membrane, that actin assembly is processive and that membrane tethering is maintained.

What other roles do WH2 domains play in the establishment or maintenance of actin networks for motility? The interaction of N-WASP with actin filament barbed ends may be a general mechanism for recruiting other regulatory molecules to the membrane-actin interface. One potential candidate is the NPF, SCAR/WAVE. It remains unclear how SCAR/WAVE proteins are recruited and activated at the leading edge of migratory cells. Experiments in cells have also demonstrated a role for actin filaments as possible diffusion barriers that trap regulatory proteins at the leading edge (Weisswange et al., 2005). This may be

a general mechanism that ensures persistent signaling and/or actin assembly at the leading edge of cells.

**Physical regulation at the membrane-actin interface**

If the interactions between WH2 domains, actin monomers and actin filaments are weak, then how can this set of interactions withstand the pulling forces generated (in the nanonewton scale; (Marcy et al., 2004))? In cells, actin filaments at the membrane surface form a highly branched, tight-knit network. Based on these data, we believe that these connections are multivalent, low-affinity but high-avidity interactions. One question is why have cells adopted this form of mechanism to maintain connections between the cytoskeleton and membrane. There are other biological processes that utilize this form of low-affinity, but high avidity interactions. Leukocyte rolling and tethering, the mechanism by which leukocytes dynamically attach and detach from the blood vessel wall (Calle et al., 2006) uses this similar type of mechanism. Both of these dynamic systems utilize the combination of multivalent, weak interactions to collectively provide strong tethering, yet allow for rapid breaking of interactions.

Actin-based motility is a biological process that is not only regulated biochemically, through signaling proteins and polymerization regulatory proteins, but also physically, through adhesion between membrane proteins, lipids and the actin network and by the fluidity of the membrane surface. What is the specific

mechanism of physical regulation? In one model, tethered filaments maintain adhesion of the actin network and "pull" against the membrane while detached filaments elongate and "push" against the membrane (Mogilner and Oster, 2003). In another model, pushing and pulling are not separated: elongating filaments are constituitively bound to the membrane (Dickinson et al., 2004; Dickinson and Purich, 2002). Our findings on the actin assembly process can be extrapolated to form hypotheses on physical regulation of actin-based motility. We found that the addition of the actin polymerization inhibitor, Latrunculin B, to motility reactions *in vitro* did not result in catastrophic detachment of actin comet tails. This result suggests that actin polymerization is not required for tethering. Further, this observation implies that actin polymerization may be required for detachment or breakage of tethering bonds. This is consistent with our results that demonstrate that inhibition of Arp2/3 complex activity does not cause detachment of actin comet tails from the membrane. Thus, our data are consistent with a combination of the two presented models. WH2 domain interactions with actin filament barbed ends may provide a continual state of adhesion but do not produce force, while nucleation by the Arp2/3 complex may be required to break the tethering bonds and generate force against the membrane (Alberts and Odell, 2004).

**Vesicle motility reconstituted with pure components.**

Our biomimetic system extends previous platforms to include more physiological components (i.e. signaling components and a membrane substrate)

which ultimately open new avenues of study *in vitro*. This system will allow us to study how switch-like cycles (i.e. RhoGTPase) and lipid fluidity or diffusion of molecules in the membrane affect actin network organization.

While in the cell, molecules dynamically exchange between the membrane and cytosol, in current biomimetic systems, NPFs are adsorbed to plastic or membrane surfaces. The nonspecific nature of this adsorption renders them constituitively active and unregulated (Bernheim-Groswasser et al., 2002). Cellular signaling molecules and lipids like PI(3,4,5)P3 do not localize to the membrane constituitively nor exist at high concentrations at a cell's resting state. Signaling molecules are inactive and cycle between on and off states. Our system utilizes components that are either autoinhibited (N-WASP) or bound by inhibitors (Cdc42/GDI) (Buck et al., 2004; Hoffman et al., 2000).

One key element of our system involves the GTPase cycle. Although we specifically use GTP$\gamma$S to activate Cdc42, we envision the future incorporation of the complete GTPase pathway upstream of N-WASP. This includes the use of hydrolyzable GTP and GTPase activating proteins (GAPs) that inactivate RhoGTPases. The incorporation of an inhibitory pathway may further sharpen polarization sites: the membrane-actin interface may protect signaling complexes from inhibition. In the same regard, stray signaling molecules away from the polarization site may be quickly inactivated.

An important variable is the proper order of addition of actin assembly factors towards the generation of polarized actin networks. We note this critical variable is as of yet underappreciated by the field. The order of N-WASP recruitment from solution to the membrane can produce two distinct mechanisms of polarized tail formation. We propose that this new mechanism is based on a positive feedback loop between actin polymerization and N-WASP recruitment to the membrane. This mechanism is closest to a model previously proposed to explain symmetry breaking based on stochastic fluctuations of actin polymerization (van Oudenaarden and Theriot, 1999); that slight asymmetries in actin polymerization can lead to amplification and persistence of the asymmetry.

A key component of our biomimetic system is the use of a synthetic lipid bilayer. Experiments have shown that the actin network can regulate the fluidity of the membrane surface (Liu and Fletcher, 2006). Likewise, it will be interesting to determine how fluidity of the membrane affects the formation and maintenance of actin networks. NPFs and RhoGTPases that are localized to the membrane surface can diffuse along the membrane. This mobility may allow molecules to cluster and concentrate on fluid membranes. Thus, we believe it is essential to observe the components of actin-based motility in a physiologically relevant state.

Along the same lines, we have shown that the incorporation of cholesterol into PIP2 membranes slightly enhances the actin polymerization activity of N-

WASP in bulk solution assays (Papayannopoulos et al., 2005). Further, the composition of the membrane may affect the different modes of symmetry breaking. At extremely high concentrations of PIP2, N-WASP may localize too quickly to the membrane and polymerize a dense shell of actin. There may be a threshold of PIP2 concentration which distinguishes the different modes of symmetry breaking possibly by regulating the concentration of active N-WASP at the membrane surface. Our preliminary results suggest that PIP2 levels may play some positive role in Cdc42 recruitment and ultimately enhance N-WASP activation. Thus, a synthetic lipid bilayer, which can be manipulated to allow examination of these factors, is essential in the further study of N-WASP and membrane motility. The development of this novel biomimetic system will advance the study of actin assembly and made it possible for us to discover a new role for WH2 domains in membrane movement.

# Appendix A

## Pathogen Motility in WT and RA/RA cells

Pathogens hijack the host cell actin machinery for intracellular motility and cell-to-cell invasion (Munter et al., 2006). They assemble polarized actin comet tails to propel themselves through the cytoplasm or in some cases along the membrane surface. *Shigella Flexneri* and Vaccinia virus both require N-WASP for their motility. *Shigella Flexneri* expresses the bacterial surface protein IcsA to recruit N-WASP to its surface and to promote its intracellular motility. Actin comet tails are assembled directly on the bacterial surface. On the other hand, *Vaccinia virus*, which resides on the outside of the cell, inserts the viral protein A36R into the host cell cytoplasm to also recruit N-WASP for formation of its actin comet tail. Interestingly, the actin comet tail is not directly attached attached to the virus but, rather is tethered to the membrane on which *Vaccinia virus* is bound to. In other words, the membrane is sandwiched between *Vaccinia virus* and the actin comet tail. Since these pathogen systems require N-WASP for their motility, we wondered whether they also required WH2-mediated membrane-actin tethering.

We infected v-Src$^{+}$/N-WASP$^{-/-}$ cells transduced with WT and RA/RA GFP N-WASP with *ShigellafFlexneri* and Vaccinia Virus and monitored pathogen motility. *Shigella flexneri* formed actin comet tails equally well in WT and RA/RA GFP-N-WASP cells (Fig. A1 A). Motile *Shigella flexneri* also moved with similar speeds in WT versus RA/RA cells (Mean velocities: WT = 11.13 ± 6.4 μm/min, n = 50; RA/RA = 12.96 ± 4.5 μm/min, n = 50) (Fig. A1 B). Strikingly, infection of

these cells with Vaccinia virus yielded a difference in comet tail lengths. Vaccinia virus comet tails in RA/RA cells were significantly shorted than those made in WT cells (Fig. A2 A, B).

The difference between these two bacterial motility systems is the presence of the membrane used by Vaccinia virus. While the speeds of Vaccinia virus in WT and RA/RA cells were not measured, the difference in tail lengths suggest that there will be a possible difference in speeds. If this is the case, then it suggests that tethering of actin filaments may be different on membrane surfaces than on less fluid surfaces like the bacterial cell surface.

Recent experimental evidence (Samarin et al., 2003; Soo and Theriot, 2005) and computational analysis (Alberts and Odell, 2004; Dickinson and Purich, 2002) demonstrate that membrane adhesion of the actin network is rate-limiting in pathogen motility. One of these models predicted that if the number of adhesive bonds is directly proportional to the density of the actin comet tail, then the average speed of the bacteria should be inversely correlated with speed. In other words, less tethering results in faster movement. In vitro, R438A is defective in membrane-actin adhesion. Consistent with the model above, prior to detaching, R438A propelled-lipid beads moves faster than WT lipid beads. If this model also holds true for pathogen motility in cells, then the attachment defect exhibited in our WH2 mutations in vitro would result in faster pathogen motility in vivo. It will be interesting to further examine the motility of Vaccinia Virus in RA/RA cells.

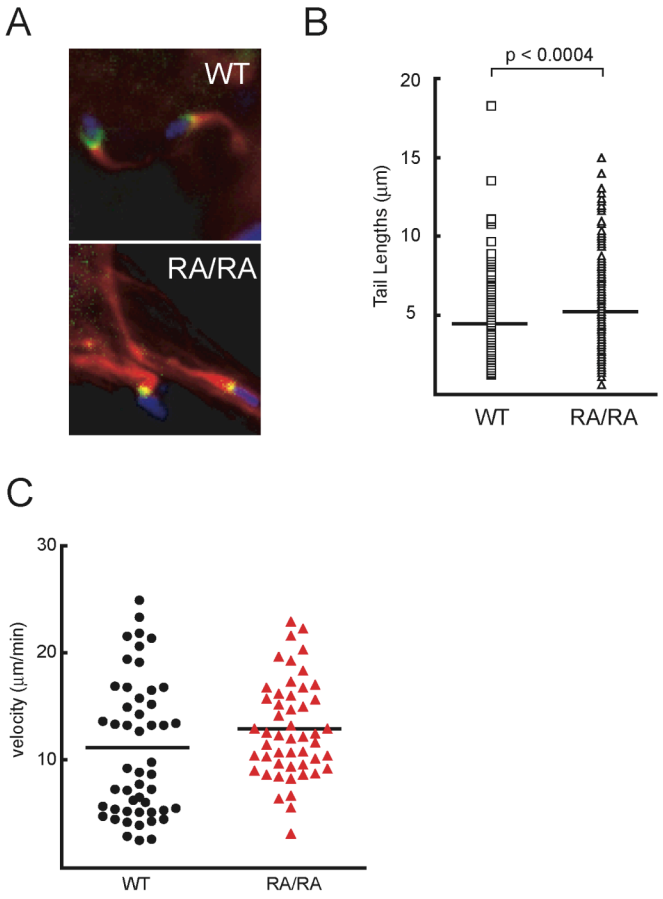


**Fig. A1 *Shigella flexneri* motility in v-Src$^{+}$/N-WASP$^{-/-}$ cells transduced with WT and RA/RA GFP N-WASP.**

(A) Representative images of *Shigella flexneri* comet tails. Cells infected with *Shigella flexneri* were fixed with 4% formaldehyde and stained with Alexa594 phalloidin and DAPI (1 μg/ml). (B) Comet tail lengths were measured in WT and RA/RA cells in (A). Analysis was performed blind. (C) WT and RA/RA GFP-N-WASP cells were plated on fibronectin-coated 35 mm glass bottom Petri dishes (Mattek). After 24 h, cells were infected with *Shigella flexneri*. Moving *Shigella flexneri* were identified by imaging the GFP-N-WASP localized to the bacteria.

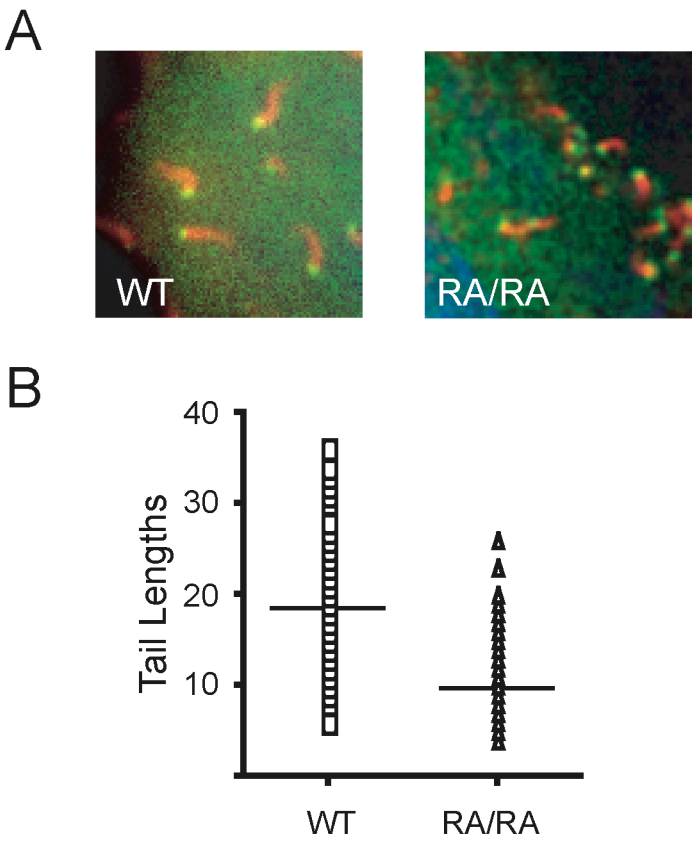


**Fig. A2 Vaccinia virus motility in v-Src$^{+}$/N-WASP$^{-/-}$ cells transduced with WT and RA/RA GFP N-WASP.**

(A) Representative images of Vaccinia virus comet tails. Cells infected with Vaccinia virus were fixed with 4% formaldehyde and stained with Alexa594 phalloidin and DAPI (1 μg/ml). (B) Comet tail lengths were measured in WT and RA/RA cells in (A). Analysis was performed blind.

### *Shigella Flexneri* motility assays

*Shigella flexneri* was grown in bovine heart infusion media (BHI). An overnight culture was grown in BHI, diluted 1:100, and grown to mid-logarithmic phase (optical density at 600nm ~ 0.3). Bacteria were pelleted, and resuspended in DMEM containing 10% FBS. The bacteria were overlayed onto a cell monolayer at a multiplicity of infection of 100, and the infection was initiated by centrifuging the plates at 700 g for 10 min. The plates were transferred to a 37°C incubator for 90 min to allow for internalization. To remove and kill extracellular bacteria, cell monolayers were washed with PBS and resuspended with medium containing 50 μg/ml gentamicin. Cells were transferred to a 37°C incubator for 120 min to allow for shigella motility. Cells were fixed with 4% formaldehyde and permeabilized with 0.5 % Triton-X-100 in cytoskeleton buffer. The cells were then stained with DAPI (1 mg/ml) and Alexa-594 phalloidin (Molecular Probes). Coverslips were mounted using Vectashield (Vector Laboratories), and imaged on an Olympus Inverted microscope using a 40x dry objective. Comet tails were visualized by fluorescence microscopy. The comet tail lengths were quantified using ImageJ and the medians were calculated and plotted using GraphPad Prism. The comet tail lengths were analyzed using the Mann-Whitney test.
To measure Shigella Flexneri speeds, cells plated on 35 mm glass bottom dishes (Mattek), were infected with Shigella flexneri as described above and visualized by fluorescence microscopy. Bacterial speeds were measured by imaging GFP-N-WASP localized to the poles of moving bacteria.

**Vaccinia virus motility assays were performed in collaboration with the laboratory of Dan Kalman (Emory University) (Reeves et al., 2005).**

# Appendix B

# References

Alberts, J. B., and Odell, G. M. (2004). In silico reconstitution of Listeria propulsion exhibits nano-saltation. PLoS Biol *2*, e412.

Baksh, M. M., Jaros, M., and Groves, J. T. (2004). Detection of molecular interactions at membrane surfaces through colloid phase transitions. Nature *427*, 139-141.

Baldassarre, M., Ayala, I., Beznoussenko, G., Giacchetti, G., Machesky, L. M., Luini, A., and Buccione, R. (2006). Actin dynamics at sites of extracellular matrix degradation. Eur J Cell Biol *85*, 1217-1231.

Bear, J. E., Svitkina, T. M., Krause, M., Schafer, D. A., Loureiro, J. J., Strasser, G. A., Maly, I. V., Chaga, O. Y., Cooper, J. A., Borisy, G. G., and Gertler, F. B. (2002). Antagonism between Ena/VASP proteins and actin filament capping regulates fibroblast motility. Cell *109*, 509-521.

Bernheim-Groswasser, A., Wiesner, S., Golsteyn, R. M., Carlier, M. F., and Sykes, C. (2002). The dynamics of actin-based motility depend on surface parameters. Nature *417*, 308-311.

Blanchoin, L., and Pollard, T. D. (2002). Hydrolysis of ATP by polymerized actin depends on the bound divalent cation but not profilin. Biochemistry *41*, 597-602.

Blanchoin, L., Pollard, T. D., and Mullins, R. D. (2000). Interactions of ADF/cofilin, Arp2/3 complex, capping protein and profilin in remodeling of branched actin filament networks. Curr Biol *10*, 1273-1282.

Boukellal, H., Campas, O., Joanny, J. F., Prost, J., and Sykes, C. (2004). Soft Listeria: actin-based propulsion of liquid drops. Phys Rev E Stat Nonlin Soft Matter Phys *69*, 061906.

Brabek, J., Constancio, S. S., Shin, N. Y., Pozzi, A., Weaver, A. M., and Hanks, S. K. (2004). CAS promotes invasiveness of Src-transformed cells. Oncogene *23*, 7406-7415.

Brieher, W. M., Coughlin, M., and Mitchison, T. J. (2004). Fascin-mediated propulsion of Listeria monocytogenes independent of frequent nucleation by the Arp2/3 complex. J Cell Biol *165*, 233-242.

Buck, M., Xu, W., and Rosen, M. K. (2004). A two-state allosteric model for autoinhibition rationalizes WASP signal integration and targeting. J Mol Biol *338*, 271-285.

Calle, Y., Burns, S., Thrasher, A. J., and Jones, G. E. (2006). The leukocyte podosome. Eur J Cell Biol *85*, 151-157.

Cameron, L. A., Footer, M. J., van Oudenaarden, A., and Theriot, J. A. (1999). Motility of ActA protein-coated microspheres driven by actin polymerization. Proc Natl Acad Sci U S A *96*, 4908-4913.

Cameron, L. A., Svitkina, T. M., Vignjevic, D., Theriot, J. A., and Borisy, G. G. (2001). Dendritic organization of actin comet tails. Curr Biol *11*, 130-135.

Chen, W. T. (1989). Proteolytic activity of specialized surface protrusions formed at rosette contact sites of transformed cells. J Exp Zool *251*, 167-185.

Chereau, D., Kerff, F., Graceffa, P., Grabarek, Z., Langsetmo, K., and Dominguez, R. (2005). Actin-bound structures of Wiskott-Aldrich syndrome protein (WASP)-homology domain 2 and the implications for filament assembly. Proc Natl Acad Sci U S A *102*, 16644-16649.

Cohen, M. S., Zhang, C., Shokat, K. M., and Taunton, J. (2005). Structural bioinformatics-based design of selective, irreversible kinase inhibitors. Science *308*, 1318-1321.

Cooper, J. A., Walker, S. B., and Pollard, T. D. (1983). Pyrene actin: documentation of the validity of a sensitive assay for actin polymerization. J Muscle Res Cell Motil *4*, 253-262.

Destaing, O., Saltel, F., Geminard, J. C., Jurdic, P., and Bard, F. (2003). Podosomes display actin turnover and dynamic self-organization in osteoclasts expressing actin-green fluorescent protein. Mol Biol Cell *14*, 407-416.

Dickinson, R. B., Caro, L., and Purich, D. L. (2004). Force generation by cytoskeletal filament end-tracking proteins. Biophys J *87*, 2838-2854.

Dickinson, R. B., and Purich, D. L. (2002). Clamped-filament elongation model for actin-based motors. Biophys J *82*, 605-617.

Dueber, J. E., Yeh, B. J., Chak, K., and Lim, W. A. (2003). Reprogramming control of an allosteric signaling switch through modular recombination. Science *301*, 1904-1908.

Egile, C., Loisel, T. P., Laurent, V., Li, R., Pantaloni, D., Sansonetti, P. J., and Carlier, M. F. (1999). Activation of the CDC42 effector N-WASP by the Shigella flexneri IcsA protein promotes actin nucleation by Arp2/3 complex and bacterial actin-based motility. J Cell Biol *146*, 1319-1332.

Egile, C., Rouiller, I., Xu, X. P., Volkmann, N., Li, R., and Hanein, D. (2005). Mechanism of filament nucleation and branch stability revealed by the structure of the Arp2/3 complex at actin branch junctions. PLoS Biol *3*, e383.

Erickson, J. W., and Cerione, R. A. (2004). Structural elements, mechanism, and evolutionary convergence of Rho protein-guanine nucleotide exchange factor complexes. Biochemistry *43*, 837-842.

Evans, J. G., Correia, I., Krasavina, O., Watson, N., and Matsudaira, P. (2003). Macrophage podosomes assemble at the leading lamella by growth and fragmentation. J Cell Biol *161*, 697-705.

Giardini, P. A., Fletcher, D. A., and Theriot, J. A. (2003). Compression forces generated by actin comet tails on lipid vesicles. Proc Natl Acad Sci U S A *100*, 6493-6498.

Heo, W. D., Inoue, T., Park, W. S., Kim, M. L., Park, B. O., Wandless, T. J., and Meyer, T. (2006). PI(3,4,5)P3 and PI(4,5)P2 lipids target proteins with polybasic clusters to the plasma membrane. Science *314*, 1458-1461.

Hertzog, M., van Heijenoort, C., Didry, D., Gaudier, M., Coutant, J., Gigant, B., Didelot, G., Preat, T., Knossow, M., Guittet, E., and Carlier, M. F. (2004). The beta-thymosin/WH2 domain; structural basis for the switch from inhibition to promotion of actin assembly. Cell *117*, 611-623.

Higgs, H. N., Blanchoin, L., and Pollard, T. D. (1999). Influence of the C terminus of Wiskott-Aldrich syndrome protein (WASp) and the Arp2/3 complex on actin polymerization. Biochemistry *38*, 15212-15222.

Ho, H. Y., Rohatgi, R., Lebensohn, A. M., Le, M., Li, J., Gygi, S. P., and Kirschner, M. W. (2004). Toca-1 mediates Cdc42-dependent actin nucleation by activating the N-WASP-WIP complex. Cell *118*, 203-216.

Hoffman, G. R., Nassar, N., and Cerione, R. A. (2000). Structure of the Rho family GTP-binding protein Cdc42 in complex with the multifunctional regulator RhoGDI. Cell *100*, 345-356.

Hufner, K., Higgs, H. N., Pollard, T. D., Jacobi, C., Aepfelbacher, M., and Linder, S. (2001). The verprolin-like central (vc) region of Wiskott-Aldrich syndrome protein induces Arp2/3 complex-dependent actin nucleation. J Biol Chem *276*, 35761-35767.

Hussain, N. K., Jenna, S., Glogauer, M., Quinn, C. C., Wasiak, S., Guipponi, M., Antonarakis, S. E., Kay, B. K., Stossel, T. P., Lamarche-Vane, N., and McPherson, P. S. (2001). Endocytic protein intersectin-l regulates actin assembly via Cdc42 and N-WASP. Nat Cell Biol *3*, 927-932.

Isambert, H., Venier, P., Maggs, A. C., Fattoum, A., Kassab, R., Pantaloni, D., and Carlier, M. F. (1995). Flexibility of actin filaments derived from thermal fluctuations. Effect of bound nucleotide, phalloidin, and muscle regulatory proteins. J Biol Chem *270*, 11437-11444.

Jurdic, P., Saltel, F., Chabadel, A., and Destaing, O. (2006). Podosome and sealing zone: specificity of the osteoclast model. Eur J Cell Biol *85*, 195-202.

Kaksonen, M., Sun, Y., and Drubin, D. G. (2003). A pathway for association of receptors, adaptors, and actin during endocytic internalization. Cell *115*, 475-487.

Kapoor, T. M., and Mitchison, T. J. (2001). Eg5 is static in bipolar spindles relative to tubulin: evidence for a static spindle matrix. J Cell Biol *154*, 1125-1133.

Kelly, A. E., Kranitz, H., Dotsch, V., and Mullins, R. D. (2006). Actin binding to the central domain of WASP/Scar proteins plays a critical role in the activation of the Arp2/3 complex. J Biol Chem *281*, 10589-10597.

Kirschner, M., Gerhart, J., and Mitchison, T. (2000). Molecular "vitalism". Cell *100*, 79-88.

Kitamura, T., Onishi, M., Kinoshita, S., Shibuya, A., Miyajima, A., and Nolan, G. P. (1995). Efficient screening of retroviral cDNA expression libraries. Proc Natl Acad Sci U S A *92*, 9146-9150.

Klopfenstein, D. R., Tomishige, M., Stuurman, N., and Vale, R. D. (2002). Role of phosphatidylinositol(4,5)bisphosphate organization in membrane transport by the Unc104 kinesin motor. Cell *109*, 347-358.

Kuo, S. C., and McGrath, J. L. (2000). Steps and fluctuations of Listeria monocytogenes during actin-based motility. Nature *407*, 1026-1029.

Laurent, V., Loisel, T. P., Harbeck, B., Wehman, A., Grobe, L., Jockusch, B. M., Wehland, J., Gertler, F. B., and Carlier, M. F. (1999). Role of proteins of the Ena/VASP family in actin-based motility of Listeria monocytogenes. J Cell Biol *144*, 1245-1258.

Linder, S., Nelson, D., Weiss, M., and Aepfelbacher, M. (1999). Wiskott-Aldrich syndrome protein regulates podosomes in primary human macrophages. Proc Natl Acad Sci U S A *96*, 9648-9653.

Liu, A. P., and Fletcher, D. A. (2006). Actin polymerization serves as a membrane domain switch in model lipid bilayers. Biophys J *91*, 4064-4070.

Loisel, T. P., Boujemaa, R., Pantaloni, D., and Carlier, M. F. (1999). Reconstitution of actin-based motility of Listeria and Shigella using pure proteins. Nature *401*, 613-616.

Luxenburg, C., Addadi, L., and Geiger, B. (2006). The molecular dynamics of osteoclast adhesions. Eur J Cell Biol *85*, 203-211.

Marchand, J. B., Kaiser, D. A., Pollard, T. D., and Higgs, H. N. (2001). Interaction of WASP/Scar proteins with actin and vertebrate Arp2/3 complex. Nat Cell Biol *3*, 76-82.

Marcy, Y., Prost, J., Carlier, M. F., and Sykes, C. (2004). Forces generated during actin-based propulsion: a direct measurement by micromanipulation. Proc Natl Acad Sci U S A *101*, 5992-5997.

Martin, A. C., Welch, M. D., and Drubin, D. G. (2006). Arp2/3 ATP hydrolysis-catalysed branch dissociation is critical for endocytic force generation. Nat Cell Biol *8*, 826-833.

Mizutani, K., Miki, H., He, H., Maruta, H., and Takenawa, T. (2002). Essential role of neural Wiskott-Aldrich syndrome protein in podosome formation and degradation of extracellular matrix in src-transformed fibroblasts. Cancer Res *62*, 669-674.

Mogilner, A. (2006). On the edge: modeling protrusion. Curr Opin Cell Biol *18*, 32-39.

Mogilner, A., and Oster, G. (2003). Force generation by actin polymerization II: the elastic ratchet and tethered filaments. Biophys J *84*, 1591-1605.

Mullins, R. D., Heuser, J. A., and Pollard, T. D. (1998). The interaction of Arp2/3 complex with actin: nucleation, high affinity pointed end capping, and formation of branching networks of filaments. Proc Natl Acad Sci U S A *95*, 6181-6186.

Munter, S., Way, M., and Frischknecht, F. (2006). Signaling during pathogen infection. Sci STKE *2006*, re5.

Palmgren, S., Ojala, P. J., Wear, M. A., Cooper, J. A., and Lappalainen, P. (2001). Interactions with PIP2, ADP-actin monomers, and capping protein regulate the activity and localization of yeast twinfilin. J Cell Biol *155*, 251-260.

Pantaloni, D., Boujemaa, R., Didry, D., Gounon, P., and Carlier, M. F. (2000). The Arp2/3 complex branches filament barbed ends: functional antagonism with capping proteins. Nat Cell Biol *2*, 385-391.

Papayannopoulos, V., Co, C., Prehoda, K. E., Snapper, S., Taunton, J., and Lim, W. A. (2005). A polybasic motif allows N-WASP to act as a sensor of PIP(2) density. Mol Cell *17*, 181-191.

Pardee, J. D., and Spudich, J. A. (1982). Purification of muscle actin. Methods Cell Biol *24*, 271-289.

Pear, W. S., Nolan, G. P., Scott, M. L., and Baltimore, D. (1993). Production of high-titer helper-free retroviruses by transient transfection. Proc Natl Acad Sci U S A *90*, 8392-8396.

Pollard, T. D., and Borisy, G. G. (2003). Cellular motility driven by assembly and disassembly of actin filaments. Cell *112*, 453-465.

Prehoda, K. E., Scott, J. A., Mullins, R. D., and Lim, W. A. (2000). Integration of multiple signals through cooperative regulation of the N-WASP-Arp2/3 complex. Science *290*, 801-806.

Quinlan, M. E., Heuser, J. E., Kerkhoff, E., and Mullins, R. D. (2005). Drosophila Spire is an actin nucleation factor. Nature *433*, 382-388.

Reeves, P. M., Bommarius, B., Lebeis, S., McNulty, S., Christensen, J., Swimm, A., Chahroudi, A., Chavan, R., Feinberg, M. B., Veach, D.*, et al.* (2005). Disabling poxvirus pathogenesis by inhibition of Abl-family tyrosine kinases. Nat Med *11*, 731-739.

Rohatgi, R., Ma, L., Miki, H., Lopez, M., Kirchhausen, T., Takenawa, T., and Kirschner, M. W. (1999). The interaction between N-WASP and the Arp2/3 complex links Cdc42-dependent signals to actin assembly. Cell *97*, 221-231.

Rozelle, A. L., Machesky, L. M., Yamamoto, M., Driessens, M. H., Insall, R. H., Roth, M. G., Luby-Phelps, K., Marriott, G., Hall, A., and Yin, H. L. (2000). Phosphatidylinositol 4,5-bisphosphate induces actin-based movement of raft-enriched vesicles through WASP-Arp2/3. Curr Biol *10*, 311-320.

Samarin, S., Romero, S., Kocks, C., Didry, D., Pantaloni, D., and Carlier, M. F. (2003). How VASP enhances actin-based motility. J Cell Biol *163*, 131-142.

Shah, K., and Shokat, K. M. (2002). A chemical genetic screen for direct v-Src substrates reveals ordered assembly of a retrograde signaling pathway. Chem Biol *9*, 35-47.

Snapper, S. B., Takeshima, F., Anton, I., Liu, C. H., Thomas, S. M., Nguyen, D., Dudley, D., Fraser, H., Purich, D., Lopez-Ilasaca, M.*, et al.* (2001). N-WASP deficiency reveals distinct pathways for cell surface projections and microbial actin-based motility. Nat Cell Biol *3*, 897-904.

Soo, F. S., and Theriot, J. A. (2005). Adhesion controls bacterial actin polymerization-based movement. Proc Natl Acad Sci U S A *102*, 16233-16238.

Spinardi, L., Rietdorf, J., Nitsch, L., Bono, M., Tacchetti, C., Way, M., and Marchisio, P. C. (2004). A dynamic podosome-like structure of epithelial cells. Exp Cell Res *295*, 360-374.

Svitkina, T. M., Bulanova, E. A., Chaga, O. Y., Vignjevic, D. M., Kojima, S., Vasiliev, J. M., and Borisy, G. G. (2003). Mechanism of filopodia initiation by reorganization of a dendritic network. J Cell Biol *160*, 409-421.

Taunton, J., Rowning, B. A., Coughlin, M. L., Wu, M., Moon, R. T., Mitchison, T. J., and Larabell, C. A. (2000). Actin-dependent propulsion of endosomes and lysosomes by recruitment of N-WASP. J Cell Biol *148*, 519-530.

van der Gucht, J., Paluch, E., Plastino, J., and Sykes, C. (2005). Stress release drives symmetry breaking for actin-based movement. Proc Natl Acad Sci U S A *102*, 7847-7852.

van Oudenaarden, A., and Theriot, J. A. (1999). Cooperative symmetry-breaking by actin polymerization in a model for cell motility. Nat Cell Biol *1*, 493-499.

Volkman, B. F., Prehoda, K. E., Scott, J. A., Peterson, F. C., and Lim, W. A. (2002). Structure of the N-WASP EVH1 domain-WIP complex: insight into the molecular basis of Wiskott-Aldrich Syndrome. Cell *111*, 565-576.

Waterman-Storer, C. M., Desai, A., Bulinski, J. C., and Salmon, E. D. (1998). Fluorescent speckle microscopy, a method to visualize the dynamics of protein assemblies in living cells. Curr Biol *8*, 1227-1230.

Wedlich-Soldner, R., Altschuler, S., Wu, L., and Li, R. (2003). Spontaneous cell polarization through actomyosin-based delivery of the Cdc42 GTPase. Science *299*, 1231-1235.

Weisswange, I., Bretschneider, T., and Anderson, K. I. (2005). The leading edge is a lipid diffusion barrier. J Cell Sci *118*, 4375-4380.

Welch, M. D., and Mullins, R. D. (2002). Cellular control of actin nucleation. Annu Rev Cell Dev Biol *18*, 247-288.

Wiesner, S., Helfer, E., Didry, D., Ducouret, G., Lafuma, F., Carlier, M. F., and Pantaloni, D. (2003). A biomimetic motility assay provides insight into the mechanism of actin-based motility. J Cell Biol *160*, 387-398.

Yamaguchi, H., Lorenz, M., Kempiak, S., Sarmiento, C., Coniglio, S., Symons, M., Segall, J., Eddy, R., Miki, H., Takenawa, T., and Condeelis, J. (2005). Molecular mechanisms of invadopodium formation: the role of the N-WASP-Arp2/3 complex pathway and cofilin. J Cell Biol *168*, 441-452.

Yamaguchi, H., Miki, H., Suetsugu, S., Ma, L., Kirschner, M. W., and Takenawa, T. (2000). Two tandem verprolin homology domains are necessary for a strong activation of Arp2/3 complex-induced actin polymerization and induction of microspike formation by N-WASP. Proc Natl Acad Sci U S A *97*, 12631-12636.

Yamaguchi, H., Pixley, F., and Condeelis, J. (2006). Invadopodia and podosomes in tumor invasion. Eur J Cell Biol *85*, 213-218.

Yarar, D., To, W., Abo, A., and Welch, M. D. (1999). The Wiskott-Aldrich syndrome protein directs actin-based motility by stimulating actin nucleation with the Arp2/3 complex. Curr Biol *9*, 555-558.

Zamanian, J. L., and Kelly, R. B. (2003). Intersectin 1L guanine nucleotide exchange activity is regulated by adjacent src homology 3 domains that are also involved in endocytosis. Mol Biol Cell *14*, 1624-1637.

UCSF Library Release

Publishing Agreement
It is the policy of the University to encourage the distribution of all theses and dissertations. Copies of all UCSF theses and dissertations will be routed to the library via the Graduate Division. The library will make all theses and dissertations accessible to the public and will preserve these to the best of their abilities, in perpetuity.

Please sign the following statement:
I hereby grant permission to the Graduate Division of the University of California, San Francisco to release copies of my thesis or dissertation to the Campus Library to provide access and preservation, in whole or in part, in perpetuity.

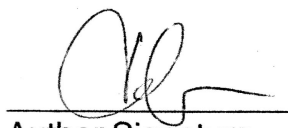

Author Signature

032707
Date